

**PROVISIONAL DRAFT**

Subject to Revision  
**DO NOT QUOTE OR RELEASE**  
Pending Approval by Director  
U.S. Geological Survey

ORIGINAL

*FLOW AND SEDIMENT TRANSPORT IN THE COLORADO RIVER  
BETWEEN LAKE POWELL AND LAKE MEAD*

*J. Dungan Smith and Stephen Wiele*  
U.S. Geological Survey  
Water Resources Division  
Boulder, Colorado

RECEIVED

APR 30 1991  
Jim Wilson  
CHEYENNE, WYOMING  
(USGS)

**GCES OFFICE COPY  
DO NOT REMOVE!**

ABSTRACT

In the Marble and Grand Canyons of the Colorado River the riparian environment is sensitive to the discharge and discharge history of the River which are tightly controlled by the Glen Canyon Dam. As a consequence, the manner in which the Glen Canyon Dam is operated can substantially benefit or damage the riparian environment of Grand Canyon National Park. In order to ascertain the relationship between water discharge at the Dam and the flow-affected downstream environment, a detailed physical understanding of the fluid mechanical and sediment transport processes in this river between Lake Powell and Lake Mead, as well as accurate flow and sediment transport models are essential. Only recently have the data necessary to develop and test such models been procured, and this paper is the first attempt to use this information as a foundation for comprehensive algorithms to compute flow and sediment transport in the Marble and Grand Canyon segments of the Colorado River. Owing to the absence of detailed topographic data for this river corridor, a reach-averaged approach was taken; therefore, the effective roughness coefficient had to be determined empirically. Topographic cross-sections that previously had been obtained every mile along the River were averaged for regions of similar riverbed geology generating mean channel geometries for ten characteristic reaches. These data were combined with (1) cross-sectionally averaged velocities, which were determined from discharge at the time of the topographic study, and (2) a set of dye advection measurements in order to calculate roughness coefficients as a function of stage for each of the ten characteristic reaches. A discharge wave phase speed also was used for this purpose, but the number of characteristic reaches had to be reduced for this calculation because of the length of the wave. From the geometries of the characteristic reaches and the stage-dependent roughness coefficients for each of them, all of the important reach-averaged flow properties were calculated and tabulated. Suspended sand transport was then determined based on the

calculated velocity fields and boundary shear stresses. We show that a substantial amount of suspended sand has been retained in the upstream part of the system because of the increasing mean river width and that some is retained there by the peak power mode of operation of the Dam. The latter occurs because the shape of the discharge wave changes between the Dam and the mouth of the Little Colorado River, reducing the duration of the period of peak discharge and forcing deposition of suspended sand on the channel bottom. Our results indicate that it is possible to construct flow and sediment transport models of sufficient accuracy to be used as the basis for delicate dam management decisions.

## INTRODUCTION

The Colorado River not only serves as a major access route to much of the Grand Canyon National Park, but its flow and consequent sediment transport also determine, in large measure, the salient characteristics of the narrow river corridor at the bottoms of the Marble and Grand Canyons (see Figure 1). Moreover, since 1963 discharge in this river has been controlled to a very high degree by hydroelectric power production at the Glen Canyon Dam. Under normal conditions no clastic sediment passes through this structure, so most of the sand that forms the substrate of the riparian environment is a relic of pre-dam conditions or has been added to the Colorado by the Paria and Little Colorado Rivers, which enter the main stem 27km (0.8 miles downstream from Lees Ferry, the location from which distance along the river is measured) and 125km (at River Mile 61.4) downstream from the Dam respectively. The issues of sand transport into the Colorado River, redistribution of sand along the Colorado, and loss of sand from this river to Lake Mead are of major environmental concern, and in order to address these issues satisfactorily a comprehensive understanding of flow in this coarse-gravel-bedded river is necessary. In particular, accurate, well tested, physically based algorithms for computation of flow and sediment transport are required for: (1) proper interpretation of physical, chemical and biological field data collected in the riparian corridor as it relates to river flow history, especially but not exclusively with respect to bank and bar processes, (2) accurate calculation of rates of sediment accumulation or loss from the system under various discharge histories imposed on the River by hydroelectric power production or spillage of water at the Glen Canyon Dam, and (3) prediction of

redistribution of sediment along the channel in response to long term changes in water discharge in the main stem and sediment discharges from the major tributaries.

### Nature of the Geomorphic System

Between Lake Powell and Lake Mead the Colorado River flows through the Marble and Grand Canyons. In this segment it is cut deeply into a sequence of rocks ranging from Jurassic to PreCambrian in age and varying from sandstone and shale through limestone to gneiss and schist in composition. At a discharge 25,000cfs (708 m<sup>3</sup>/s) the River has a mean surface width of 80.5m and a mean depth of 6.9m, but the reach-averaged surface width at this discharge varies from 60m in the Inner Granite Gorge to 110m somewhat upstream of Furnace Flats depending primarily on the rock type at river level.

The most obvious geomorphologic characteristics of the river corridor in this region arise from its deep incision. The steep walls of the main canyon promote the formation of talus slopes along the edges of the River, and the steep walls of the tributaries make the canyon floor susceptible to blockage by fans of coarse gravel resulting from debris flows and floods originating in these tributaries. As was pointed out by Dolan and others (1978), and as has been emphasized by Howard and Dolan (1981) and more recently by Webb (1992), most of the rapids in the Marble and Grand Canyons are due to deposits of this type. The fluid mechanical consequence of a debris fan in this system is to produce a hydraulic control at the site of maximum width and depth constriction. This leads to an upstream pool from the damming effect of the hydraulic control followed by a rapid that begins at the site of least cross-sectional area. In many instances, there also are pools somewhat downstream of the rapids. According to Smith (in preparation) the downstream pools are produced by the impacts of boulders that have saltated down the face of the debris barriers during large pre-dam floods on the main stem. At the beginning of a high flow event there is likely to be sand and gravel covering the beds of the downstream pools, but as the flow increases in intensity the sand goes into suspension and the gravel is crushed and removed. Under the most extreme conditions Smith claims that a substantial fraction of the sediment on the beds of these pools is removed and the incoming boulders impact directly on bedrock pulverizing it, and thereby permitting local excavation of the bed of the river. In pre-dam times these downstream pools, therefore,

served as sites for rapid particle size reduction, contributing in a major way to the removal of coarse, tributary derived, material from the main channel. In essence, they are the direct result of what Smith believes to be the major bedrock excavation mechanism in active, deeply incised rivers. As a consequence of the incision, the dominant geomorphological characteristics of the river corridor arise from the interplay of random hydrologic events in small tributaries that have caused large mass movements through them, and large pre-dam discharges in the main stem, with local variations in these characteristics resulting from the bedrock geology at river level.

Were there no other sediment sources, the bed of the Colorado River in the Marble and Grand Canyons would be coarse gravel derived primarily from the debris fans. Significant amounts of fine material, however, were transported down the main stem in pre-dam times, and some always has been added from floods in the Paria and Little Colorado Rivers. Superimposed on what otherwise would have been a gravel bedded stream, therefore, was a significant flux of silt and sand produced by erosion of the fine grained sedimentary rocks that cover the Colorado Plateau. Currently no silt or sand bypasses the Glen Canyon Dam, but fine material derived from the Paria and Little Colorado Rivers is still transported through the Grand Canyon and into Lake Mead. The average annual sand load derived from debris flows and floods on all of the other tributaries appears to be substantially less than that contributed by the Paria and Little Colorado River. At discharges above 10,000cfs ( $283\text{m}^3/\text{s}$ ) this sand fraction moves through the otherwise coarse bedded system largely in suspension, and relative to the gravel it has a very short residence time in the system.

In pre-dam times, this segment of the Colorado River was swept each Spring by snow melt floods that were more than five times greater in daily discharge than have been most post-dam releases, and as indicated above, the current geomorphology of the system clearly reflects the processes that occurred during these high flow events. The Glen Canyon Dam has substantially reduced the maximum daily discharges that occur each year, but it also has cut off the supply of sand from the main stem above the mouth of the Paria River. As a consequence, with the exception of future debris flows, the deposits of which can be reworked only in minor ways by the present and expected low main stem flows, the morphology of the fluvial system is fixed. Neither in pre-dam nor current times has enough sand been

added to the system relative to its transport capacity to allow the fine material to exert a dominant control on river geomorphology. Basically what is supplied to the system is transported throughout it, the balance being maintained locally through expansion and contraction of the fraction of the channel bed covered by sand. These sand patches could not smooth the bed of the channel in pre-dam times because most of the material was washed through by the large snow melt floods each Spring, and they cannot smooth the bed of the channel at present because the supply is still too low for the imposed discharge.

As has always been the case, the lateral bars of the system (composed primarily of sand) are in areas of flow convergence, but grow or shrink in response to the supply of the sand from upstream, the discharge history of the river, and the geometry of the channel (imposed primarily by mass movement processes). From a geologic point of view all of the sand deposits are ephemeral. As the stage rises sand is eroded from local areas of boundary shear stress divergence and it is deposited in zones of boundary shear stress convergence, the latter being especially common in regions of flow separation along the edges of the channel. In pre-dam times these flow separation, or eddy deposits, also contained a significant amount of silt. Owing to the normal tendency for eddy bars to fill embayments along river channels, for them to collect fragments of riparian plants some of which can root, and for them to maintain elevated ground water tables for extended periods of time, they produce extremely important substrates for riparian biological activity, particularly in arid regions and specifically along the Colorado River in the Grand Canyon. In fact, Smith (1991) claims that eddy deposits comprise the major means of channel straightening and bank repair in many active rivers. Channel edge deposition in the Colorado River is especially effective at high stage, when the river surface is elevated well above the eddy bars, when the eddy circulation is strong, and when there is more sediment in suspension. Large perched sand deposits from pre-dam and relatively recent high stage events also serve as the campsites of preference for rafters and hikers.

#### **Nature of the Management Problem**

As a consequence of major changes in both the flow and the sediment transport regimes in the Colorado River between Lake Powell and Lake Mead, the riparian system can no longer operate as it did

in pre-dam times. At present the Dam is operated primarily for power production during times of peak demand each day, and as a consequence, a large amplitude discharge wave is released daily. It has been argued that the rise and fall of the water surface in association with these large amplitude discharge waves promotes erosion of the most desirable eddy beaches and should be banned. The question thus arises as to whether the Glen Canyon dam could be operated to optimize power production while at the same time satisfying the constraints of the "Law of the River" and minimizing the environmental damage now being done to the Grand Canyon National Recreation Area and Grand Canyon National Park. Until recently the latter was not considered an important factor in dam operations, but it is likely that environmental considerations eventually will become of great importance in dam management decisions. In this system as well as in many others, substantial improvement in environmental protection probably can be effected with minimal revenue loss, if the flow and sediment transport processes in the river are thoroughly understood, carefully modeled, and properly taken into account when developing operational plans. Balancing the various environmental and economic factors involved in the operation of a dam is a political consideration, but the development of a solid scientific understanding that permits operational decisions to be made with insight, and the environmental consequences of those decisions to be made clear, is a scientific and environmental engineering issue.

In 1989 the U.S. Geological Survey generated a plan for comprehensive examination of the flow, sediment transport, and water quality in the Colorado River between Lake Powell and Lake Mead. The goal was to develop the foundations of knowledge required for astute management of this river. This plan was devised partly in support of Phase II of GCES (Glen Canyon Environmental Studies) but also in response to a critical national need for sound scientific information on the basic hydraulic, sediment transport, geomorphic, and environmental chemical processes controlling the riparian environment of the Colorado River in the Marble and Grand Canyons. At the time the U.S.G.S. plan was composed, conjecture on how dam operations had affected and were affecting the downstream environment far outweighed any scientific knowledge on this issue. A primary goal of the facet of the U.S. Geological Survey plan with which this report is concerned was to develop a comprehensive understanding of flow and sediment transport in the Colorado river such that fluid mechanically based

water and sediment transport models could be developed, and used as management tools. This report presents results of the first phase of analysis of data collected in 1991 as part of the U.S. Geological Survey field program.

It is the view of the authors of this report that first the flow and second the sediment transport that arises in response to a particular discharge history must be thoroughly understood if the system or any part of it is to be properly managed or truly protected. *Short of changing the design of the intake structures at the Dam, or adding sediment to the River from a slurry pipeline, management of the riparian environment is through the rate at which water is discharged at the Glen Canyon Dam as a function of time, and if an accurate understanding of the consequences of such discharges is not developed then effective management of the system is impossible.* Moreover, without such knowledge past, present and future studies pertaining to the effects of operation of the Glen Canyon Dam cannot be put into a proper scientific context, and thus are likely to be misinterpreted and misused. Knowing the relationship of environmental phenomena to discharge and discharge history is essential if results from detailed field studies are to be generalized properly. A thorough understanding of flow and sediment transport in the Colorado River between Lake Powell and Lake Mead is essential for sensitive management of the riparian environment of Grand Canyon National Park, and such an understanding can only be obtained through a carefully designed, well balanced research project that includes an innovative field measurement program, a comprehensive, fluid mechanically based data analysis component and state-of-the-art mathematical modeling.

## CHARACTERIZATION OF THE FLOW

### Field Measurements

The above mentioned U.S. Geological Survey research plan was based in part on the expectation that high resolution air photogrammetry would be used by the Bureau of Reclamation to make a high precision topographic map of the River corridor and that this important information would be available for the analysis phase of the project. Unfortunately this basic topographic information has not yet been procured. To date only fifty of approximately three hundred miles of the River have been mapped. As

might be expected, the lack of this essential data has had a negative impact on the flow and sediment transport modeling program, because high accuracy flow and sediment transport calculations cannot be carried out for local areas in a river for which the bed and bank topography is known only crudely, if at all. As a consequence, the analysis presented in this paper is for the large scale system and is based on 199 cross-sections measured with an echo sounder approximately every mile between Lees Ferry and Diamond Creek (see Figure 1) by Richard Wilson of the U.S. Geological Survey.

Owing to the typical large daily variation in discharge at the Glen Canyon Dam, stage as a function of location and time is an extremely important variable. Consequently a network of approximately 50 temporary, internally recording pressure gages was deployed along the gorge. By late, 1990, gages were emplaced approximately every five miles between Lees Ferry and Lake Mead and were recording usable data. In the first half of calendar year 1991, the pressure transducer at each of these measurement sites was being sampled only once every fifteen or once every thirty minutes making determination of rapid changes in stage quite inaccurate. By mid-summer 1991, however, the relatively crude data loggers that were emplaced initially had been replaced by ones able to measure average river surface elevation every five minutes. All of the pressure transducers were carefully calibrated and delicately emplaced by Robert Gauger of the Flagstaff Field Office of the U.S. Geological Survey, and this temporary stage gage network has yielded an extremely high quality data set, one that has made possible the conclusions contained in this report. Data from this network has been especially important in light of the absence of detailed topography for the river corridor.

Accurate velocity measurements as a function of stage at specific sites along a river are useful only when the topography and bed roughness at those sites also are known. In the absence of detailed topographic information, regionally averaged velocity data such as obtained from dye studies is of greater value. Therefore, four large scale dye studies were planned by Julia Graf of the Tucson Office of the U.S. Geological Survey. Two of these have been carried out to date and the results are described by Graf (1992). These were accomplished during: (1) a steady discharge of 15,000cfs ( $425\text{m}^3/\text{s}$ ) and (2) a flow in which the discharge varied from 3,000cfs ( $85\text{m}^3/\text{s}$ ) to 26,000cfs ( $736\text{m}^3/\text{s}$ ) repetitively for eight days. Nevertheless, additional data are badly needed for a steady discharge of 5,000cfs ( $142\text{m}^3/\text{s}$ ) and

for a steady flow with a peak discharge at or above power plant capacity (32,000cfs or  $907\text{m}^3/\text{s}$ ).

Information from each steady dye study provides a direct constraint on the reach-averaged bed roughness at the stage of that dye release. In addition, dye advection data from a large amplitude, unsteady flow provides a sensitive test of a discharge wave propagation model.

### Modeling Flow in Long Segments of Large Rivers

When attempting to understand flow and flow related characteristics such as sediment transport in large rivers it is rarely feasible or advantageous to construct a three-dimensional model of the entire fluvial system. In these situations the most effective modeling strategy is to construct a simple global algorithm that predicts the general properties of the flow in any given segment of the system and then to use this global algorithm to drive quasi steady, multi-dimensional models for specific sites of particular interest. The local models then can be used to evaluate the detailed flow and sediment transport structures in reaches of known morphology and roughness, and to evaluate some of the parameters required in the global model. For example, our large scale model of the flow in the Colorado River between Lees Ferry and Diamond Creek contains an empirically determined roughness coefficient field. If one were to set these roughness coefficients theoretically, the effects of large roughness elements on the riverbed and the effects of rapids would have to be calculated using local models of rough bedded straight reaches (such as that of Wiberg and Smith, 1991), of curved reaches (such as those of Smith and McLean, 1984, and Nelson and Smith, 1987) and of debris-fan-caused constrictions (such as currently under development by Wiele and Smith).

In order to construct an accurate one-dimensional flow model it is necessary to have either a continuous field of cross-sectional area as a function of stage or a discretely sampled field from which a spectrum that contains a full representation of the essential variations can be calculated: Moreover, for an accurate two- or three-dimensional model not only must this requirement be met, but also a continuous or densely sampled field of cross-sections is necessary. In most parts of the Colorado River, this means that cross-sections would have to be measured every 20m or so, instead of every mile (1.6km) along the trace of the River. Owing to the absence of topographic information for the bed and banks of the

Colorado River sufficient to permit construction of three-, two-, or even one-dimensional flow and sediment transport models, a reach-averaged approach had to be taken. If the extent of a characteristic reach is chosen carefully and if that reach is long compared to the major variations in the system, then effects arising from convective accelerations associated with bed and bank topography in a small scale model will show up as effective roughness in the large scale one. Although this simplifies the problem immensely and makes global computations relatively simple, it also makes computation of the roughness impossible without empirical input, or at least without the use of a large set of local models employed as described in the previous paragraph, and it requires that the topography used in the model be accurately averaged over the characteristic reaches.

Cross-sectionally averaged velocities calculated from information procured during a topographic investigation carried out at nearly steady discharges ranging from 25,500cfs ( $722\text{m}^3/\text{s}$ ) to 32,000cfs ( $903\text{m}^3/\text{s}$ ) by Richard Wilson (Wilson, 1986), a dye study carried out by Julia Graf (Graf, 1992) at a steady discharge of 15,000cfs ( $425\text{m}^3/\text{s}$ ), and the phase speed of a discharge wave that varied between 5,000cfs ( $142\text{m}^3/\text{s}$ ) and 15,000cfs ( $425\text{m}^3/\text{s}$ ) were used to set the roughness coefficient field as a function of stage and downstream position in the version of our reach-averaged flow model presented in this report. Only after appropriate topographic information for the river corridor becomes available will reliable reach-averaged flow calculations for discharges above 30,000cfs ( $850\text{m}^3/\text{s}$ ) be possible or will the calculations required to set the roughness coefficient field theoretically be feasible. In a reach-averaged model, the downstream gravitational force averaged over a lengthy streamwise segment of the river is balanced against the frictional force on the wetted boundary of that segment of the river to produce a reach-averaged boundary shear stress and a reach-averaged hydraulic radius. If the reaches are chosen so that convective accelerations between them are small and the reach-averaged boundary shear stress can be calculated with high accuracy from the reach-average slope times the hydraulic radius for the reach times the specific weight of the fluid. For this calculation the hydraulic radius for the reach is defined as the volume of water in the reach divided by the wetted surface area in the reach.

#### Reach-Averaged Geometry of the Colorado River

PROVISIONAL DRAFT

Subject to Revision  
DO NOT QUOTE OR RELEASE  
Pending Approval by Director  
U.S. Geological Survey

In the Colorado River both the cross-sectional area and the cross-sectional shape vary significantly with downstream distance on the scale of a fraction of a river width; therefore, cross-sections taken at spacings greater than this are of little value for deterministic analysis. At present, the only moderately complete set of river channel cross-sections is the one procured by Wilson. It was this data set with which Randall and Pemberton (1987) had to work when they produced the first numerical models for flow and sediment transport in the Colorado River. Aware that Wilson's data set was by itself insufficient for their one-dimensional algorithm, these authors tried to use a field of river widths to expand it. Unfortunately, there is insufficient correlation between the width of this part of the Colorado River, which is relatively easily measured from the air photographs taken at a stage of 5,000cfs ( $142\text{m}^3/\text{s}$ ), and its cross-sectional area, because large changes in local depth, associated with past geomorphic events, exert a greater local control on cross-sectional area than does river surface width. In this report we, therefore, have chosen to take a stochastic approach, and to average the available topographic data over zones of similar geometric characteristics. Although this does not minimize convective accelerations as is often a goal of reach-averaging, the great lengths of our reaches force inertial effects to be small.

Inside a given geologically defined zone of reasonable lateral extent, a reach-averaged cross-sectional area, a reach-averaged surface width, a reach-averaged depth, and a reach-averaged cross-sectional shape can be constructed from the Wilson cross-sections for the stage at which the measurements in that zone were made. Our reach-averaged cross-sectional shapes were obtained by scaling each individual profile with its surface width then averaging the scaled profiles in groups associated with the chosen zones. Each reach-averaged cross-sectional shape was then rescaled, by the appropriate mean surface width for the stage at which the set of measurements was made, and the banks were extrapolated linearly to higher elevations. There is no apparent reason for the river, on the average over a reach tens of kilometers in extent, to have an asymmetrical cross-section; therefore, to provide a larger population of cross-sections for the statistical analysis we forced the channel to be symmetrical by averaging the left and right halves of the profiles. In addition to reach-averaged values, standard

deviations of surface width, cross-sectional area, mean depth, and cross-sectional shape also were calculated.

To aid in delineating characteristic reaches, the Wilson data set was filtered with a fifteen point running mean. The filtered data set has the advantage of providing a continuous distribution of key geometric properties from Lees Ferry to Diamond Creek, but it suffers from the fact that the morphologic characteristics of the river channel vary primarily with canyon-bottom bedrock geology and that changes from one geologically controlled zone to the next are more abrupt than the length scale of the filter that had to be used to get an acceptably smooth result. The fifteen point filtered channel properties are displayed in Figures 2 and 3. The solid line in Figure 2 displays mean surface width and the dashed line displays the running standard deviation of surface width from the fifteen point analysis, as a function of distance down river from Lees Ferry. Similarly, Figure 3 shows the running mean cross-sectional area and its standard deviation as a function of River Mile, the solid line displaying the former and the dashed line representing the latter. From each local width and local cross-sectional area, a cross-sectionally averaged depth also can be calculated. These results then can be filtered to yield a running mean depth. In both of these two figures, a blocky structure to the running means is clearly evident; moreover, by comparing these graphs to the Colorado River in Grand Canyon Guide (Stevens, 1983), it becomes clear that each of the zones of approximately constant value corresponds with a zone of characteristic geology. We therefore have defined the set of characteristic reaches using Figures 2 and 3, in terms of riverbed geology and channel geometry. The full set of reaches that we have chosen to use is delineated in Table I. This group is similar to the eleven morphologic zones defined in an analogous manner by Graf and Schmidt (1990) and some of our reaches are essentially the same as theirs, but others differ because of our greater reliance on filtered profiles. These ten divisions of the River between Lees Ferry and Diamond Creek will be denoted *morphologically similar reaches*, thereby indicating the dominant criteria by which they were defined.

After segmenting the river as described above and as displayed in Table I, block means and standard deviations were computed for each of the segments. Figures 4, 5, and 6 compare the block averaged values of surface width, cross-sectional area, and flow depth respectively for all of the

morphologically similar reaches to the fifteen point running means of these variables. Also shown in Figures 4, 5, and 6 are the block averaged values of the variables plus and minus one standard deviation. The dashed line in Figure 7 shows the block averaged cross-sectional shape for the entire set of profiles, and the solid line in this figure indicates the block averaged cross-sectional shape for the entire channel assuming that it must be symmetrical. The dotted lines in Figure 7 give the symmetrical shape plus and minus one standard deviation. A full set of cross-sectional shapes for the ten morphologically similar reaches is included as Appendix I, while some of the more interesting cross-sections are displayed in combination in Figures 8 through 11.

Figure 8 compares the cross-sectional shapes for three reaches in which there is limestone and massive, calcareously cemented sandstone (RM 0-11) or just limestone (RM 23-50, RM 140-169) at river level and shows that there is no significant difference between these reaches. Consequently the profiles from all three locations were combined. Similarly, Figure 9 compares the cross-sectional shape of the River as it cuts through the Supai Group with that for the Inner Granite Gorge where the Zoroaster Granite and Vishnu Schist are at river level. These profiles similarly do not differ appreciably and, therefore, have been combined. In contrast, Figure 10 displays the block averaged cross-sectional shapes for the river channel as it cuts through Tapeats Sandstone and Bright Angel Shale between Nankoweap Creek (RM 52) and Lava Canyon (RM 65) as compared to where it cuts through the same Cambrian rocks between Fern Glen Canyon (RM 168) and Whitmore Wash (RM 188). The upstream reach is represented by the upper profile and the downstream one is represented by the next one down in the figure. The difference between these two shapes represents sand and gravel in the reaches below Nankoweap Creek (RM 52) and near the mouth of the Little Colorado River (RM 61), the origin of which is discussed in the section of this report on sediment transport. Although most of the downstream section was once filled with Pleistocene Lava, the presence then removal of this volcanic material clearly has not had a significant effect on the channel cross-sectional geometry. Also shown in Figure 10 is the profile for the channel cut through Vishnu Schist between Whitmore Wash (RM 188) and Diamond Creek (RM 225), where the River is much narrower and deeper. The block averaged cross-sectional profiles for the reaches that were discussed and grouped previously in this paragraph are contrasted in

Figure 11 to demonstrate the substantial differences between the river channels through Cambrian clastic sedimentary rocks (shallowest), limestone (next shallowest), PreCambrian sedimentary rocks and schist (next deepest), and Zoroaster Granite and Supai Group (deepest). It is useful to examine the statistics for each of these reaches, as given in Table II, in conjunction with the cross-section displayed in Figure 11.

Using as measures of resolution both the standard deviations for the chosen blocks of data and the differences between the left and right halves of the channel in each block as given in Appendix I, the set of cross-sections was compacted. As might be expected, the sub-groups that were combined come from reaches with similar geologic characteristics, especially in regard to the response of the rocks bounding the river channel to impacts. The only possible surprises are that the sandy beds of the Supai Group react similarly to the Zoroaster Granite - Vishnu Schist of the Upper Granite Gorge, and that the Pleistocene lava in the lower canyon seems to have had little effect on river geomorphology. The most common characteristic morphology is that for the zones in which limestone and calcareously cemented, eolian sandstone are at river level, namely River Miles 0.8 to 5.5 where the Kaibab and Toroweap limestones and the Coconino Sandstone are at river level, River Miles 23.2 to 48.8 in which the Redwall and then the Muav limestones are at river level, and reach 139.7 to 169.1 in which Redwall and Muav (primarily the latter) are again at river level. Although a quantitative analysis of the processes producing these characteristic morphologies is not the goal of the present report, it is clear that there is a straight forward correspondence between the consequences of incision, the bedrock type at river level, the flow, and the geometry of the river channel.

#### **Reach-Averaged Flow Properties at Stages of 15,000cfs ( $425\text{m}^3/\text{s}$ ) and Above**

Now that cross-sections have been constructed for each of the morphologically defined reaches of the Colorado River in the Marble and Grand Canyons, this information can be combined with reach-averaged river slope and reach-averaged velocity data to produce reach-averaged boundary shear stresses, reach-averaged bed roughness, and tables that permit computation of shear velocity, cross-sectionally averaged velocity, and discharge as functions of stage. Four dye studies were planned in order to determine reach-averaged velocity fields, but only two of these have been carried out to date; moreover,

only one of these two was undertaken during an extended period of steady flow. This was accomplished during Research Flow E in late May, 1991, when the discharge was 15,000cfs ( $425\text{m}^3/\text{s}$ ). Data from this dye study are used in this section to determine reach-average velocities and then roughnesses for each of the ten morphologically similar reaches. Dye concentration measurements were not obtained at or near the boundaries of the reaches defined by our channel geometry analysis because of logistical constraints. Nevertheless, the dye velocity varied surprisingly little with downstream distance in this experiment (Graf, 1992), and it is easy to interpolate the measured velocities of the dye cloud peak to get accurate estimates of cross-sectionally averaged velocity, namely the velocity to which the dye cloud peak most closely responds, for each of the morphologically similar reaches. All measurements of the velocity of the dye cloud peak for Research Flow E are within five per cent of one meter per second.

Using the geometric properties of each morphologically similar reach to determine its hydraulic radius as a function of flow depth, and using the reach-averaged slope in combination with this hydraulic radius to obtain reach-averaged boundary shear stress and shear velocity, allows computation of the effective roughnesses of each of these reaches at a discharge of 15,000cfs ( $425\text{m}^3/\text{s}$ ). None of the methods by which channel bed friction normally is parameterized is appropriate for a river of such high relative roughness. Only a method, in which the form drag on each of the common geometric elements of the channel bed is computed and then summed, can yield a satisfactory velocity field and hence an accurate relationship between cross-sectionally averaged velocity and shear velocity, permitting computation of bed friction, as a function of stage for each morphologically similar reach. This could be done by applying a modified version of the method of Wiberg and Smith (1991) to a statistical representation of the channel bed were the appropriate topographic information available, and this will be done when the required information is obtained. In the meantime, a more empirical method must be employed. To do this we shall assume that the reach-averaged velocity field is estimated at any point in the cross-section by expressions that apply to steady, horizontally uniform open channel flows of low relative roughness, namely

$$u = \frac{u_*}{k} \ln \frac{z}{z_0} \quad z \leq z_b = 0.20h \quad (1a)$$

$$u = \frac{u_*}{k} \left( \beta \left( \frac{z}{h} \right) - \frac{1}{2} \left( \frac{z}{h} \right)^2 \right) - 0.18 \beta + \ln \frac{0.20h}{z_0} \quad (1b)$$

$$z \geq z_0 = 0.20h$$

where  $u_* = (\tau_0/\rho)^{1/2}$  is the shear velocity,  $\tau_0$  is the boundary shear stress,  $\rho$  is the density of the fluid,  $z$  is the distance above the riverbed,  $h$  is the depth of the flow at the location of interest,  $k = 0.408$  is VonKarman's constant,  $z_0$  is a parameter that characterizes the effective roughness of the flow below and upstream of the location of interest, and  $\beta = 6.24$  is a parameter. This velocity profile assumes an eddy viscosity of  $K = ku_*z(1-z/h)$  below  $0.20h$  and  $K = ku_*h/\beta$  above this level. Integrating the velocity profile represented by (1) over the flow depth yields

$$q = \langle u \rangle h = \frac{u_*}{k} \left( \ln \frac{h}{z_0} - 0.74 \right) h \quad (2)$$

where  $q$  is the discharge per unit width at the location of interest and  $\langle u \rangle$  is the vertically averaged velocity at that location.

In actuality, lateral stresses should be taken into account, and the eddy diffusivity for momentum should be derived in terms of distance from the bed along rays that are normal to the isovel field and that intersect the channel boundary perpendicularly. For broad shallow channels, however, the error introduced by computing the appropriate integrals along vertical lines rather than along these difficult to calculate rays is small except near the banks and (2) can be employed as a reasonable approximation. In the Colorado River, a much greater error than that produced by neglecting lateral stresses in (2) is incurred by the use of (1) or its integral (2) instead of calculating a velocity field with an appropriate modification of the method of Wiberg and Smith. Equation (2), or its numerical equivalent if a more general local flow algorithm is employed (eg. that of Wiberg and Smith), must be integrated across the channel to get discharge from the discharge per unit width which is given by (2). This must be done numerically, because of the dependence of the shear velocity and the logarithmic term on local flow depth. The cross-stream integrated version of (2), however, can be written in the form:

$$Q = U b h = \frac{U_*}{k} \left( \ln \left( a_h \frac{R}{(z_0)_{av}} \right) - 0.74 \right) b h \quad (3)$$

where  $U_*$  is based on the hydraulic radius  $R$  of the characteristic reach rather than the local flow depth,  $(z_0)_{av}$  is the depth weighted average value of the roughness parameter, and  $a_h$  is a coefficient that makes this analytic expression equal to the numerical result. In (3),  $b$  represents the surface width of the flow,  $h_{av}$  denotes average depth, and  $U$  denotes the cross-sectionally averaged velocity. Also we define a friction coefficient  $B$  by

$$B = \frac{1}{k} \left( \ln \left( a_h \frac{R}{(z_0)_{av}} \right) - 0.74 \right) \quad (4)$$

Often  $a_h$  is included in the value of  $z_0$ , and we shall follow that procedure here. From the reach-averaged values of the cross-sectionally averaged velocity obtained with the dye study, we can now compute values of  $B$  and  $z_0$ , at a discharge of 15,000cfs ( $425\text{m}^3/\text{s}$ ). These values are given in Table III.

Also, values of  $U$ , hence  $B$  and  $z_0$ , can be calculated for the discharges at which the cross-sections were obtained by Wilson. Typically the profiles within a given morphologically similar reach were procured at a more or less constant discharge, so a reasonably accurate cross-sectionally averaged velocity can be calculated for each of these reaches. These velocities are given in Table III along with the calculated values of  $B$  and  $z_0$ . This procedure demonstrates that  $z_0$  increases with stage, therefore,  $z_0$  and  $B$  also have to be evaluated at other discharges, especially one around 5,000cfs ( $142\text{m}^3/\text{s}$ ).

Unfortunately no dye or topographic information with which to do this is available, and next to the construction of a detailed topographic map of the river corridor, procurement of cross-sectionally averaged velocity data from a dye study at a discharge of 5,000cfs ( $142\text{m}^3/\text{s}$ ) is of the highest priority.

In the absence of flow velocity information, a travel time versus distance curve for one of the Research Flow discharge waves had to be used.

Up to this point the mean geometric properties of the river channel and the quasi-steady response of the flow system have been examined. Only topographic profiles and reach-averaged velocity data have been used to do this. To improve on these quasi-steady flow results additional reach-averaged velocity information at lower and higher discharges relative to 15,000cfs ( $425\text{m}^3/\text{s}$ ) and much better topographic information for the riverbed and the river banks from the 25,000cfs ( $708\text{m}^3/\text{s}$ ) to the 100,000cfs ( $2,830\text{m}^3/\text{s}$ ) levels are required. Currently accurate calculations are not possible for discharges above 25,000cfs ( $708\text{m}^3/\text{s}$ ) in most of the upstream reaches and above 32,000cfs ( $906\text{m}^3/\text{s}$ ) in the lower ones because the available cross-sections do not extend above these levels.

#### Determination of the Friction Coefficient for Low Discharges

Not only did the values of the friction coefficient vary between the two high flow cases for which it was set, but also all of the calculations of discharge wave speed based on stage independent friction parameters or extrapolated stage-dependent values led to underestimates of the wave speed during the research flows for which we had accurate data from the temporary stage gage network. Our calculations all indicated that the bed of the river becomes effectively smoother as the stage drops, and demonstrated that this effect had to be taken into account if suitable routing algorithms were to be constructed. The friction parameters determined above for each of the morphologically similar reaches were for discharges at or close to the peak values of both the 5,000cfs ( $142\text{m}^3/\text{s}$ ) to 15,000cfs ( $425\text{m}^3/\text{s}$ ) and the 3,000cfs ( $85\text{m}^3/\text{s}$ ) to 26,000cfs ( $736\text{m}^3/\text{s}$ ) research flows (B and D respectively); therefore, the phase speeds for these research flows or results from the unsteady dye study could, in principal, be used to determine the low stage friction parameters for each of the morphologically similar reaches. The dye study, however, was carried out at such a highly variable discharge [3,000cfs ( $85\text{m}^3/\text{s}$ ) to 26,000cfs ( $736\text{m}^3/\text{s}$ ) at the Dam] that the stage (and discharge) of the trough increased substantially with downstream distance, making the velocity data for this research flow very difficult to use for determination of a low flow friction parameter.

Owing to a more rapid rise in trough level stage with downstream distance for Research Flow D than for Research Flow B, the trough discharges for both of these were about the same in the middle

third of the river segment between the Dam and Diamond Creek requiring the low stage friction parameter to be the same for both cases in this segment of the River. Preliminary calculations indicated that the data being used to constrain the friction parameter were not accurate enough to justify making a distinction between the two trough discharge values in the upper and lower thirds of the River; therefore, a single value was set for flows of discharges from 4,400cfs ( $125\text{m}^3/\text{s}$ ) to 5,400cfs ( $153\text{m}^3/\text{s}$ ) in the upper River and from 5,500 ( $156\text{m}^3/\text{s}$ ) to 6,200cfs ( $176\text{m}^3/\text{s}$ ) in the lower river. This procedure led to a reasonable characterization of friction for low discharge flows, but before the temporary stage gage network is removed it is important that a comprehensive low stage dye study be carried out to set this friction coefficient definitively. With only one low stage friction parameter to be determined and two phase speeds to use for this purpose at each morphologically similar reach, a simple test of the flow algorithm became possible. Consequently, the low stage friction coefficient was set using Research Flow B so that all of the data from Research Flow D could be used to verify the algorithm. For the preliminary model that is the focus of this report, the strongest confirmation of its validity is its ability to reproduce the travel time trace of the discharge wave for the latter Research Flow.

The wavelength of the discharge wave produced during Research Flow B is approximately 170km and that for Research Flow D is nearly 240km. As a consequence, these waves respond to the average geometry of not one but several morphologically similar reaches at a time, and in order to compare measured and calculated phase speeds, a smaller set of average cross-sections, each containing more of the individually measured cross-sections, had to be constructed. The locations and average properties of these longer reaches are shown in Table IV. In addition, flow calculations for systems of highly variable stage are quite sensitive to bank shape, and it is likely that not enough cross-sections were available to characterize the bank shape as accurately as required in most of the morphologically similar reaches listed in Table II. In any case, a reduction in the number of reaches used in flow calculation was required in order to stabilize the calculations and produce consistent results. For the geometrically defined reaches of Table IV, those upstream of River Mile 140 were treated individually, but the long reach downstream of River Mile 140 was broken into three segments in order to permit the stage and discharge of the trough to adjust properly; therefore, there are five geometrically defined reaches, but

seven *hydraulically characterized reaches*. The cross-sectional profiles for each of these reaches are shown in Figures 12 through 16. The format in these figures is the same as that for Figure 7.

Results of our flow model are presented in Table V for each of the seven hydraulically characterized reaches, and for the entire Lees Ferry to Diamond Creek segment of the River. Using this table all of the important hydraulic parameters can be estimated at any or all of these eight segments for any steady discharge below 35,000cfs ( $846\text{m}^3/\text{s}$ ) at the Glen Canyon Dam. Moreover, even the most extreme diurnal variations in discharge are predominantly quasi steady in their primary reach-average characteristics, and the information presented in this table also is necessary for computation of the salient properties of the daily discharge waves. The salient morphologic and flow properties also are displayed graphically in Figures 17, 18 and 19 for the entire Lees Ferry to Diamond Creek segment of the River.

The results of this preliminary model, as displayed in Table V, are not likely to change drastically but may change somewhat as the inputs to it are improved and as the model is carefully compared to measurements currently being made with the temporary stage gage network. Moreover, the accuracy, reliability, and generality of the model will increase immensely after additional dye studies are carried out, and when accurate topographic data for the riparian corridor of the entire River are made available. Nevertheless, the model as it now stands; (1) demonstrates the feasibility of making the type of flow and, consequently, sediment transport calculations required for relating discharge at the Dam to both clear and subtle downstream effects, thereby enabling sensitive and insightful management of the riparian environment of the Colorado River in the Marble and Grand Canyons, and (2) provides a badly needed means with which researchers can connect detailed field studies of all types to the discharge histories responsible for the physical, chemical and biological phenomena being investigated, and thereby enabling them to relate properly their findings to the operational history of the Glen Canyon Dam. As mentioned above, the present model cannot be used reliably for discharges in excess of 25,500cfs ( $708\text{m}^3/\text{s}$ ) in the upper river and 32,000cfs ( $906\text{m}^3/\text{s}$ ) in the lower river, because the topographic cross-sections did not extend above these levels and there is essentially no topographic information with which to calculate reach-averaged geometric properties above these levels.

## Mechanics of the Discharge Wave

Next it is desirable to examine the unsteady response of the system and for this some theoretical background is necessary. The continuity equation for incompressible flow is

$$\frac{\partial u}{\partial x} + \frac{\partial v}{\partial y} + \frac{\partial w}{\partial z} = 0 \quad (5)$$

where  $u$  is the velocity component in the downstream ( $x$ ) direction,  $v$  is the velocity component in the cross-stream direction, and  $w$  is the velocity component in the near vertical ( $z$ ) direction (that is, perpendicular to the average channel slope). Integrating this equation with respect to  $z$  yields

$$\frac{\partial \langle u \rangle h}{\partial x} + \frac{\partial \langle v \rangle h}{\partial y} = - \frac{\partial h}{\partial t} \quad (6)$$

where  $\langle u \rangle$  is the velocity component in the downstream direction averaged over the flow depth at any point in the river,  $\langle v \rangle$  is the cross-stream velocity component averaged over the flow depth at that point, and  $h$  is the depth at that point. Integrating (6) in the cross-stream direction gives

$$\frac{\partial}{\partial x} \left( \int_{-b/2}^{b/2} \langle u \rangle h \, dy \right) = - \frac{\partial}{\partial t} \int_{-b/2}^{b/2} h \, dy \quad (7a)$$

That is,

$$\frac{\partial Q}{\partial x} = - \frac{\partial A}{\partial t} \quad (7b)$$

where  $A$  is the cross-sectional area of the flow and  $Q$  is the discharge.

If we let  $Q = Q_0 + Q_{\Delta} f(\theta)$  and  $A = A_0 + A_{\Delta} f(\theta)$  where  $Q_0$  represents the discharge of the steady flow at the trough, sometimes called the base flow, and  $A_0$  is the cross-sectional area of this flow

at the site of interest,  $Q_{\Delta}$  is the difference between the maximum and minimum discharges of the discharge wave, and  $A_{\Delta}$  is the change in cross-sectional area corresponding to the change in discharge. The function  $f(\Theta)$  represents the shape of the wave and  $\Theta = \alpha x - \omega t$  where  $\alpha = 2\pi/\lambda$  is the wave number,  $\omega = 2\pi/T$  is the angular frequency,  $\lambda$  is the length of the wave,  $T$  is its period, and  $C = \lambda/T = \omega/\alpha$  is its phase speed. Substituting the expressions for  $Q_{\Delta}$  and  $A_{\Delta}$  into (7b) and solving for  $C$  gives

$$C = \frac{Q_{\Delta}}{A_{\Delta}} = \frac{Q_p - Q_o}{A_p - A_o} \quad (8)$$

where  $Q_p$  is the peak discharge and  $A_p$  is the cross-sectional area of the peak flow. Alternately we can write  $A = bh$  and  $Q = Ubh$  where  $U = U_*B$  and  $U_* = (U_*)_p(h/h_p)^{1/2}$  substitute into (7b) to find

$$C = U_p \left( \frac{h}{h_p} \right)^{1/2} \frac{\left( \left( \frac{3}{2}b + hb' \right) \frac{B}{B_p} + hb \frac{B'}{B_o} \right)}{(b + hb')} \quad (9)$$

where the primes denote differentiation with respect to  $h$  and the variables subscripted with  $p$  denote evaluation at the peak discharge. Equations (8) and (9) both require the wave to remain constant in shape and height, but they also represent first approximations for waves that are changing shape slowly. Equation (9) shows that the discharge wave will deform at least as  $(h/h_p)^{1/2}$  as it propagates, becoming more asymmetrical with distance downstream from its origin.

#### Measured Properties of the Discharge Wave

The temporary stage gage network produces immensely valuable information with regard to the properties of the discharge waves as they propagate from the Glen Canyon Dam to Lake Mead. In this report, however, only the segment between the Dam and Diamond Creek has been investigated in detail because there is no topographic information for the reaches beyond River Mile 225. The amplitudes of the discharge waves vary locally in response to the ever-changing cross-section of the River, but the

wave shape at a given site is more robust. Stage is measured at specific sites so each stage-discharge curve depends on the cross-sectional area at the location of the gage. Moreover, in order to prevent contamination of the data by surface waves, sites typical were selected in pools upstream of rapids, biasing the data set toward wider reaches. Nevertheless, the general trend in discharge wave height with downstream distance for two research flows can be seen clearly in Figure 20. Between the Dam and Furnace Flats the waveheight decreases as the peak moves from the narrow gorge in limestone and well indurated sandstone to the wide sections through the soft Cambrian and PreCambrian sedimentary rocks. The wave height then increases as the wave propagates through the Upper Granite Gorge, and it remains more or less constant until the wave enters the wide reaches downstream of Fern Glen Canyon. Both of the curves representing amplitude as a function of downstream distance display the same structure. The differences are due to environmentally and instrumentally induced drift, and comparison of normalized versions of the two curves provides a good estimate of the precision of the network. Pressure transducers lying on a sandy bed can scour or be partially covered by the fine sediment, whereas pressure transducers lying on bedrock sometimes get moved into deeper water by the flow. These events are made evident by changes in the field calibration of the instrument, but the data in Figure 20 have not yet been corrected for changes in instrument depth or for the cross-sectional profile at the measurement site as compared to that for the morphologically similar reach in which the measurement site is located. The higher curve in this figure represents the height of the discharge wave during the 3,000cfs ( $85\text{m}^3/\text{s}$ ) to 26,000cfs ( $736\text{m}^3/\text{s}$ ) research flow in late May, 1991, and the lower curve represents the height of the discharge wave during Research Flow B in February, 1991. Using Table II one can see the general correspondence between wave height and the reach-averaged geometric properties of the river corridor.

Of particular interest in this report are the shapes of the discharge waves for these February and May research flows. Owing to the initial sparse sampling of the discharge waves by the data recorders, seven of the eight cycles of each research flow were combined. The variance for this procedure was very small, especially when the first wave was omitted from the analysis; therefore, the approach provided a very accurate composite wave shape. Each research flow was preceded by several days of steady 5,000cfs ( $142\text{m}^3/\text{s}$ ) discharge, and typically this had a lower stage than the trough of the 5,000cfs

( $142\text{m}^3/\text{s}$ ) to  $15,000\text{cfs}$  ( $425\text{m}^3/\text{s}$ ) discharge wave at the Dam, that is, the trough discharge increased with downstream location. Consequently the first wave of each research flow sequence had to accommodate this effect, and was a slightly different shape. For the same reason, it also had a slightly lower peak discharge. The mean wave shape for each of the temporary stage gage sites was normalized by its height. These normalized wave shapes were then averaged for all of the sites in each morphologically similar reach. A sequence of three such waves is plotted in Figure 21 for Research Flow B. In this figure the dashed line represents the shape of the wave just downstream from Lees Ferry, the dashed line with double dots represents the shape of the same wave in the vicinity of Phantom Ranch, and the dotted line represents the shape of this discharge wave just upstream of Diamond Creek. Two very important features of the discharge wave field can be observed immediately from this sequence of curves. First, the wave has a much broader top just downstream of the Dam than it does in the Upper Granite Gorge, and its top is broader in the Upper Granite Gorge than it is upstream of Diamond Creek; that is, the duration of the high velocity flow decreases with downstream distance in the discharge wave, reducing both the amount of water and the amount of sediment that can be carried by the wave form. Second, the wave becomes substantially more asymmetrical with downstream distance, the leading edge growing ever steeper, and the trailing edge becoming less steep. The latter is a consequence of both reduction in the duration of the peak flow and the tendency for the wave phase speed to be greater at higher stages as indicated by (9).

A complete sequence of discharge wave shapes is shown in Figure 22 for the morphologically similar reaches between Lees Ferry and Phantom Ranch. Note that the trends of peak flow duration reduction and increasing leading edge steepness of the discharge wave are monotonic. Figure 23 is analogous to Figure 21, but for Research Flow D. The wave shapes for Research Flows B and D are essentially the same in the reach just downstream of Lees Ferry, but the higher wave of Research Flow D transforms even more quickly than that of Research Flow B. This also is clear from Figure 24, which shows the shapes of the discharge waves in the morphologically similar reaches between Lees Ferry and Phantom Ranch. Here one can again see the monotonic trends in reduction of peak discharge duration and leading edge steepening and can note by the greater dispersion of the lines in the upper left-hand

corner of Figure 24 relative to those in the same area on Figure 22, the more rapid transformation of the higher amplitude discharge wave. This also can be seen by comparing the solid and dashed lines in Figure 25, the former being for Research Flow B and the latter being for Research Flow D. Note particularly the very steep leading edge and sharp, almost triangular, crests and troughs for the higher amplitude discharge wave.

As can be seen by visual inspection of any of these figures, all other things being equal, the change in shape of the discharge wave reduces the area under it: Therefore, in order to conserve mass the trough discharge must rise. Also the trailing edge of the first wave extends an ever increasing distance under the wave following it, causing the trough leading the later wave to rise up the back of the former wave. Position of the peak of the discharge wave relative to the preceding trough is displayed graphically in Figure 26 for both research flows, the upper curve being for B and the lower one being for D. Note that the transformation is greatest for the larger wave and in the upper half of the River for both waves. Measured trough stage relative to the stage of the preceding 5,000cfs ( $142\text{m}^3/\text{s}$ ) steady flow is shown in Figure 27 for these two research flows. The more rapid transformation of the higher discharge wave produces a much more rapid rise in trough stage (trough discharge) with downstream distance; that is, the dashed line in Figure 27, which is for Research Flow B, has a smaller upward slope than the dashed line with double dots, which represents trough level stage for Research Flow D. The trough level rises at about the same rate as the wave height decays, thus, when corrected for changes in cross-sectional area, the stage of the peak stays about the same throughout the entire Marble and Grand Canyon segments of the Colorado River. Water discharge varies approximately as the square of the stage, but sediment transport varies with a much higher power of this variable. Much more sediment, therefore, is transported by the peak flow than by lower discharges, and sediment transport rates are forced to reduce with downstream distance as a consequence of this drastic change in wave shape.

Regardless of the shape of the wave released at the Dam, all discharge waves will evolve toward a quasi triangular shape similar to those shown for the reach just upstream of Diamond Creek in Figure 27. Distortion of the shape of the discharge wave released at the Dam is greatest in the reach between the Dam and the Little Colorado River; therefore, the nature of the flow and sediment transport in this

reach can be controlled somewhat by the operation of the Dam. Production of a relatively square wave at the Dam has the disadvantage of causing more erosion of the eddy beaches but the advantage of retaining more sediment in the zone between the Paria and Little Colorado Rivers for the same average daily sediment discharge. In contrast, were a symmetrical triangular wave produced at the Dam, the leading edge would steepen and the trailing edge would flatten, but the change in shape would not create a substantial rise in trough discharge and it would not promote much deposition of sediment in the upstream reaches of Marble Canyon. This type of wave probably would not significantly reduce the rate of downramping in the downstream section of the River, and it might not change the upramping rate very much below Phantom Ranch. Thus it appears that the nature of the discharge wave produced at the Dam has its greatest effect on the flow and sediment transport just downstream of the Dam. Although the wave height decreases substantially between the Dam and Furnace Flats, as shown in Figure 20, the trough stage rises and, in fact, the actual peak stage, as mentioned above, does not decrease substantially in this reach or over the entire river segment.

One of the most easily and most accurately measured flow parameters, when a network of stage gages is available, is wave travel time, from which wave phase speeds can be determined with high accuracy. Wave travel time is an extremely sensitive parameter, and a model that aims to predict this property must be very accurate at any given locality. Errors in roughness and channel cross-section cause errors in flow velocity that often accumulate with downstream distance. Unfortunately stage dependence of the roughness coefficient as discussed in a previous section of this report makes such computations extremely difficult. In the case at hand, this difficulty was circumvented by using discharge wave phase speed to calculate the low-stage roughness coefficient. Wave travel time as a function of River Mile is shown for both Research Flows B and D in Figure 28. In addition, model predictions are displayed by the dashed line and the dashed line with single dots in this figure. Only the average properties can be compared between the measured and calculated travel times because of the reach-averaged nature of the model, and it would be interesting to attempt to predict local variations in wave phase speed, but this must remain undone until detailed topographic information for more of the river corridor becomes available. Examination of Figure 28 indicates that use of dye advection data in

combination with the wave travel time curve for the 5,000cfs ( $142\text{m}^3/\text{s}$ ) to 15,000cfs ( $425\text{m}^3/\text{s}$ ) research flow produces roughness coefficients that can be employed to predict the properties of the even more extreme 3,000cfs ( $85\text{m}^3/\text{s}$ ) to 26,000cfs ( $736\text{m}^3/\text{s}$ ) research flow, indicating that our model can be used with reasonable confidence for unsteady flows that range between about 5,000cfs ( $142\text{m}^3/\text{s}$ ) and 30,000cfs ( $850\text{m}^3/\text{s}$ ). Greater confidence at low discharges could be gained by completion of a dye study at a discharge around 5,000cfs ( $142\text{m}^3/\text{s}$ ), and for discharges above about 30,000cfs ( $850\text{m}^3/\text{s}$ ) little can be said with confidence until the topography of the riparian corridor has been mapped.

### SEDIMENT TRANSPORT

Sediment transport in natural systems typically is complicated by important but difficult to resolve variations in the near-bottom velocity field induced by bed and bank topography. This certainly is the case in the Colorado River between Lake Powell and Lake Mead. Moreover, until the riparian corridor has been mapped properly, an accurate investigation of the intricacies of sand transport in this segment of the River will not be possible. Nevertheless, many important large scale patterns of erosion, transport and deposition can be deduced using the flow model that has been described previously in this report, in conjunction with general geomorphic and sediment transport principles. If the micro-environments are more or less similar in each of the hydraulically characterized reaches, then the gross patterns of erosion and deposition in the river are controlled by the reach to reach variations in velocity and boundary shear stress. As pointed out in the Introduction to this report, the morphology of the Colorado River in the Marble and Grand Canyons is that of a gravel bedded fluvial system. Although sand lenses are the primary focus of this report, they are transient and they rarely modify the geomorphology of the system in any profound manner. Their main manifestation is as patches on the bottom and along the sides of the channel. These patches have some effect on the near-bed flow typically by making the bottom locally smoother, but they generally exist as a consequence of larger scale flow patterns.

The general physical principle that governs erosion and deposition rates in sediment transporting systems is conservation of mass, and it usually is applied in the form of the erosion equation:

$$\frac{\partial z}{\partial t} = -\frac{1}{\epsilon_b} \left( \frac{\partial V_s}{\partial t} + \nabla \cdot \underline{q}_s \right) \quad (10)$$

Here  $z$  is the elevation of the bed,  $\partial z/\partial t$  is the rate of deposition,  $\epsilon_b$  is the concentration of sediment in the bed,  $V_s$  is the volume of sediment per unit area of bed stored in a column of water above the bottom,  $q_s$  is the sediment discharge per unit width, and  $\nabla \cdot \underline{q}_s$  is the divergence of this local sediment discharge. Equation (10) states that rate of deposition is proportional to the rate of loss of sediment from storage in the water column ( $\partial V_s/\partial t$ ), and the rate of removal of sediment from that being transported ( $\nabla \cdot \underline{q}_s$ ). In rivers,  $|\partial V_s/\partial t|$  is typically much less than  $|\nabla \cdot \underline{q}_s|$ , hence (10) simplifies to:

$$\frac{\partial z}{\partial t} = -\frac{1}{\epsilon_b} (\nabla \cdot \underline{q}_s) \quad (11)$$

Reach-averaging (11) yields

$$\left( \frac{\partial z}{\partial t} \right)_{av} = -\frac{1}{\epsilon_b} \frac{\partial Q_s}{\partial x} \quad (12)$$

where  $(\partial z/\partial t)_{av}$  is the reach-averaged rate of deposition,  $Q_s$  is the reach-averaged sediment discharge, and  $x$  is the down-river direction. If the wetted surface of a reach were entirely covered with sand then  $Q_s$  would depend monotonically on the reach-averaged boundary shear stress, and the chain rule could be used to write

$$\left( \frac{\partial z}{\partial t} \right)_{av} = -\frac{1}{\epsilon_b} \frac{\partial Q_s}{\partial \tau_b} \frac{\partial \tau_b}{\partial x} \quad (13)$$

Equations (12) and (13) clearly demonstrate that erosion and deposition are related to downstream changes in sediment discharge which are related, in turn, to downstream changes in flow properties.

From (13) it is clear that in a sand bedded river for which the entire perimeter of the channel is mobile, the dominant geomorphic adjustment to changing boundary shear stress is an adjustment of

channel cross-section until the boundary shear stress becomes constant in the streamwise direction. In contrast, for a system in which sand is distributed in patches over gravel, it is the sediment transport rate and not the boundary shear stress that is adjusted. This is accomplished by changing the area of the river bed covered by sand. On a reach-average scale, suspended sand transport is supported by the presence of sand on the bed. Suspended load transport results from the upward diffusion and downstream advection of sediment and, therefore, it requires the highest concentration of suspended material to be in the immediate vicinity of the bed. This can only be the case if the gravel bed is locally covered with sand. When there is a decrease in sediment flux, deposition expands the area of the bed covered by sand and thereby increases the efflux of material from the depositional site until the sediment discharge becomes constant. This happens quite quickly at high transport rates but very slowly at low transport rates because in the latter situation the sand transport is confined primarily to the sand bedded part of the channel. The rate at which this adjustment occurs when the bed is being eroded also depends on the sediment discharge (namely the rate at which material can be removed), but it also depends on the thickness of the sand deposit on the riverbed (namely the amount that must be eroded). It is this type of adjustment that occurs in the Marble and Grand Canyon segments of the Colorado River.

Equilibrium suspended sand transport also can be computed locally for systems in which the material of interest only partially covers the bed. To do this the bed is first assumed to be floored by a thin layer of sand. In regions of local boundary shear stress divergence (erosion) this layer is soon removed, whereas in areas of boundary shear stress convergence (deposition) it becomes thicker. For an equilibrium system this approach soon evolves sand patches that are the appropriate sizes and are in the appropriate locations for the imposed flow conditions. In natural systems patch structure is often quite complex, and it usually is very difficult with field methods to determine patch locations and patch areas with the accuracy required for usable sediment transport calculations. Therefore, application of this computational approach often is necessary. An appropriate upstream source must be included in all equilibrium calculations. This might be an eroding patch of sand at the mouth of a tributary, a distributed flux from a patchy source or a cross-sectionally averaged flux. Moreover, the input flux might be adjusted to satisfy a measured downstream sediment discharge, as will be done subsequently in

this section. Any increase in the imposed sediment flux will produce deposition in the reach until the influx and efflux are the same and the patch sizes will adjust accordingly. A decrease in it will produce erosion until equilibrium is again attained. Sediment transport varies nonlinearly with boundary shear stress and, therefore, suspended sand fluxes are strongly weighted toward periods of high flow. By calculating the sediment transport rate that would occur in the deepest half of a given channel as a function of time for a complicated hydrograph and then calculating the stage that would produce the same average flux, an effective sediment transporting stage can be estimated for any system with a complicated, time dependent hydrograph. This is best done with a global model, but once this effective stage has been determined, patches can be produced where a deterministic or stochastic representation of the bed topography will place them using a local model. After an appropriate upstream source has been added, such that the patches grow or shrink until an equilibrium pattern is produced, transient calculations can be carried out to determine variations around this long term equilibrium state.

Sediment transport in topographically complex systems, such as the Colorado River, is extremely sensitive to variations in flow and bed topography, and these must be modeled accurately either with a fully deterministic or partly deterministic and partly stochastic model. Small scale roughness is almost always treated stochastically, but larger scale flow patterns often need to be calculated with a multi-dimensional flow algorithm such as the quasi three-dimensional one of Smith and McLean (1984; see also Nelson and Smith 1987). If the bed is coarse and poorly sorted the method of Wiberg and Smith (1991) can be used to good advantage. Moreover, in complicated reaches where the bed roughness is composed of gravel, but sand is moving over it, the method of Wiberg and Smith can and should be combined with the quasi three-dimensional model of Smith and McLean. Use of the appropriate topography for the gravel bed underlying the sand layer permits the drag on protruding roughness elements to be determined so that the near-bed momentum defect can be calculated and the flow in the immediate vicinity of the bed estimated with the accuracy required for proper sediment transport calculations. When investigating longer reaches and segments such as in the present case, a stochastic treatment of channel geometry as well as bed topography, is the most effective approach and that is the procedure that ultimately needs to be taken with regard to sand transport calculations in the

Marble and Grand Canyon reaches of the Colorado River. Unfortunately, this cannot be done at present because the required topographic information has not yet been obtained. Although the tools to carry out accurate sediment transport calculations are available, and the need for such calculations is acute, we do not yet have the basic information to use these powerful methods. Therefore, a simpler and somewhat less accurate approach will be taken in this report.

To avoid the need to know the near-bed velocity field accurately, we shall assume that the sand patches are of moderate lateral extent and that they are connected in the streamwise direction in a manner such that the high relative roughness acts to produce low cross-sectionally averaged and interior velocities, but that the bed over the small sand patches is geometrically smooth. Under these circumstances the vertically integrated velocity over the sand patches in the deepest part of the channel (that is, at the site of the highest local boundary shear stress) in each of the characteristic reaches is given by

$$\langle u \rangle = \bar{u} (h_m/h)^{1/2} \quad (14)$$

where  $h_m$  is the channel centerline depth and  $h$  is the average depth for the cross-section. In a river channel of normal roughness,  $\langle u \rangle$  is the same as the most probable actual velocity about 40% of the local flow depth above the bottom. Combining this relationship with (1) and (14) gives a near-bed velocity field at the center of the channel

$$\bar{u} (h_m/h)^{1/2} = \frac{u_*}{k} \ln \left( \frac{0.40 h_m}{z_0} \right) \quad (15)$$

If we also assume that there is a sand patch with a geometrically smooth surface at this location and that this patch affects the near-bed velocity field but not that in the interior of the water column, because of the extremely high lateral diffusion of momentum in the region well above the boundary, we can find the shear velocity and the boundary shear stress on the sand patch from (15) using the method of Wiberg and

Rubin (1989) to calculate the appropriate  $z_0$  for the sand patch. This local value of  $z_0$  for flow over a geometrically smooth sand patch will be denoted  $(z_0)_s$ .

Once the shear stress on the surface of the sand patch is known, the sand concentration  $(C_a)$  at a precisely prescribed distance  $(z_a)$  from the riverbed can be calculated using an equation first suggested by Smith and McLean (1977) and later modified by Wiberg and Smith (in preparation), namely

$$\epsilon_a = 0.0045 \epsilon_b \left( \frac{C_b}{C_c} - 1 \right) \quad (16a)$$

$$z_a = S_B \quad (16b)$$

In (16),  $\tau_c$  is the critical shear stress for the initiation of sediment motion as given by the Shields diagram (or the initial motion theory of Wiberg and Smith, 1987),  $\epsilon_b$  is the concentration of sediment in the bed, and  $S_B$  is the height to which sediment grains of the size and physical properties of interest would hop if they were in the saltation motion field. Grains being transported in suspension are lifted off a sediment bed by the same forces that produce saltation, and as they rise from the bed they are subjected to small scale pressure gradients resulting from the turbulent flow. If the forces on the grains from the turbulent fluctuations are small relative to the grain weight then the particles will saltate, but if these forces are large relative to the grain weight then some of the grains will be plucked from their trajectories and carried upward and into suspension. A substantial fraction of the flight time of a saltating grain is spent near the top of its trajectory, making this the most probable distance above the riverbed from which non-cohesive sediment grains will be carried into suspension. The height  $S_B$  depends on the dimensionless boundary shear stress (Shields stress,  $\tau_* = \tau_b / (\rho_s - \rho) g D$ , where  $(\rho_s - \rho) g$  is the specific weight of the submerged grain) and the grain diameter ( $D$ ), and it can be calculated using Figure 29. The coefficient in (16a) has been determined from the field data of Smith and McLean (1977a), from the laboratory measurements of Guy and others (1966) and from the saltation theory of Wiberg and Smith (198), so it can be used with considerable confidence.

Above the sediment bed modern suspended sediment transport theory can be employed (see Smith, 1977; Smith and McLean 1977a and 1977b, and Gelfenbaum and Smith, 1986). Using (1) and the diffusion coefficients for momentum that go with these velocity profiles, in conjunction with (16), and an appropriate setting velocity for the material in transit, suspended sand concentration profiles can be calculated, multiplied by the appropriate velocity profile and then integrated over the flow depth to get suspended sand discharge per unit width over the deepest part of the channel. This concentration profile is

$$\frac{e_s}{1-e_s} = \frac{e_a}{1-e_a} \left( \left( \frac{z_a}{z} \right) \left( \frac{1-z/h}{1-z_a/h} \right) \right)^{R_s} \quad z \leq z_b \quad (17a)$$

$$\frac{e_s}{1-e_s} = \frac{e_a}{1-e_a} \left( \left( \frac{z_a}{z_b} \right) \left( \frac{1-z_b/h}{1-z_a/h} \right) \right)^{R_s} \exp\left(-\beta \left( \frac{z}{h} - \frac{z_b}{h} \right)\right) \quad (17b)$$

$z \geq z_b$

where  $z_b = 0.20h_m/p_s = w_s/k(u^*)_s$  is the Rouse number,  $w_s$  is the setting velocity for the sediment, and  $(u^*)_s$  is the value of  $u^*$  calculated from (15).

In the relatively crude suspended sand transport model presented in this report we have calculated the suspended sand flux per unit width, as described above, only for the deepest part of the channel, and then we multiplied this value by the fraction of the perimeter of the channel covered by sand, rather than calculating the unit suspended sand discharge as a function of local depth and integrating this result in the cross-channel direction numerically. Such a procedure does not produce a particularly large error because only a small fraction of the wetted perimeter of the narrow morphologically similar reaches is covered by sand, and in the broader, shallower reaches the flow depth does not vary significantly in the cross-stream direction. Until better topographic information is available a more sophisticated approach probably is not warranted. Moreover, the procedure used here yields a simple, convenient relationship between sediment discharge and fraction of the bed covered by sand.

Suspended sand fluxes increase very rapidly with stage. This is displayed in Figures 30 and 31 for Research Flows B and D respectively. In these figures the shapes of the stage, water discharge, and sediment discharge curves are compared. For Research Flow B the stage and water discharge curves have about the same shape, but the sediment discharge curve is much more peaked. This means that the daily average sediment discharge is much higher for a normal peak power producing flow than it is for a steady flow of the same average water discharge. Figure 31 for Research Flow D displays a greater deviation in the shape of the discharge wave relative to the stage wave and a much more sharply peaked sediment discharge curve, hence, an even higher daily suspended sand discharge for approximately the same average water discharge. In fact, for Research Flow D almost all of the suspended sand transport occurs within 10% of the peak stage. This means that there is a substantial convergence in sediment transport rate as a function of distance downstream from the Dam under normal peak power production conditions, and this wave-transformation-forced-convergence in suspended sand transport causes more deposition of sediment in the upstream most part of Marble Canyon than would be the case under condition of steady suspended sand transport at the same daily average sediment discharge. This also is the case for the same daily water discharge as long as there is excess sand in the bar at the mouth of the Paria River, but the high sediment transport rates associated with high stage peak power production obviously will deplete this source more rapidly than would be the case at lower peak and steady flow stages. A persistent discharge scenario of this type will cause the sand patches on the bed of the river to increase in area, but this in turn will make the reach more susceptible to erosion by transient events of very high stage.

If the riverbed were in equilibrium with the sediment fluxes given by the Grand Canyon (Phantom Ranch) rating curve during Research Flows B and D then 19% and 12% of the bed of the morphologically similar reach in which that gage is located would be covered by sand respectively. If the same percentages of the bed were covered in every hydraulically characterized reach, then the suspended sand discharges for these research flows would be as shown in Figure 33, and if the system were operated in this mode long enough for the sediment discharges to become the same from reach to reach, then the fractions of the beds in each of the hydraulically characterized reaches covered by sand

would be as given in Figure 34. In reality the system is never in equilibrium, but the area of channel bed covered by sand probably varies between these two states depending on the recent operational history of the Dam. The thicknesses of the sand patches control only their rates of decreases in size, and it is very unlikely that there is sufficient sand in the system for it to remain out of equilibrium for more than a decade or so. Furthermore, erosion of thick sand patches on the bed of the river cannot enhance local sand fluxes by enough to have a significant long-term impact on the eddy beaches. These eddy deposits are approximately in equilibrium with the sand deposits on the bed of the channel. Eventually the suspended sand transport rates measured at the National Canyon Cableway will be used to determine the fraction of sand on the bed of the 140 to 169 hydraulically characterized reach. Once this has been done, the reach just upstream of the Grand Cam or gage can be mapped so that the Grand Canyon gage site can be properly calibrated, as was done with the National Canyon gage site in 1991. Then results from the Grand Canyon gage can be compared to those of the model to determine exactly how far out of equilibrium the sediment transport system in the lower canyon has been operating and how closely the Grand Canyon suspended sand rating curve represents equilibrium sand transport conditions in the Canyon.

#### SUMMARY AND CONCLUSIONS

This report presents a careful analysis of field measurements made specifically for the purpose of understanding flow and sediment transport in the Colorado River between Lake Powell and Lake Mead, along with simple, but accurate algorithms for computation of reach-averaged flow and sediment transport under the range of environmental conditions represented by the data. It focuses on that segment of this river and those stages for which topographic information is available. The approach is general, but the necessary input information is limited. When this additional information becomes available, the models will be expanded to cover the reaches below Diamond Creek and stages near and above power plant capacity including those attained during the mid-1980s and in pre-dam times. The present model is not strictly valid for discharges above 26,000cfs ( $736\text{m}^3/\text{s}$ ) in the upper River and for discharges above 32,000cfs ( $907\text{m}^3/\text{s}$ ) in the lower River, but it probably can be extrapolated with some confidence to

present peak-power-production-capacity of the Dam. Dam managers certainly would be remiss, however, in not procuring the information required for extending the models to all pre- and post-dam flows that have affected and will affect the river corridor. Until accurate calculations have been carried out for the flow and sediment transport conditions of the mid-1980's, postulated consequences of these high discharge conditions must be considered speculative. The topographic data required to extend the models to these high discharge conditions are not particularly difficult to procure.

Further tests of the model developed in this paper will be made using data from other research flows, particularly those of July of 1991, and results from analysis of the 3,000cfs ( $85\text{m}^3/\text{s}$ ) to 26,000cfs ( $736\text{m}^3/\text{s}$ ) dye study will be used to test model predictions over this range of conditions. It is important to note that the above stated discharge range is for the Dam and that the trough discharge at Diamond Creek during this research flow never went below about 6,200cfs ( $176\text{m}^3/\text{s}$ ). Only low steady discharges from the Dam produce similarly low discharges at the downstream end of the system. Flow calculations for normal discharge ranges indicate that control over downstream flow and sediment transport is subtle and must be considered in light of accurate global and local flow models. The latter have not been addressed in this report, but currently are being developed for several reaches for which detailed topographic information is available. Eventually, these local models will be spliced together with the global one in order to interpret important field measurements previously made at specific sites; nevertheless, many important consequences of past and proposed flow and the sediment transport scenarios can be evaluated in detail using a reach-averaged model.

From a sediment transport point of view, the results presented in this report are particularly important as they provide a solid foundation on which reliable suspended sand transport computations can be based. Such calculations yield specific predictions about the effects of steady and unsteady flows on redistribution and loss of sand added to the system by the Paria and Little Colorado Rivers, and they clearly demonstrate that some sediment is and will continue to be retained rather effectively in the upper canyon by its geometry. Also they show that sand can be held or redistributed in the upper part of Marble Canyon by the shape of the daily discharge wave that is produced at the Dam. Our results demonstrate that the amount of sand retained in the upper part of the system can be controlled quite

precisely, and that operational strategies for the Dam could be developed to store sand in the upstream part of the system in preparation for high stage beach building flows of reasonable duration. Our results also show that the only major control of upramping rates is through the amplitude of the discharge wave that is produced; high amplitude waves transform more rapidly and produce steeper leading edges. These high amplitude waves also are the ones with the broad trailing edges making it very difficult to alter downramping rates in the lower part of the Canyon. The high amplitude discharge waves transport more sediment than do lower amplitude ones with the same mean daily water discharge, and in the long run this results in a reduction in the amount of sand stored on the bed of the channel.

In conclusion, this paper demonstrates that flow in the Colorado River between the Glen Canyon Dam and Diamond Creek can be calculated under normal conditions with the accuracy required to evaluate reach-averaged sediment transport rates, and to determine the gross redistribution of sediment along the River under various discharge scenarios. We have shown that even a system as complicated as the Colorado River in the Grand Canyon can be understood conceptually, and with appropriate input, can be modeled effectively. Consequently, it can if desired be managed in an environmentally sensitive manner. We also have shown that the sediment transport in this system, as in many others, depends on subtle and sometimes unexpected flow characteristics.

REFERENCES

- Dolan, R., and A. Howard, Structural control of the rapids and pools of the Colorado River in the Grand Canyon, *Science*, 202, 629-631, 1978.
- Gelfenbaum, G., and J. Dungan Smith, Experimental evaluation of a generalized suspended-sediment transport theory, *Canadian Society of Petroleum Geologists, Memoir II*, 133-144, 1986.
- Graf, J. B., Traveltime and longitudinal dispersion at steady and unsteady flows, Colorado River, Glen Canyon Dam to Lake Mead, *Open-File Report*, 92-, 1992.
- Guy, H. P., D. B. Simons, and E. V. Richardson, Summary of alluvial channel data from flume experiments, 1956-1961, *Prof. Paper*, 462-J, 1966.
- Howard, A., and R. Dolan, Geomorphology of the Colorado River in the Grand Canyon, *The Journal of Geology*, 89, 3, 269-298, 1981.
- Nelson, J. M., and J. Dungan Smith, Flow in meandering channels with natural topography, *Am. Geophysical Union, Water Resources Monograph (12), River Meandering*, 69-102, 1987.
- Randle, T. J., and E. L. Pemberton, Results and analysis STARS modeling efforts of the Colorado River in Grand Canyon, *Glen Canyon Environmental Studies*, U.S. Bureau of Reclamation, Salt Lake City, Utah, 1987.
- Schmidt, J. C., and J. B. Graf, Aggradation and degradation of alluvial sand deposits, 1965 to 1986, Colorado River, Grand Canyon National Park, Arizona, *Prof. Paper*, 1493, 1990.
- Smith, J. Dungan, The role of eddies in stream mechanics, *EOS Trans. AGU*, 72, 44, *Fall Meeting Supplement*, 218, 1991.
- Smith, J. Dungan, Erosion at the bed of deeply incised rivers, *Water Resources Research*, in preparation.
- Smith, J. Dungan, and S. R. McLean, Boundary layer adjustments to bottom topography and suspended sediment, *Bottom Turbulence*, Elsevier Scientific Publishing Company, The Netherlands, 123-151, 1977.
- Smith, J. Dungan, and S. R. McLean, Spatially averaged flow over a wavy surface, *J. of Geophysical Research*, 82, 12, 1735-1746, 1977.
- Smith, J. Dungan, and S. R. McLean, A model for flow in meandering streams, *Water Resources Research*, 20, 9, 1301-1315, 1984.
- Stevens, L., *The Colorado River in Grand Canyon, A Guide*, Red Lake Books, Arizona, 1983.
- Webb, R. H., A century of environmental change in Grand Canyon, *University of Arizona Press*, in preparation.
- Webb, R. H., J. C. Schmidt, and T. S. Melis, Inter-relation among debris fans, sand bars, and the Colorado River in Grand Canyon, *J. of Geology*, in preparation.
- Wiberg, P. L., and D. M. Rubin, Bed roughness produced by saltating sediment, *J. of Geophysics Research*, 94, C4, 5011-5016, 1989.
- Wiberg, P. L., and J. Dungan Smith, A theoretical model for saltating grains in water, *J. of Geophysical Research*, 90, C4, 7341-7354, 1985.
- Wiberg, P. L., and J. Dungan Smith, Calculations of the critical shear stress for motion of uniform and heterogeneous sediments, *Water Resources Research*, 23, 8, 1471-1480, 1987.
- Wiberg, P. L., and J. Dungan Smith, Model for calculating bed load transport of sediment, *J. of Hydraulic Engineering*, 115, 1, 101-123, 1989.
- Wiberg, P. L., and J. Dungan Smith, Velocity distribution and bed roughness in high-gradient streams, *Water Resources Research*, 27, 5, 825-838, 1991.
- Wiele, S., and J. Dungan Smith, Modeling of flow in large rapids, *Water Resources Research*, in preparation.
- Wilson, R. P., Sonar patterns of Colorado riverbed, Grand Canyon, *Fourth Federal Interagency Sedimentation Conference*, 2, Las Vegas, Nevada, 1986.

TABLE I

River Level Rock Types in the *Morphologically Similar Reaches*

Span of Reach (River Miles)	Span of Reach (River Kilometers)	Dominant Rock Types
0 - 11	0 - 18	Mixed Permian Rocks
0.8 - 1.5	1.3 - 2.4	Kaibab Limestone
1.5 - 3.8	2.4 - 6.2	Toroweap Limestone
3.8 - 5.5	6.2 - 9.0	Coconino Sandstone
5.5 - 11.2	9.0 - 18.0	Hermit Shale
11 - 23	18 - 37	Pennsylvanian Clastic Rocks (Supai Group)
23 - 50	37 - 81	Mid and Lower Paleozoic Limestones
23.2 - 33.9	37.4 - 54.5	Redwall Limestone
33.9 - 48.8	54.5 - 78.8	Muav Limestone
50 - 77	81 - 125	Cambrian & PreCambrian Sedimentary Rocks
48.8 - 59.3	78.8 - 95.5	Bright Angel Shale
59.3 - 63.3	95.5 - 101.8	Tapeats Sandstone
63.3 - 77.4	101.8 - 124.8	Unkar Group
77 - 107	125 - 172	PreCambrian Metamorphic Rocks (Vishnu Schist and Zoroaster Granite)
107 - 117	172 - 189	Mixed PreCambrian Rocks
106.7 - 109.6	171.8 - 176.4	Unkar Group
109.6 - 117.3	176.4 - 188.8	Vishnu Schist
117 - 140	189 - 225	Basal Cambrian & Mixed PreCambrian Rocks
117.3 - 127.1	188.8 - 204.5	Tapeats Sandstone
127.1 - 130.7	204.5 - 210.3	Vishnu Schist
130.7 - 137.5	210.3 - 221.3	Bass Limestone
137.5 - 139.7	221.3 - 224.8	Tapeats Sandstone
140 - 169	225 - 272	Cambrian Limestone (Muav Formation)
169 - 190	272 - 306	Cambrian Clastic Rocks
169.1 - 176.6	272.1 - 284.2	Bright Angel Shale
176.6 - 178.8	284.2 - 287.7	Tapeats Sandstone
178.8 - 190.1	287.7 - 305.9	Lava over Cambrian Rocks
190 - 225	306 - 362	Basal Cambrian & PreCambrian Metamorphic Rocks
190.1 - 207.8	305.9 - 334.4	Tapeats Sandstone over Vishnu Schist
207.8 - 225.0	334.4 - 362.4	Vishnu Schist

TABLE II  
 Geometric Properties of the Morphologically Similar Reaches

In the table below,  $b$  denotes surface width in meters,  $A$  denotes cross-sectional area in square meters, and  $Q$  denotes the discharge in cubic meters per second at the time the measurements were made in each of the reaches delineated in Table I. In addition, an over bar denotes a reach averaged property and  $s$  denotes standard deviation of the subscript variable in the appropriate units. The data are from cross-sections measured every mile between Lees Ferry and Diamond Creek by Richard Wilson. Although the discharge was not constant during the Wilson study, it did not vary drastically and the data in this table provide a reasonable estimate of the geometrical characteristics of the *Morphologically Similar Reaches* at a stage of 28,000cfs ( $791 \text{ m}^3/\text{s}$ ) or so, the degree to which these variables are resolved, and their variability.

Reach (RM)	Reach (km)	$b$	$s_b$	$s_b/b$	$A$	$s_A$	$s_A/A$	$A/b$	$Q$
0 - 11	0 - 18	87.4	5.96	.068	599	23.0	.038	7.11	807
11 - 23	18 - 37	63.1	2.74	.043	520	19.5	.038	8.44	807
23 - 50	37 - 81	85.6	4.63	.054	558	25.8	.046	6.86	755
50 - 77	81 - 125	113.3	6.06	.053	592	27.7	.047	5.43	731
77 - 107	125 - 172	60.8	3.61	.059	524	34.0	.065	8.63	722
107 - 117	172 - 189	58.7	4.99	.085	469	71.0	.151	7.75	730
117 - 140	189 - 225	69.1	3.74	.054	518	31.5	.061	7.73	757
140 - 169	225 - 272	67.1	3.17	.047	457	20.6	.045	6.91	836
169 - 190	272 - 306	105.9	7.56	.071	613	47.9	.078	5.90	903
190 - 225	306 - 362	95.7	4.62	.048	645	32.1	.050	7.10	903

**T A B L E I I I**  
 Geometric and Hydraulic Properties of the Morphologically Similar Reaches at a nominal 15,000cfs  
 (42.5m<sup>3</sup>/s) and at the Average Discharge at which Wilson Made his Measurements in Each of These  
 Reaches.

	Discharge (cfs)	Discharge (m <sup>3</sup> /s)	Velocity (m/s)	Shear Velocity (m/s)	Area (m <sup>2</sup> )	Center Depth (m)	Average Depth (m)	Top Width (m)	Hyd Rad (m)	Wetted Per (m)	Friction Coef
0-11	15,000	425	0.87	0.29	488.5	7.97	5.80	84.2	5.63	43.41	3.00
0-11	28,605	810	1.29	0.32	632.9	9.64	7.20	87.6	6.88	91.65	4.09
11-23	15,000	425	0.87	0.33	488.5	11.63	7.95	61.4	7.27	33.60	2.64
11-23	28,605	810	1.45	0.34	558.3	12.68	8.66	63.9	7.85	70.46	4.50
23-50	15,000	425	0.81	0.26	524.7	8.45	6.28	83.5	6.06	43.32	3.11
23-50	26,733	757	1.28	0.27	598.7	9.30	6.94	85.9	6.66	89.58	4.75
50-77	15,185	430	0.94	0.27	457.4	5.05	4.18	109.5	4.12	55.45	3.48
50-77	25,886	733	1.13	0.31	652.4	6.77	5.63	115.7	5.52	117.96	3.62
77-107	15,291	433	0.97	0.37	446.4	10.74	7.67	58.2	6.98	31.97	2.64
77-107	25,568	724	1.39	0.39	528.7	12.11	8.67	60.9	7.78	67.81	3.56
107-117	15,291	433	0.97	0.37	446.4	10.10	7.62	58.6	6.87	32.47	2.65
107-117	25,850	732	1.62	0.37	454.3	10.24	7.74	58.7	6.96	65.22	4.37
117-140	15,291	433	1.08	0.32	400.9	8.42	6.30	63.7	5.94	33.72	3.39
117-140	26,804	759	1.42	0.35	535.0	10.43	7.74	69.1	7.20	74.22	4.06
140-176	15,327	434	1.08	0.26	401.9	8.82	6.22	64.6	5.89	34.10	4.17
140-176	29,594	838	1.72	0.28	493.7	10.14	7.16	68.1	6.71	72.53	6.64
176-190	15,397	436	1.08	0.22	403.7	5.49	4.09	98.6	4.04	50.00	4.84
176-190	31,995	906	1.46	0.27	624.5	7.65	5.90	105.9	5.76	108.45	5.43
190-225	15,291	433	1.06	0.24	408.5	5.25	4.57	89.4	4.45	45.88	4.40
190-225	31,995	906	1.35	0.30	678.6	8.18	7.15	94.9	6.80	99.77	4.26

T A B L E I V  
 Geometric Properties of the Morphologically Similar Reaches

In order to improve resolution of the bank topography for discharge wave phase speed calculations several adjacent Morphologically Similar Reaches had to be combined. This was done only for cases in which the discharges were similar at the times the measurements were made. The geometric properties of these combined reaches are presented in the table below, in which b denotes surface width in meters, A denotes cross-sectional area in square meters, and Q denotes the average discharge in cubic meters per second at the time the measurements were made. In addition, an over bar denotes a reach averaged property and s denotes standard deviation of the subscript variable in the appropriate units. The data are from cross-sections measured approximately every mile between Lees Ferry and Diamond Creek by Richard Wilson.

Reach (RM)	Reach (km)	b	s <sub>b</sub>	s <sub>p/b</sub>	A	s <sub>A</sub>	s <sub>A/A</sub>	A/b	Q
0 - 23	0 - 37	74.7	4.01	.054	558	17.0	.030	7.47	807
23 - 77	37 - 125	99.4	4.31	.043	575	19.1	.033	5.78	743
77 - 107	125 - 172	60.8	3.61	.059	524	34.0	.065	8.62	722
107 - 140	172 - 225	65.6	3.14	.048	502	31.9	.064	7.65	743
140 - 225	225 - 362	83.7	3.19	.038	553	20.4	.037	6.61	877

T A B L E V  
 Geometric and Hydraulic Properties of the seven *Hydraulically Characterized Reaches* at  
 Various Discharges and for the segment of the River between Lees Ferry and Diamond Creek

*Hydraulically Characterized Reach, 0 - 23*

Discharge (cfs)	Discharge (m <sup>3</sup> /s)	Velocity (m/s)	Shear Velocity (m/s)	Area (m <sup>2</sup> )	Center Depth (m)	Average Depth (m)	Top Width (m)	Hydraulic Radius (m)	Wetted Perimeter (m)	Friction Coefficient
2500	70.8	0.4417	0.2105	160.2	4.535	3.031	52.84	2.970	53.93	2.100
5000	141.6	0.5270	0.2513	268.7	6.426	4.349	61.77	4.222	63.63	2.100
7500	212.4	0.6308	0.2713	336.5	7.489	5.130	65.60	4.948	68.01	2.324
10000	283.2	0.7202	0.2867	393.1	8.335	5.763	68.20	5.527	71.11	2.509
12500	354.0	0.7985	0.2992	443.1	9.058	6.306	70.27	6.017	73.64	2.667
15000	424.8	0.8706	0.3102	487.7	9.684	6.783	71.90	6.443	75.69	2.810
17500	495.5	0.9751	0.3148	508.4	9.971	6.998	72.64	6.635	76.63	3.099
20000	566.3	1.0739	0.3189	527.3	10.230	7.192	73.31	6.806	77.48	3.372
22500	637.1	1.1686	0.3227	545.2	10.473	7.373	73.94	6.965	78.27	3.626
25000	707.9	1.2611	0.3262	561.3	10.689	7.554	74.29	7.119	78.83	3.871
27500	778.7	1.3309	0.3310	585.1	11.007	7.818	74.79	7.342	79.64	4.022
30000	849.5	1.3665	0.3346	612.1	11.321	8.041	75.49	7.525	80.58	4.077
32500	920.3	1.3949	0.3375	634.2	11.578	8.223	76.05	7.676	81.34	4.115
35000	991.1	1.4233	0.3404	656.3	11.836	8.406	76.62	7.827	82.11	4.152

PROVISIONAL DRAFT  
 Subject to Revision  
 DO NOT QUOTE OR RELEASE  
 Pending Approval by Director  
 U.S. Geological Survey

*Hydraulically Characterized Reach, 23 - 77*

Discharge (cfs)	Discharge (m <sup>3</sup> /s)	Velocity (m/s)	Shear Velocity (m/s)	Area (m <sup>2</sup> )	Center Depth (m)	Average Depth (m)	Top Width (m)	Hydraulic Radius (m)	Wetted Perimeter (m)	Friction Coefficient
2500	70.8	0.3677	0.1842	192.3	3.253	2.361	81.47	2.349	81.90	2.000
5000	141.6	0.4473	0.2239	316.5	4.684	3.506	90.26	3.470	91.18	2.000
7500	212.4	0.5723	0.2390	371.3	5.284	4.019	92.37	3.965	93.62	2.392
10000	283.2	0.6851	0.2499	413.1	5.733	4.403	93.83	4.333	95.33	2.742
12500	354.0	0.7865	0.2588	449.8	6.122	4.730	95.08	4.646	96.80	3.040
15000	424.8	0.8792	0.2667	482.9	6.468	5.020	96.18	4.922	98.11	3.301
17500	495.5	0.9553	0.2744	518.7	6.838	5.327	97.37	5.213	99.50	3.484
20000	566.3	1.0259	0.2814	552.2	7.180	5.608	98.46	5.478	100.79	3.649
22500	637.1	1.0919	0.2870	583.6	7.497	5.866	99.47	5.722	101.99	3.801
25000	707.9	1.1547	0.2932	613.3	7.794	6.106	100.42	5.947	103.11	3.942
27500	778.7	1.1975	0.2972	639.4	8.038	6.296	101.21	6.123	104.03	4.025
30000	849.5	1.2224	0.2996	661.4	8.226	6.433	101.81	6.248	104.74	4.059
32500	920.3	1.2473	0.3021	683.3	8.414	6.570	102.41	6.373	105.45	4.094
35000	991.1	1.2722	0.3046	705.3	8.602	6.707	103.01	6.498	106.16	4.129

Hydraulically Characterized Reach, 77 - 107

Discharge (cfs)	Discharge (m <sup>3</sup> /s)	Velocity (m/s)	Shear Velocity (m/s)	Area (m <sup>2</sup> )	Center Depth (m)	Average Depth (m)	Top Width (m)	Hydraulic Radius (m)	Wetted Perimeter (m)	Friction Coefficient
2500	70.8	0.5393	0.1738	131.3	4.137	2.707	48.52	2.656	49.45	3.100
5000	141.6	0.6450	0.2083	219.6	5.811	3.914	56.10	3.802	57.75	3.100
7500	212.4	0.7574	0.2272	280.2	6.862	4.719	59.37	4.546	61.64	3.332
10000	283.2	0.8784	0.2391	322.4	7.560	5.258	61.32	5.035	64.03	3.669
12500	354.0	0.9843	0.2493	359.6	8.159	5.718	62.89	5.447	66.01	3.954
15000	424.8	1.0810	0.2572	392.8	8.681	6.112	64.26	5.799	67.73	4.210
17500	495.5	1.2175	0.2600	406.9	8.901	6.276	64.83	5.945	68.45	4.682
20000	566.3	1.3496	0.2630	419.7	9.096	6.422	65.35	6.073	69.10	5.133
22500	637.1	1.4753	0.2655	431.8	9.282	6.559	65.83	6.194	69.71	5.557
25000	707.9	1.5960	0.2680	443.5	9.458	6.689	66.30	6.309	70.29	5.957
27500	778.7	1.6788	0.2720	463.9	9.762	6.911	67.09	6.503	71.29	6.170
30000	849.5	1.7235	0.2763	491.3	10.106	7.141	67.99	6.699	72.43	6.242
32500	920.3	1.7527	0.2787	511.0	10.352	7.304	68.64	6.837	73.24	6.280
35000	991.1	1.7819	0.2812	530.7	10.597	7.467	69.28	6.975	74.05	6.318

PROVISIONAL DRAFT  
 Subject to Revision  
 DO NOT QUOTE OR RELEASE  
 Pending Approval by Director  
 U.S. Geological Survey

Hydraulically Characterized Reach, 107 - 140

Discharge (cfs)	Discharge (m**3/s)	Velocity (m/s)	Shear Velocity (m/s)	Area (m**2)	Center Depth (m)	Average Depth (m)	Top Width (m)	Hydraulic Radius (m)	Wetted Perimeter (m)	Friction Coefficient
2500	70.8	0.4008	0.2678	176.5	5.585	3.857	45.76	3.700	47.70	1.500
5000	141.6	0.4800	0.3200	295.0	7.993	5.671	52.00	5.299	55.66	1.500
7500	212.4	0.6190	0.3366	343.3	8.904	6.340	54.14	5.871	58.47	1.837
10000	283.2	0.7489	0.3480	378.3	9.542	6.808	55.56	6.265	60.37	2.152
12500	354.0	0.8642	0.3574	409.5	10.097	7.211	56.78	6.601	62.03	2.420
15000	424.8	0.9701	0.3650	438.0	10.595	7.568	57.88	6.896	63.51	2.656
17500	495.5	1.0753	0.3710	460.9	10.987	7.844	58.75	7.125	64.68	2.897
20000	566.3	1.1739	0.3765	482.4	11.350	8.099	59.56	7.334	65.77	3.118
22500	637.1	1.2687	0.3815	502.2	11.681	8.342	60.19	7.530	66.68	3.326
25000	707.9	1.3595	0.3861	520.6	11.986	8.577	60.70	7.715	67.48	3.521
27500	778.7	1.4131	0.3901	541.8	12.296	8.790	61.29	7.879	68.33	3.617
30000	849.5	1.4455	0.3936	564.0	12.610	8.999	61.90	8.040	69.21	3.657
32500	920.3	1.4779	0.3971	586.2	12.924	9.209	62.52	8.200	70.09	3.696
35000	991.1	1.5102	0.4006	608.4	13.239	9.418	63.14	8.361	70.98	3.736

PROVISIONAL DRAFT  
 Subject to Revision  
 DO NOT QUOTE OR RELEASE  
 Pending Approval by Director  
 U.S. Geological Survey

Hydraulically Characterized Reach, 140 - 169

Discharge (cfs)	Discharge (m <sup>3</sup> /s)	Velocity (m/s)	Shear Velocity (m/s)	Area (m <sup>2</sup> )	Center Depth (m)	Average Depth (m)	Top Width (m)	Hydraulic Radius (m)	Wetted Perimeter (m)	Friction Coefficient
2500	70.8	0.3932	0.1636	180.2	3.115	2.060	87.45	2.053	87.77	2.400
5000	141.6	0.4814	0.2003	294.3	4.357	3.105	94.79	3.079	95.57	2.400
7500	212.4	0.5964	0.2176	355.8	4.998	3.669	96.96	3.627	98.09	2.743
10000	283.2	0.7546	0.2224	375.0	5.196	3.841	97.62	3.793	98.86	3.394
12500	354.0	0.9013	0.2266	392.5	5.374	3.996	98.22	3.941	99.56	3.976
15000	424.8	1.0371	0.2308	409.6	5.547	4.144	98.80	4.085	100.24	4.492
17500	495.5	1.1119	0.2394	445.6	5.910	4.454	100.02	4.383	101.66	4.650
20000	566.3	1.1788	0.2467	480.4	6.255	4.747	101.18	4.663	103.01	4.780
22500	637.1	1.2415	0.2535	513.2	6.578	5.018	102.27	4.921	104.27	4.899
25000	707.9	1.3007	0.2591	544.4	6.882	5.270	103.29	5.162	105.46	5.010
27500	778.7	1.3562	0.2653	574.2	7.169	5.507	104.25	5.387	106.58	5.115
30000	849.5	1.4088	0.2703	602.9	7.444	5.732	105.18	5.600	107.65	5.212
32500	920.3	1.4573	0.2750	631.3	7.704	5.941	106.05	5.797	108.67	5.299
35000	991.1	1.4804	0.2771	650.5	7.860	6.057	106.58	5.903	109.29	5.329

PROVISIONAL DRAFT  
 Subject to Revision  
 DO NOT QUOTE OR RELEASE  
 Pending Approval by Director  
 U.S. Geological Survey

Hydraulically Characterized Reach, 169 - 190

Discharge (cfs)	Discharge (m <sup>3</sup> /s)	Velocity (m/s)	Shear Velocity (m/s)	Area (m <sup>2</sup> )	Center Depth (m)	Average Depth (m)	Top Width (m)	Hydraulic Radius (m)	Wetted Perimeter (m)	Friction Coefficient
2500	70.8	0.4084	0.2474	173.4	4.695	3.436	50.45	3.339	51.91	1.650
5000	141.6	0.4904	0.2974	288.7	6.830	5.042	57.27	4.814	59.97	1.650
7500	212.4	0.6367	0.3129	333.6	7.599	5.617	59.38	5.329	62.58	2.036
10000	283.2	0.7809	0.3216	362.6	8.082	5.972	60.71	5.645	64.23	2.427
12500	354.0	0.9106	0.3294	388.7	8.507	6.280	61.88	5.918	65.67	2.764
15000	424.8	1.0292	0.3365	412.6	8.891	6.556	62.94	6.160	66.98	3.062
17500	495.5	1.1339	0.3426	437.1	9.276	6.829	64.00	6.400	68.29	3.309
20000	566.3	1.2328	0.3482	459.4	9.623	7.088	64.81	6.623	69.36	3.537
22500	637.1	1.3292	0.3540	479.3	9.928	7.350	65.19	6.835	70.08	3.754
25000	707.9	1.4225	0.3595	497.7	10.210	7.602	65.46	7.036	70.71	3.959
27500	778.7	1.4845	0.3641	519.3	10.517	7.849	65.90	7.231	71.47	4.074
30000	849.5	1.5171	0.3674	539.5	10.788	8.045	66.39	7.384	72.20	4.114
32500	920.3	1.5498	0.3707	559.8	11.060	8.242	66.88	7.538	72.94	4.153
35000	991.1	1.5824	0.3740	580.1	11.332	8.439	67.37	7.691	73.67	4.193

PROVISIONAL DRAFT  
 Subject to Revision  
 DO NOT QUOTE OR RELEASE  
 Pending Approval by Director  
 U.S. Geological Survey

*Hydraulically Characterized Reach, 190 - 225*

Discharge q(cfs)	Discharge q(m <sup>3</sup> /s)	Velocity (m/s)	Shear Velocity (m/s)	Area (m <sup>2</sup> )	Center Depth (m)	Average Depth (m)	Top Width (m)	Hydraulic Radius (m)	Wetted Perimeter (m)	Friction Coefficient
2500	70.8	0.4156	0.1597	170.4	2.487	2.077	82.04	2.065	82.48	2.600
5000	141.6	0.5135	0.1978	275.6	3.736	3.201	86.08	3.158	87.24	2.600
7500	212.4	0.6358	0.2149	333.9	4.407	3.809	87.64	3.738	89.30	2.959
10000	283.2	0.7856	0.2219	360.3	4.706	4.079	88.29	3.994	90.18	3.537
12500	354.0	0.9229	0.2282	383.5	4.969	4.316	88.85	4.217	90.95	4.042
15000	424.8	1.0485	0.2334	405.2	5.212	4.533	89.36	4.420	91.66	4.484
17500	495.5	1.0959	0.2448	452.2	5.734	5.000	90.42	4.853	93.15	4.474
20000	566.3	1.1366	0.2551	498.2	6.240	5.452	91.36	5.269	94.53	4.455
22500	637.1	1.1736	0.2642	542.8	6.726	5.884	92.25	5.662	95.84	4.437
25000	707.9	1.2074	0.2729	586.4	7.197	6.297	93.11	6.036	97.12	4.419
27500	778.7	1.2523	0.2801	622.0	7.578	6.630	93.81	6.336	98.15	4.474
30000	849.5	1.3034	0.2853	651.8	7.895	6.905	94.38	6.583	99.01	4.569
32500	920.3	1.3499	0.2902	680.2	8.192	7.161	94.93	6.810	99.81	4.653
35000	991.1	1.3746	0.2925	700.7	8.389	7.319	95.29	6.943	100.34	4.687

**PROVISIONAL DRAFT**  
 Subject to Revision  
 DO NOT QUOTE OR RELEASE  
 Pending Approval by Director  
 U.S. Geological Survey

Lees Ferry to Diamond Creek

Discharge (cfs)	Discharge (m**3/s)	Velocity (m/s)	Shear Velocity (m/s)	Area (m**2)	Center Depth (m)	Average Depth (m)	Top Width (m)	Hydraulic Radius (m)	Wetted Perimeter (m)	Friction Coefficient
2500	70.8	0.3969	0.2036	178.1	4.015	2.819	63.18	2.785	63.94	1.950
5000	141.6	0.4796	0.2456	295.2	5.746	4.141	71.29	4.056	72.79	1.950
7500	212.4	0.6182	0.2608	343.6	6.414	4.681	73.40	4.564	75.28	2.369
10000	283.2	0.7543	0.2700	375.5	6.845	5.032	74.61	4.891	76.76	2.792
12500	354.0	0.8766	0.2777	403.7	7.220	5.337	75.63	5.173	78.03	3.157
15000	424.8	0.9888	0.2844	429.6	7.560	5.612	76.53	5.426	79.17	3.476
17500	495.5	1.0695	0.2926	463.2	7.997	5.963	77.67	5.746	80.60	3.654
20000	566.3	1.1444	0.3003	494.9	8.402	6.288	78.71	6.042	81.91	3.812
22500	637.1	1.2142	0.3066	524.8	8.780	6.587	79.68	6.312	83.14	3.957
25000	707.9	1.2803	0.3124	553.0	9.132	6.866	80.54	6.563	84.25	4.092
27500	778.7	1.3396	0.3192	581.2	9.480	7.154	81.23	6.818	85.24	4.202
30000	849.5	1.3749	0.3229	605.1	9.746	7.355	81.83	6.991	86.04	4.255
32500	920.3	1.4026	0.3256	626.3	9.974	7.520	82.36	7.132	86.74	4.292
35000	991.1	1.4303	0.3283	647.5	10.201	7.685	82.90	7.272	87.44	4.328

PROVISIONAL DRAIN  
 Subject to Revision  
 DO NOT QUOTE OR RELEASE  
 Pending Approval by Director  
 U.S. Geological Survey

**PROVISIONAL DRAFT**  
 Subject to Revision  
**DO NOT QUOTE OR RELEASE**  
 Pending Approval by Director  
 U.S. Geological Survey

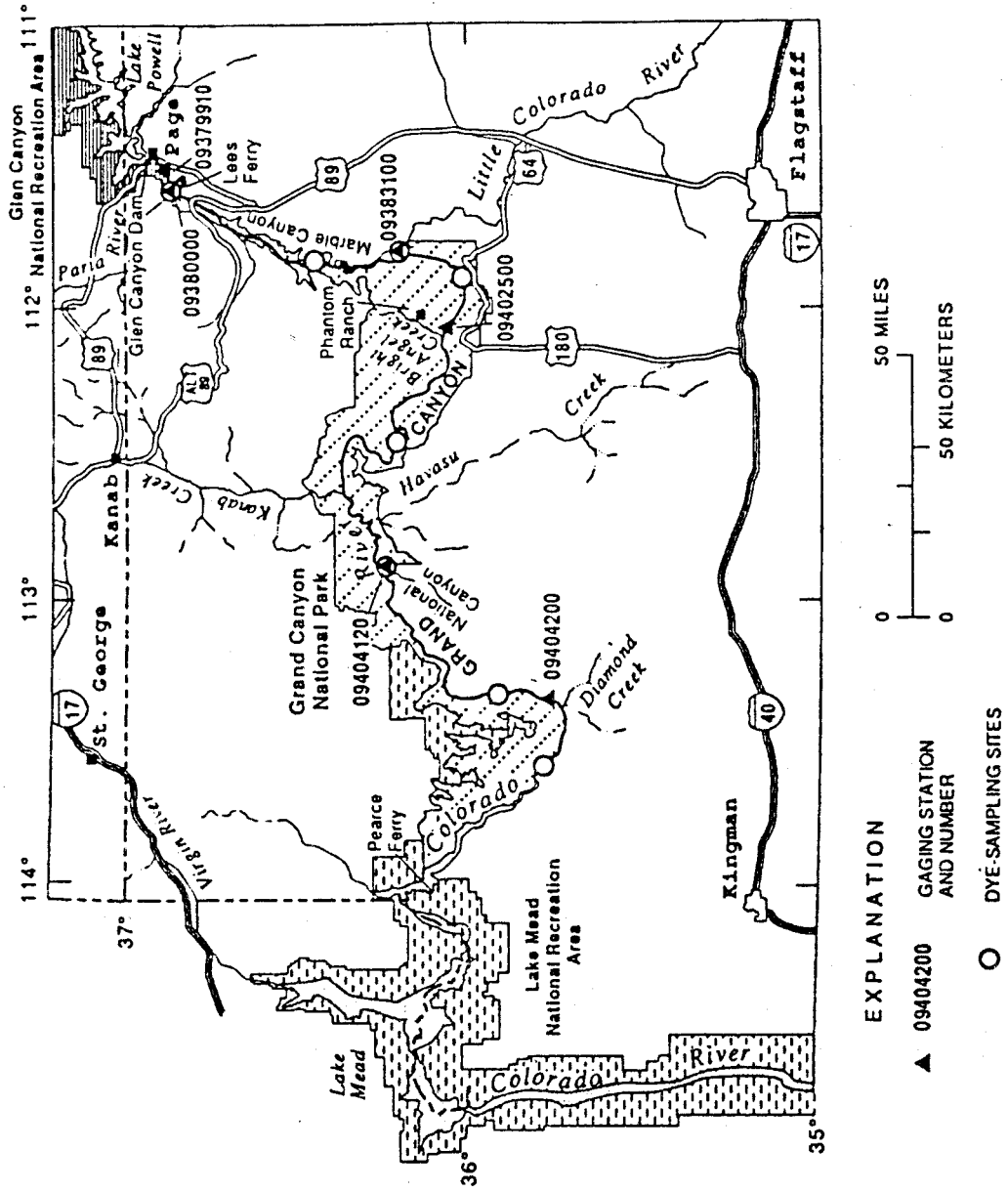
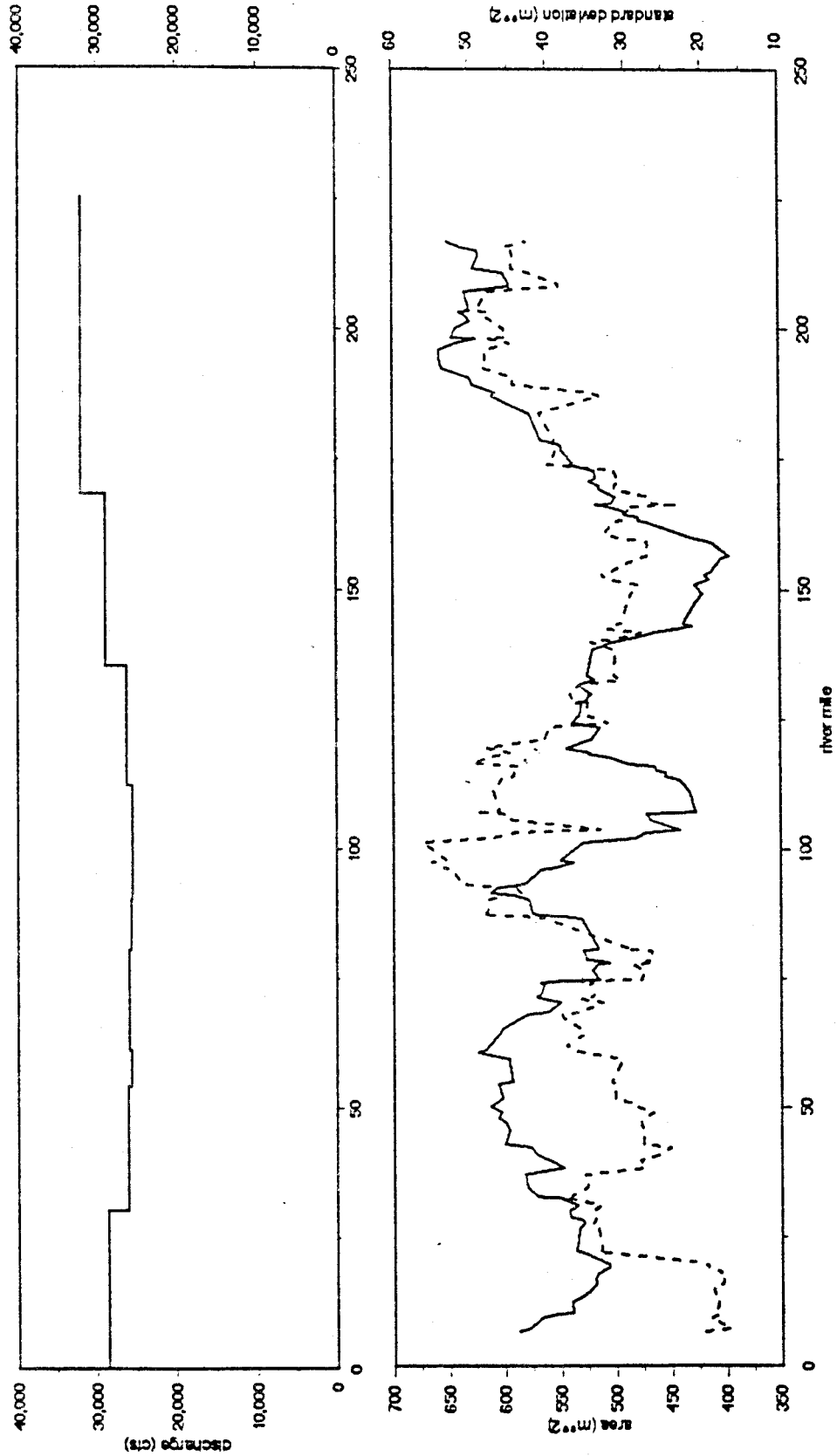
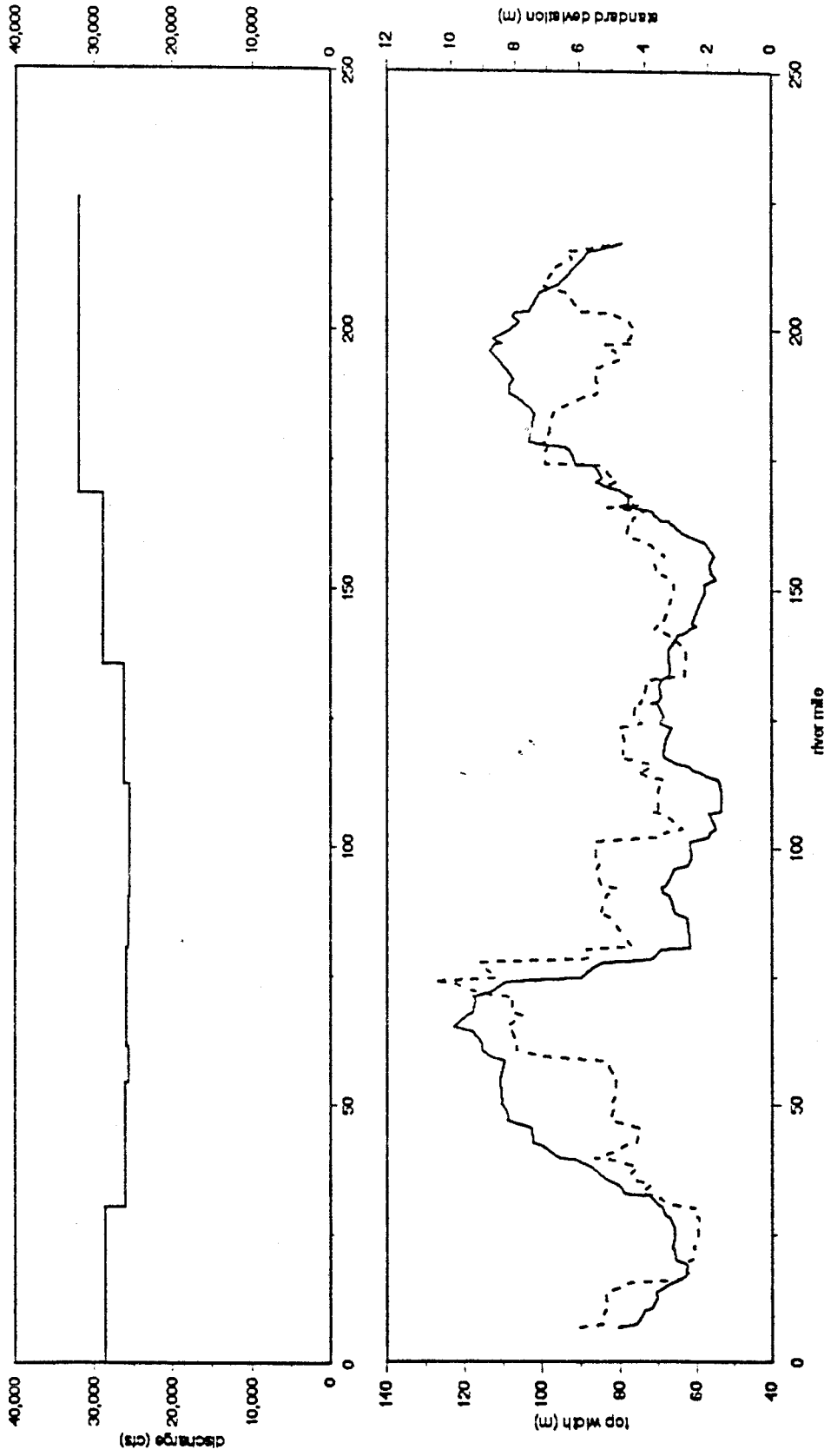


Figure 1: Map of the Colorado River through the Marble and Grand Canyons (from Graf, 1992).



**Figure 3:** Running mean (solid line) and running standard deviation (dashed line) for the cross-sectional area of the Colorado River between 25,000cfs ( $708\text{m}^3/\text{s}$ ) and 32,000cfs ( $907\text{m}^3/\text{s}$ ) as a function of River Mile. The data are from cross-sections measured approximately every mile along the River between Lees Ferry and Diamond Creek by Richard Wilson. The estimated discharge corresponding with the time and location of each group of measurements is indicated by the dotted line at the top of the figure. Note the blocky structure of these 15 point running means.

**PROVISIONAL DRAFT**  
 Subject to Revision  
 DO NOT QUOTE OR RELEASE  
 Pending Approval by Director  
 U.S. Geological Survey



**Figure 2:** Running mean (solid line) and running standard deviation (dashed line) for the surface width of the Colorado River between 25,000cfs ( $708\text{m}^3/\text{s}$ ) and 32,000cfs ( $907\text{m}^3/\text{s}$ ) as a function of River Mile. The data are from cross-sections measured approximately every mile along the River between Lees Ferry and Diamond Creek by Richard Wilson. The estimated discharge corresponding with the time and location of each group of measurements is indicated by the dotted line at the top of the figure. Note the blocky structure of these 15-point running means.

**PROVISIONAL DRAFT**  
 Subject to Revision  
 DO NOT QUOTE OR RELEASE  
 Pending Approval by Director  
 U.S. Geological Survey

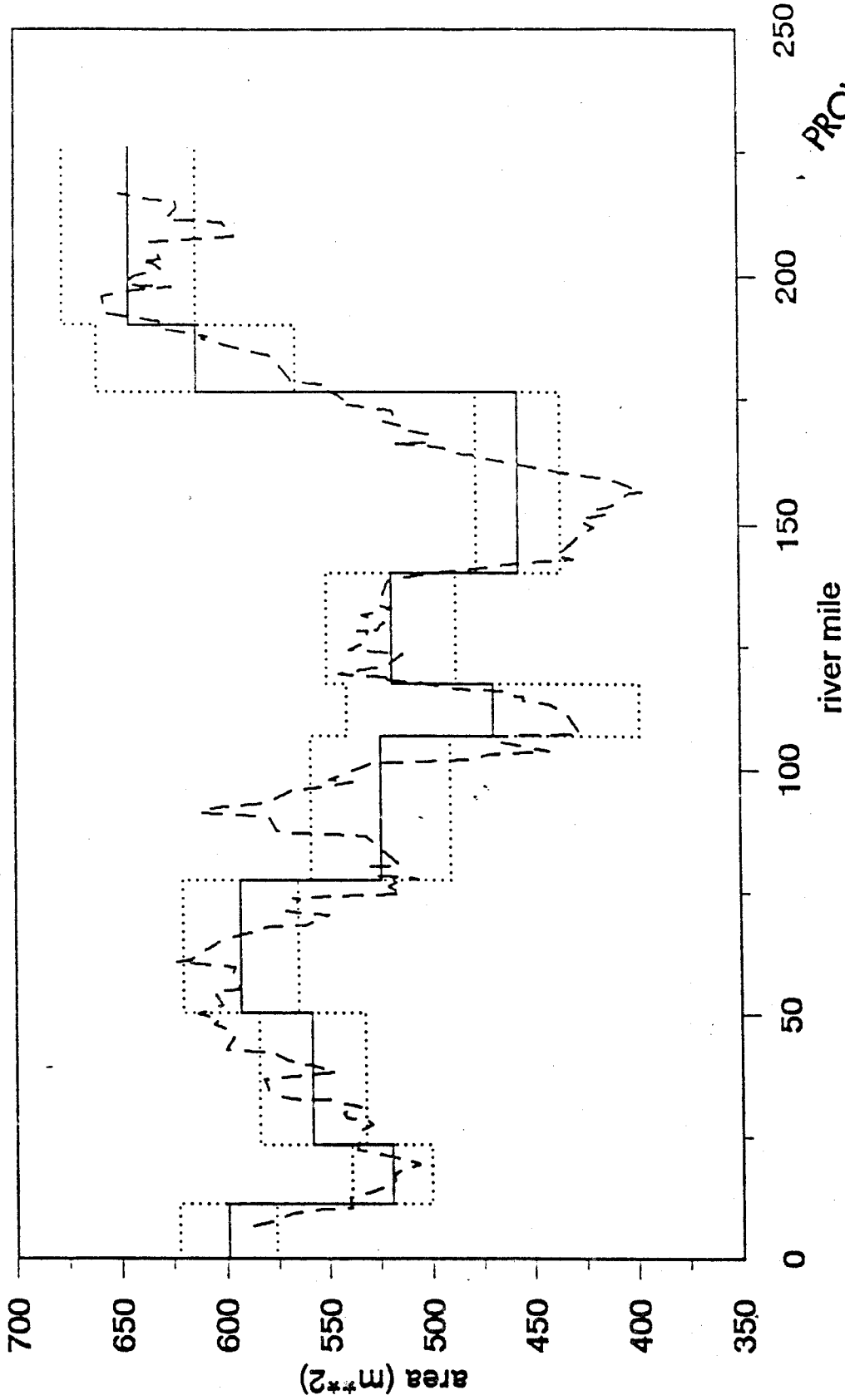


Figure 5: Block averaged means (solid line) compared to 15-point running means (dashed lines) of cross-sectional area from the Wilson profiles for reaches defined using river level and rock type and channel depth. The dotted lines show the block averaged mean values plus and minus one standard deviation. The locations and characteristics of these *Morphologically Similar Reaches* are listed in Tables I and II.

PROVISIONAL DRAFT,  
 Subject to Revision  
 DO NOT QUOTE OR RELEASE  
 Pending Approval by Director  
 U.S. Geological Survey

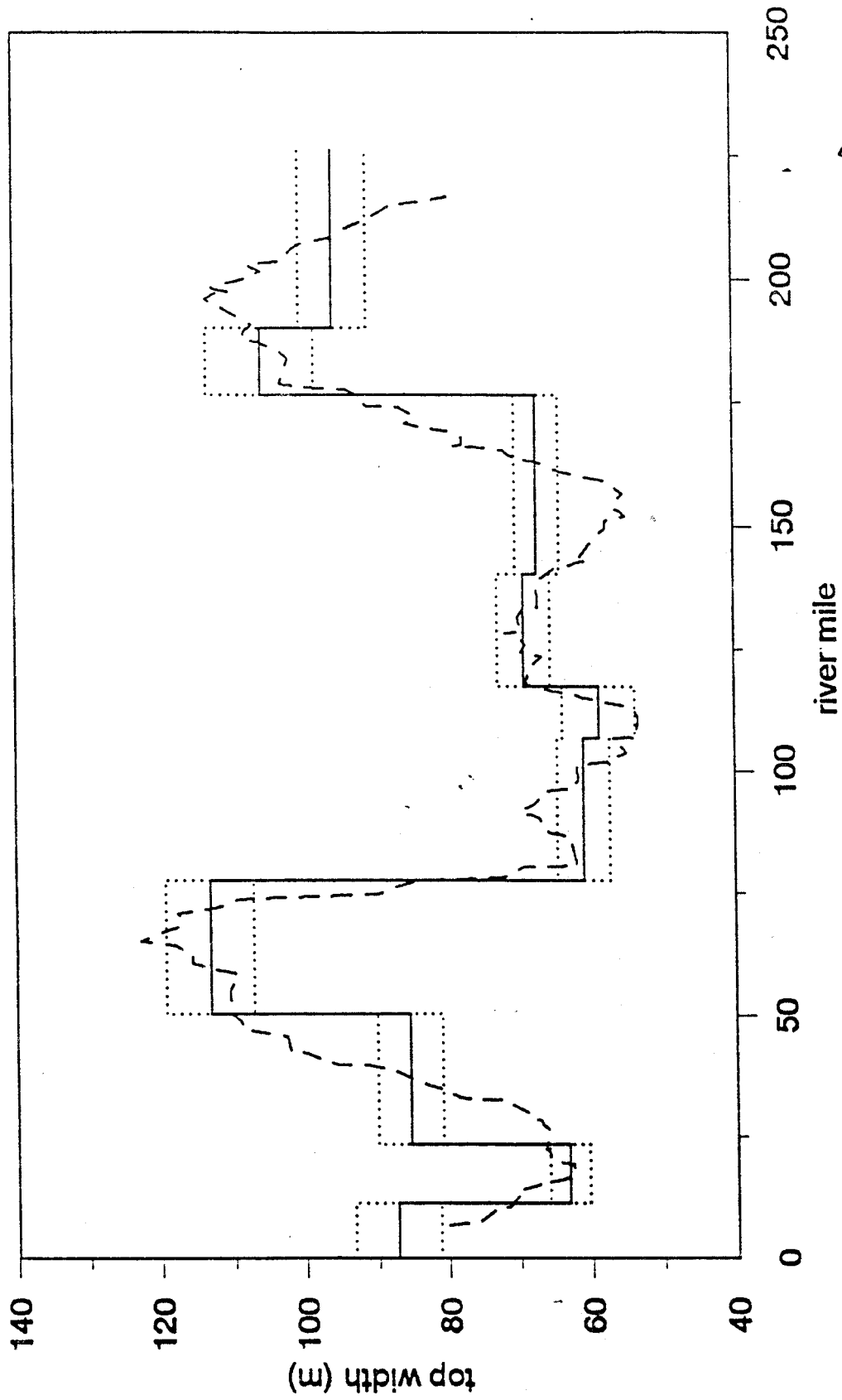
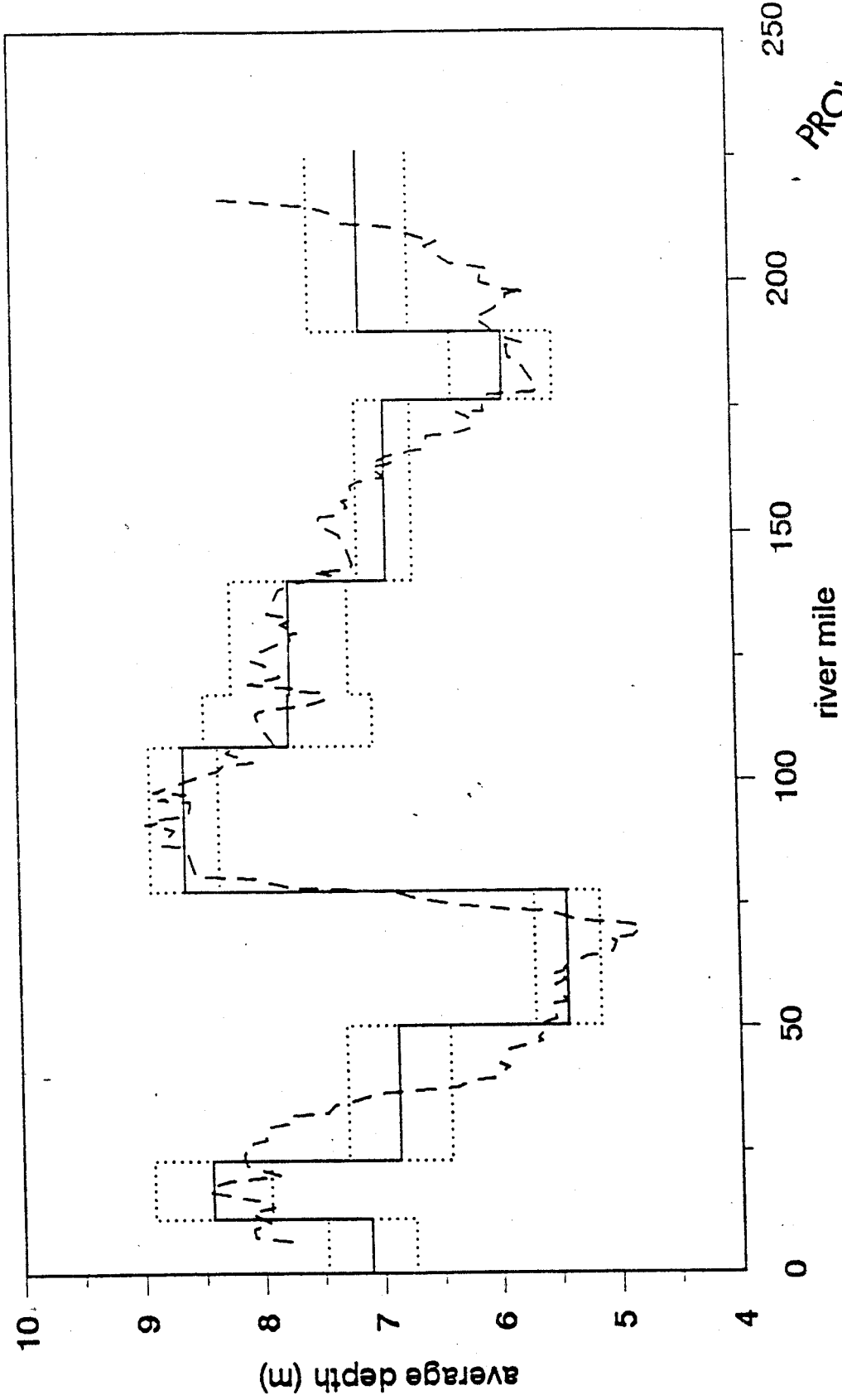


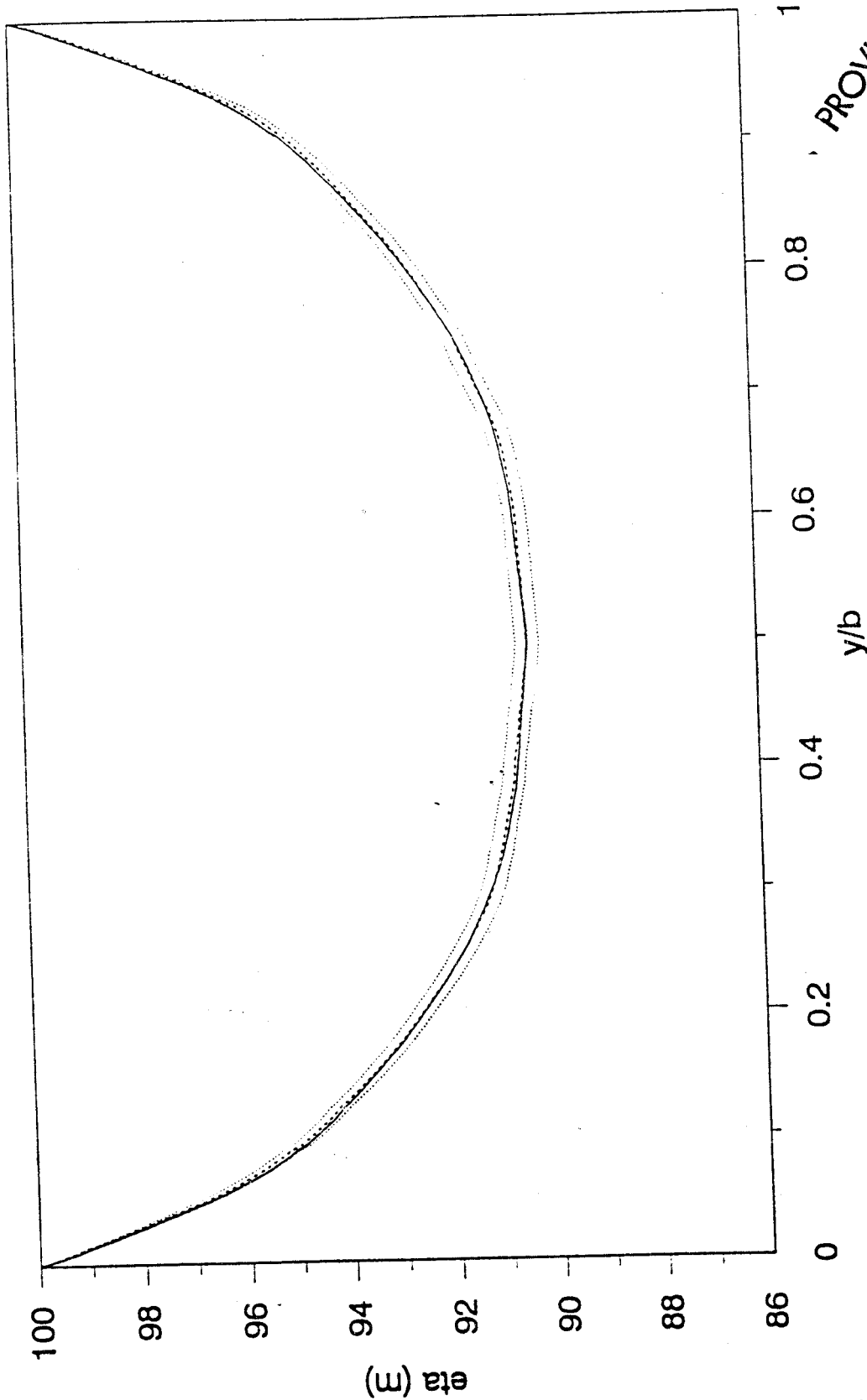
Figure 4: Block averaged means (solid line) compared to running means (dashed lines) of surface width from the Wilson profiles for reaches defined using river level rock type and cross-sectionally averaged channel depth. The dotted lines show the block averaged mean values plus and minus one standard deviation. The locations and characteristics of these Morphologically Similar Reaches are listed in Table 1.

**PROVISIONAL DRAFT**  
 Subject to Revision  
 Do NOT QUOTE OR RELEASE  
 Pending Approval by Director  
 U.S. Geological Survey



**PROVISIONAL DRAFT**  
 Subject to Revision  
**DO NOT QUOTE OR RELEASE**  
 Pending Approval by Director  
 U.S. Geological Survey

**Figure 6:** Block averaged means (solid line) compared to 15-point running means (dashed lines) of flow depth from the Wilson profiles for reaches defined using river level rock type and channel width. The dotted lines show the block averaged mean values plus and minus one standard deviation. The locations and characteristics of these *Morphologically Similar Reaches* are listed in Tables I and II.



**PROVISIONAL DRAFT**  
 Subject to Revision  
 Do NOT QUOTE OR RELEASE  
 Pending Approval by Director  
 U.S. Geological Survey

**Figure 7:** Block averaged cross-sectional shape for the entire set of channel profiles obtained by Wilson. The solid line assumes the profiles must be symmetrical and the dashed line does not enforce this constraint. The dotted lines give the block averaged mean plus and minus one standard deviation. All profiles were scaled by river width before averaging.

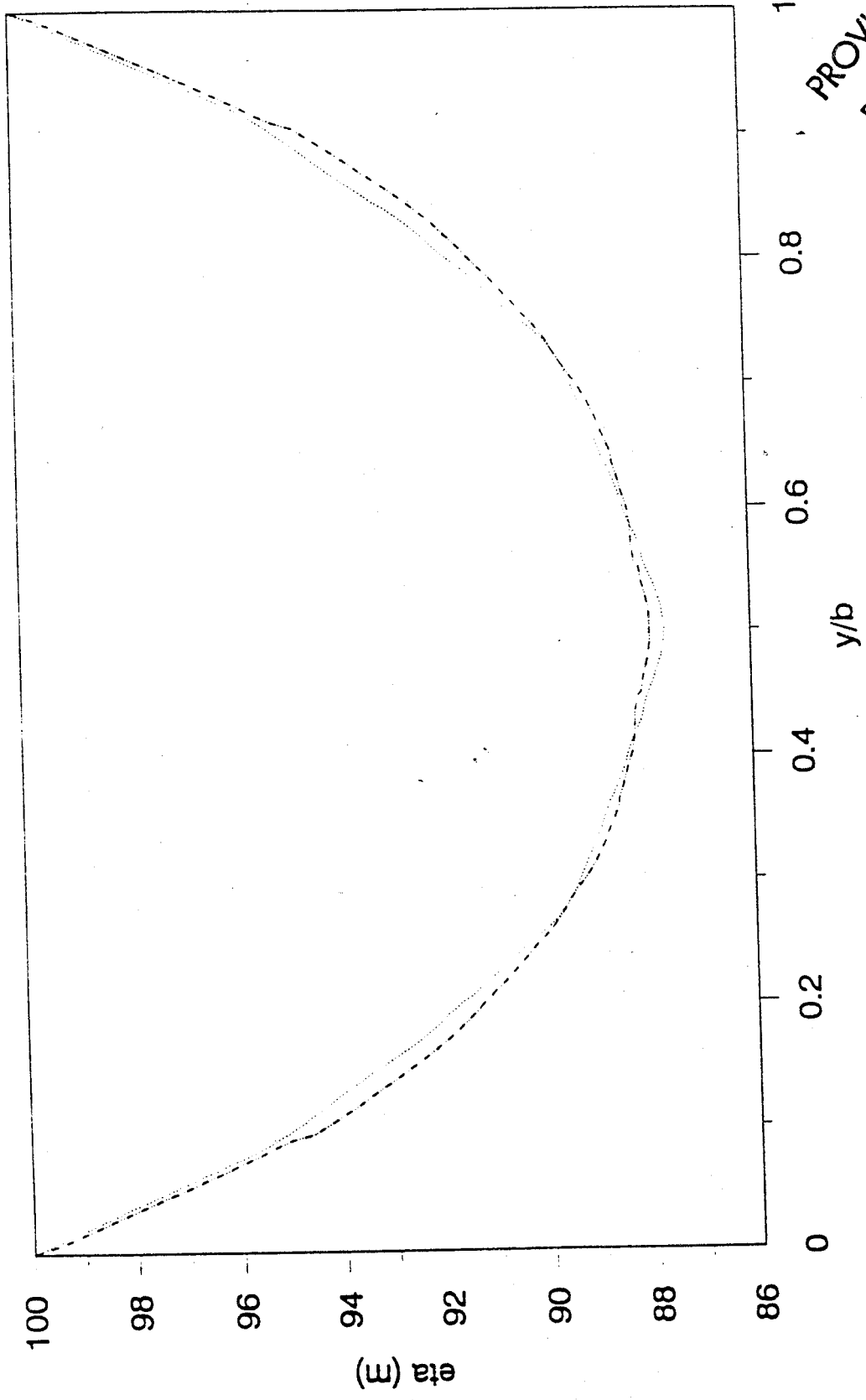


**Figure 9:** Block averaged profiles of channel shape for the 11 to 23 (dots) and 77 to 107 (dashes with double dots). The dominant rocks at river level in these reaches are sandstones of the Supai Group (11 to 23) and Zoroaster Granite and Vishnu Schist (77 to 107).

**PROVISIONAL DRAFT**  
 Subject to Revision  
**DO NOT QUOTE OR RELEASE**  
 Pending Approval by Director  
 U.S. Geological Survey

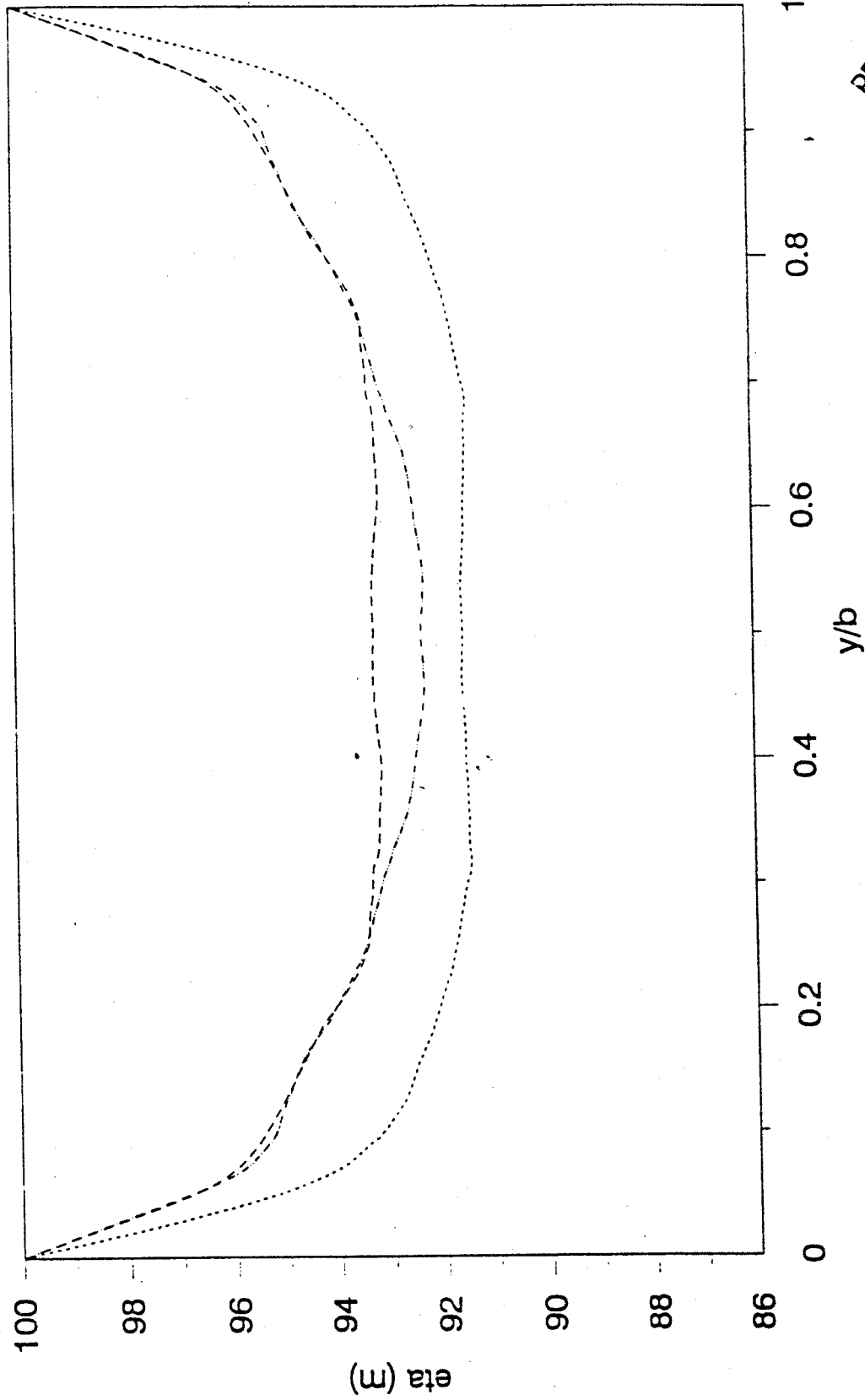
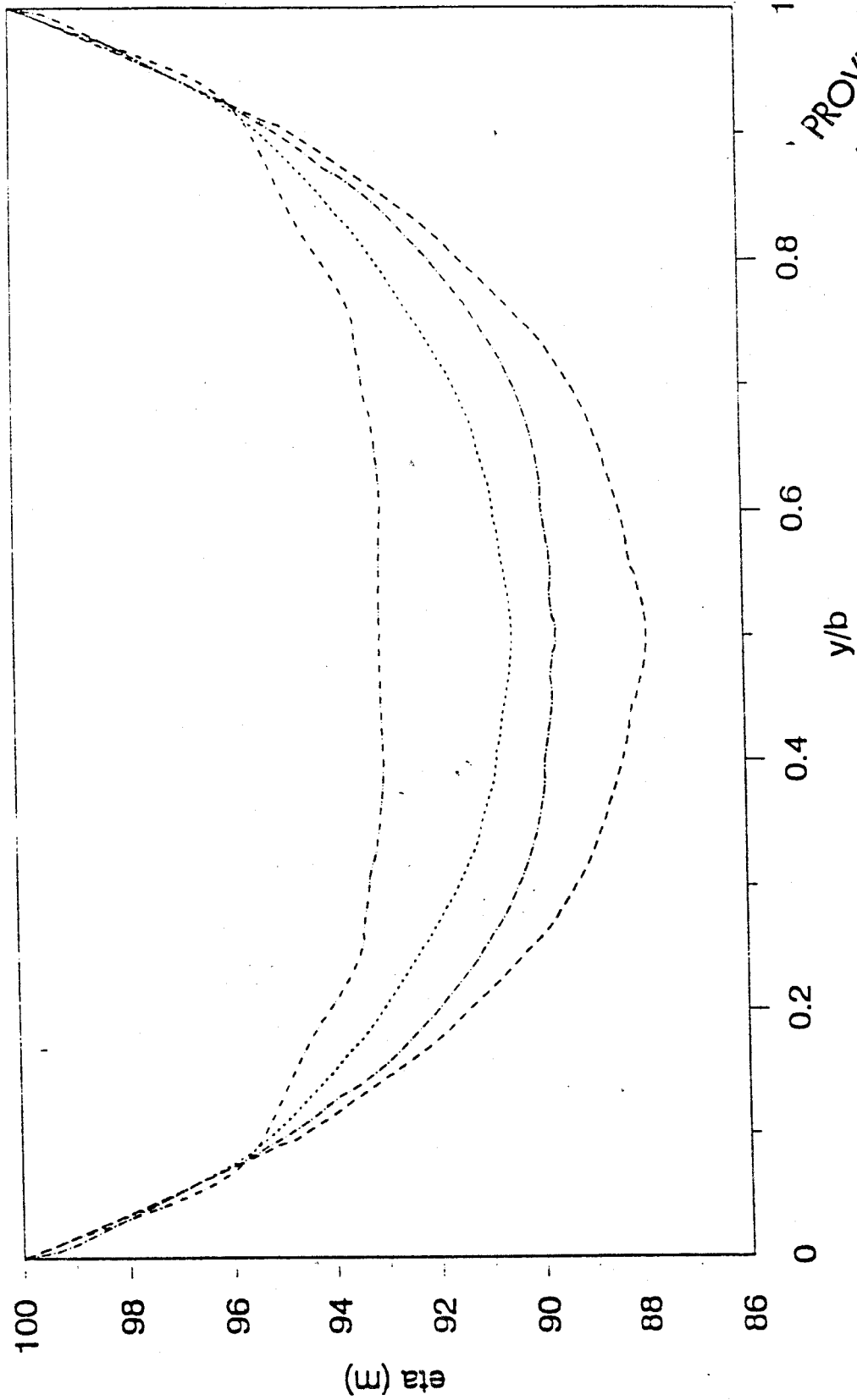


Figure 10: Block averaged profiles of channel shape for the 50 to 77 (dashes) and 169 to 190 (dashes with double dots) reaches. The dominant rocks at river level in these reaches are Bright Angel Shale and Tapeats Sandstone. The mound in the center of the upstream most reach is a result of sand and gravel lenses and bars in this depositional zone below the mouth of the Little Colorado River. Although the Pleistocene lava is present in the 169 to 190 zone, it appears to have little geomorphic effect. Also shown by the dotted line is the block averaged channel shape for the 190 to 225 reach which is in Vishnu Schist.

**PROVISIONAL DRAFT**  
 Subject to Revision  
 Do NOT QUOTE OR RELEASE  
 Pending Approval by Director  
 U.S. Geological Survey



**Figure 11:** Block averaged cross-sections for various *Morphologically Similar Reaches*. The dashed line represents the average of the data shown in Figure 9 for the reaches with Supai Sandstones and Vishnu Schist and Zoroaster Granite at river level; the dashes with single dots represent block averaged cross-sections for the 107 to 117 reach; the dotted line represents the average of the data shown in Figure 8 for the reaches with Paleozoic limestone at river level; the dashes with double dots represent the upstream most reach of those displayed in Figure 10.

**PROVISIONAL DRAFT**  
 Subject to Revision  
 DO NOT QUOTE OR RELEASE  
 Pending Approval by Director  
 U.S. Geological Survey

RM 0-23

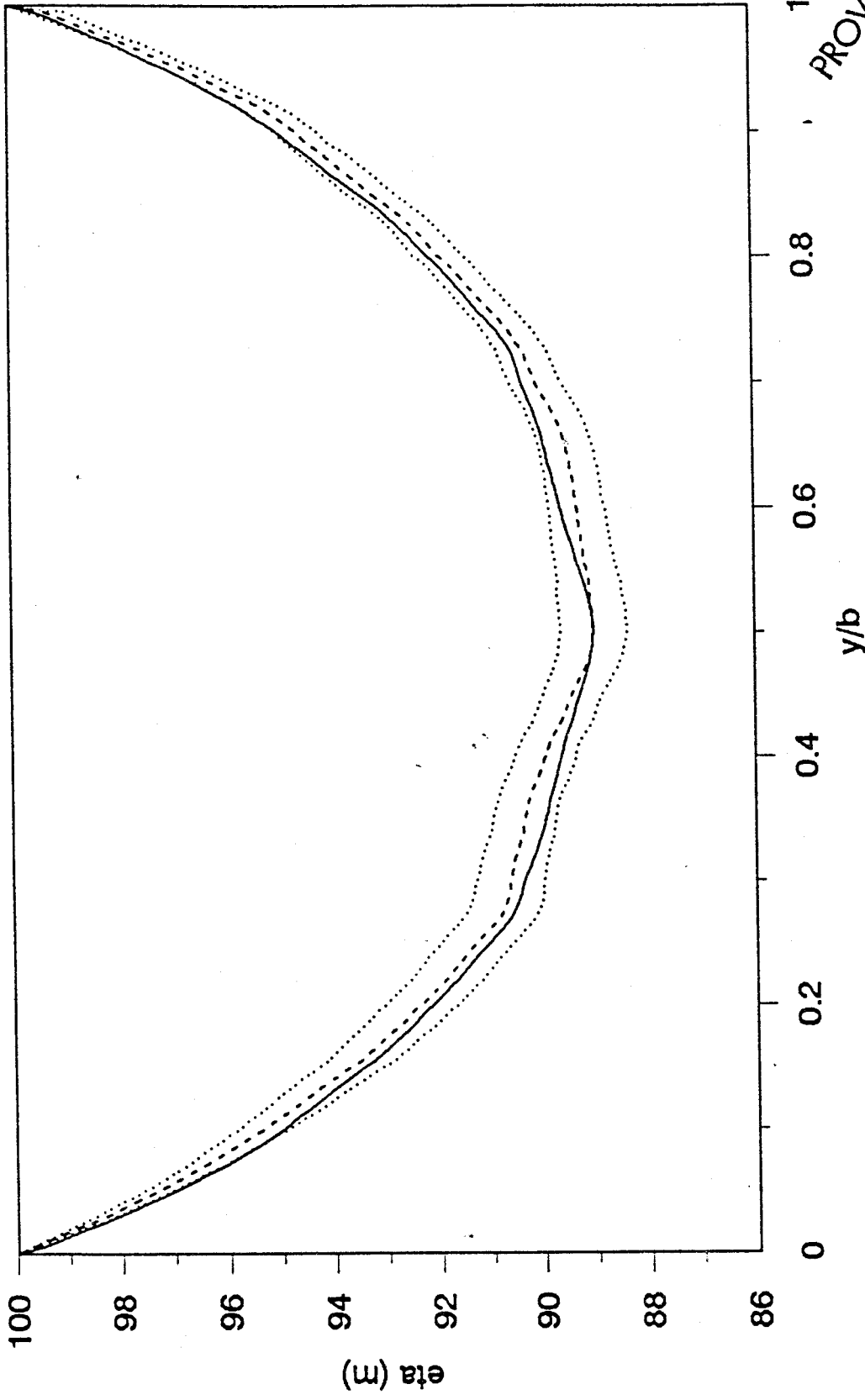
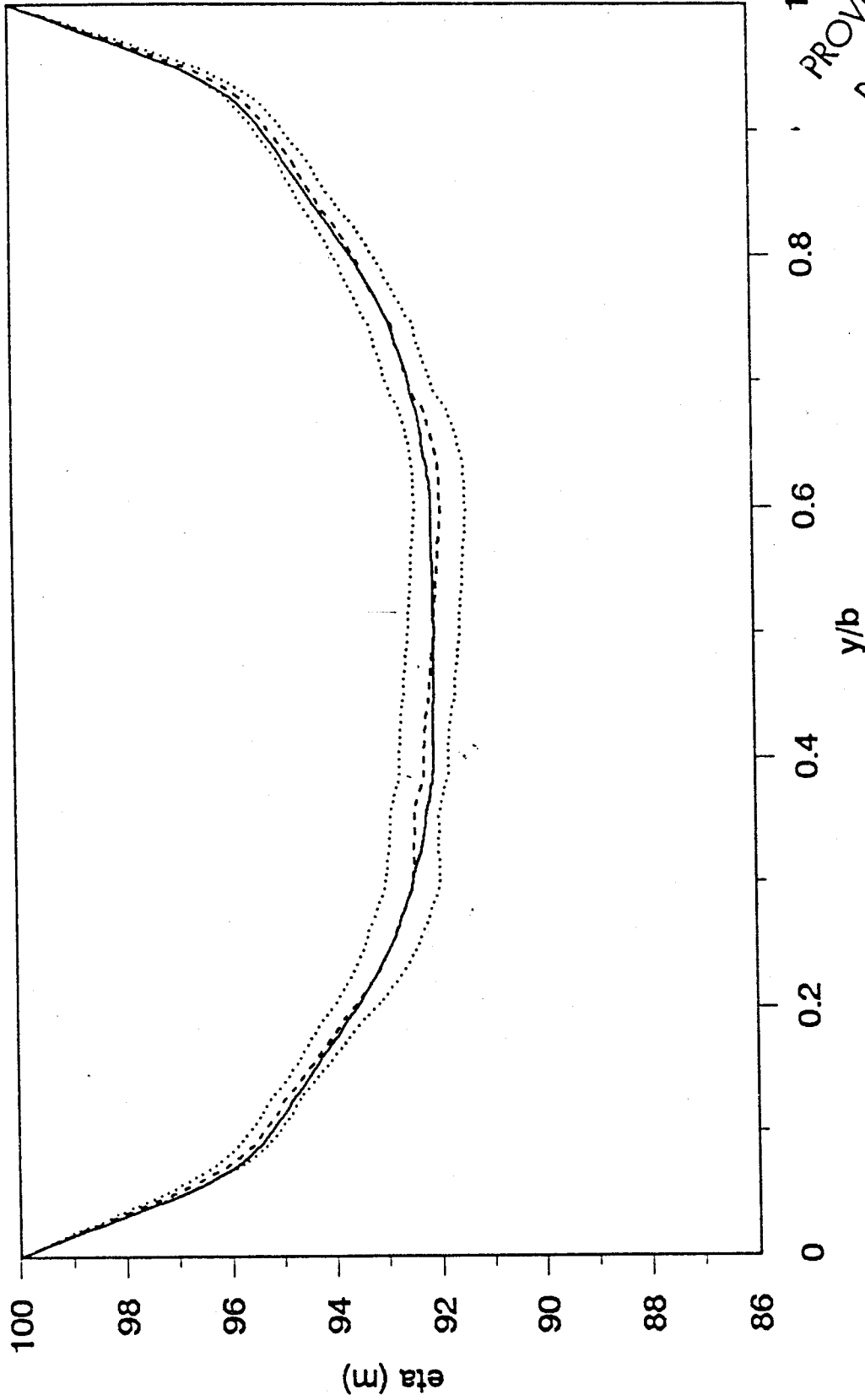


Figure 12: Block averaged cross-sectional shape for the set of channel profiles obtained by Wilson in the 0 to 23 reach. The solid line assumes the profiles must be symmetrical and the dashed line does not enforce this constraint. The dotted lines give the block averaged mean plus and minus one standard deviation. All profiles were scaled by river width before averaging.

PROVISIONAL DRAFT  
Subject to Revision  
DO NOT QUOTE OR RELEASE  
Pending Approval by Director  
U.S. Geological Survey

RM 23-77



1

0.8

0.6

0.4

0.2

0

y/b

PROVISIONAL DRAFT  
Subject to Revision  
DO NOT QUOTE OR RELEASE  
Pending Approval by Director  
U.S. Geological Survey

Figure 13: Block averaged cross-sectional shape for the set of channel profiles obtained by Wilson in the 23 to 77 reach. The solid line assumes the profiles must be symmetrical and the dashed line does not enforce this constraint. The dotted lines give the block averaged mean plus and minus one standard deviation. All profiles were scaled by river width before averaging.

RM 77-107

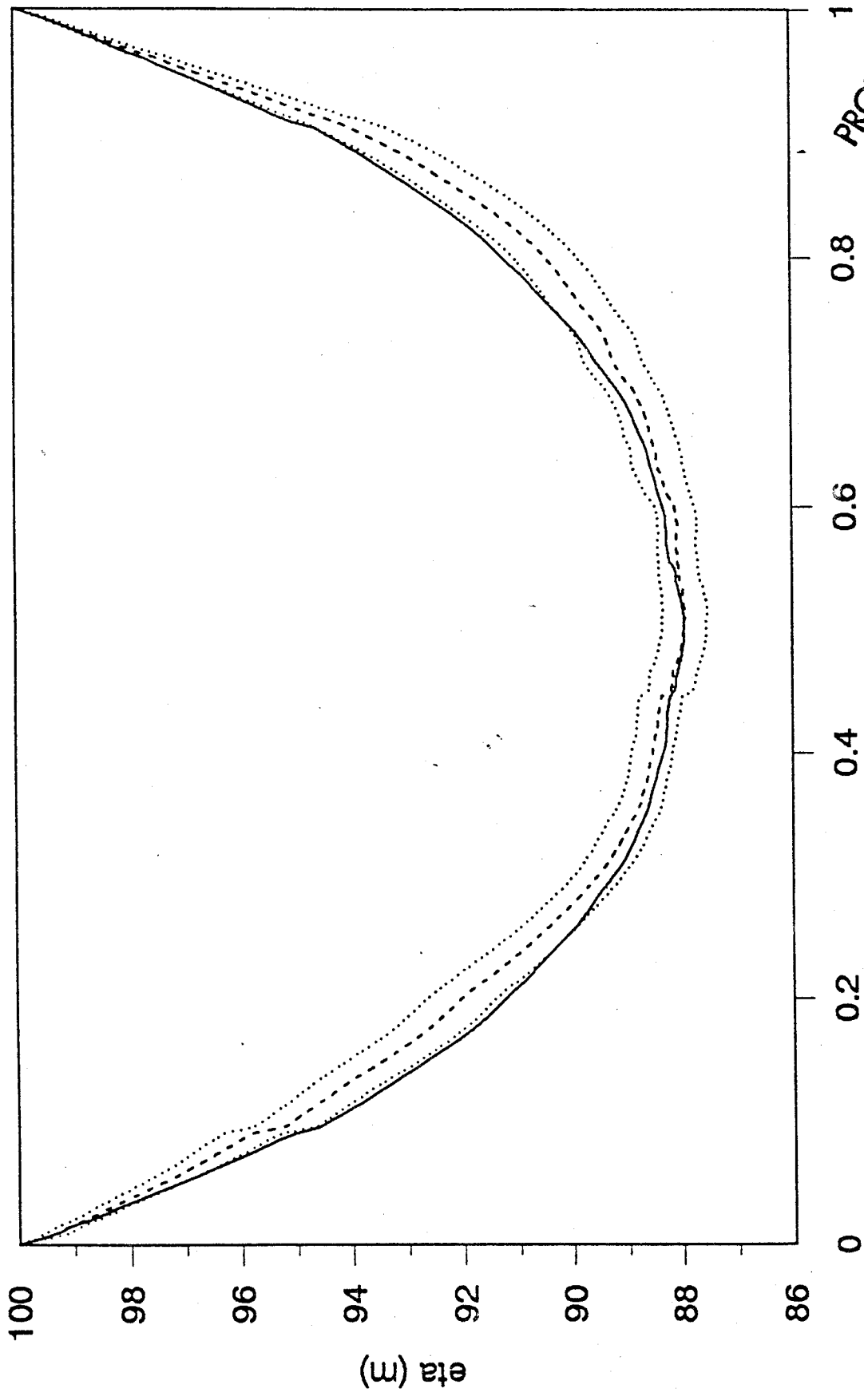


Figure 14: Block averaged cross-sectional shape for the set of channel profiles obtained by Wilson in the 77 to 107 reach. The solid line assumes the profiles must be symmetrical and the dashed line does not enforce this constraint. The dotted lines give the block averaged mean plus and minus one standard deviation. All profiles were scaled by river width before averaging.

**PROVISIONAL DRAFT**  
Subject to Revision  
**DO NOT QUOTE OR RELEASE**  
Pending Approval by Director  
U.S. Geological Survey

RM 107-140

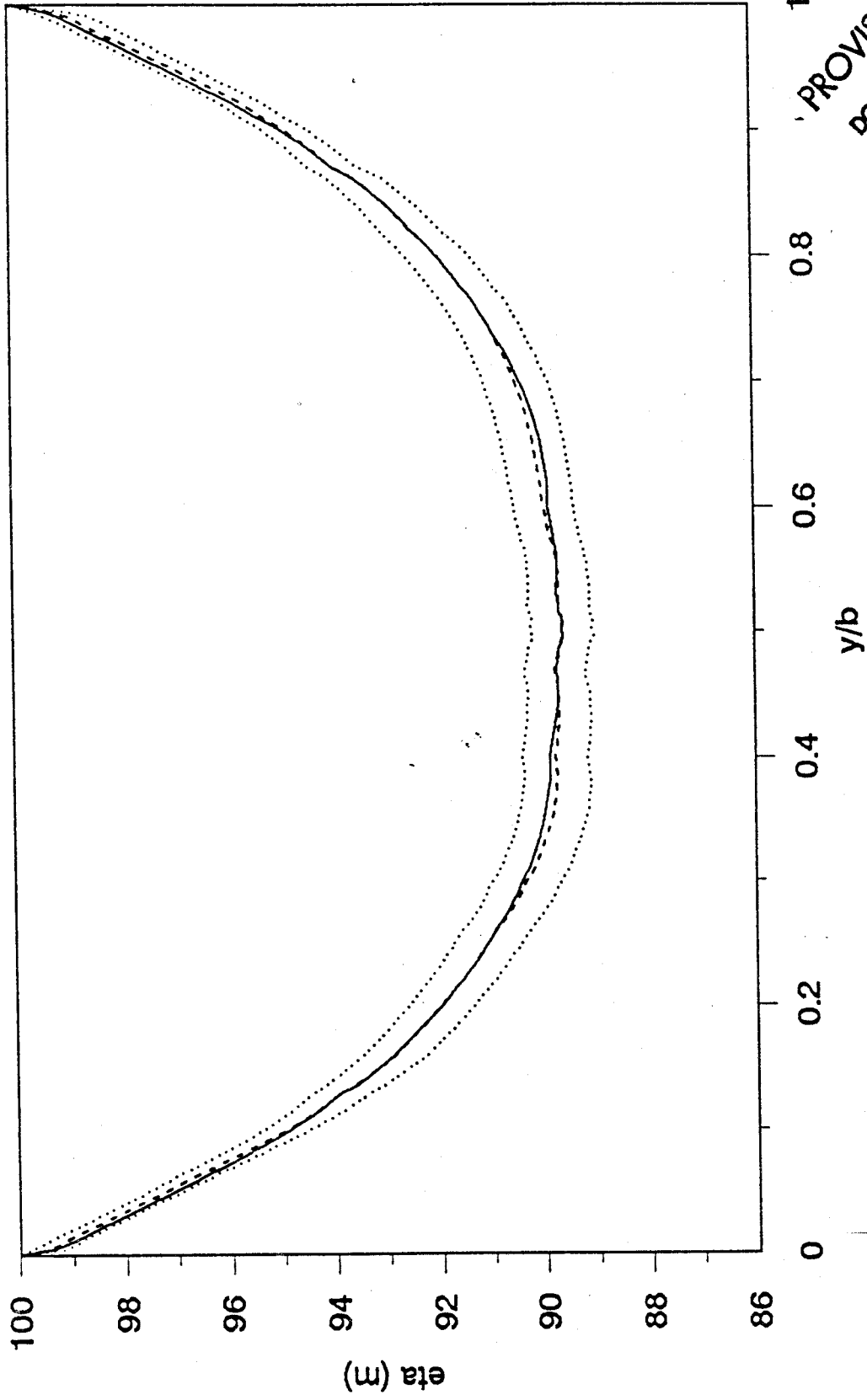


Figure 15: Block averaged cross-sectional shape for the set of channel profiles obtained by Wilson in the 107 to 140 reach. The solid line assumes the profiles must be symmetrical and the dashed line does not enforce this constraint. The dotted lines give the block averaged mean plus and minus one standard deviation. All profiles were scaled by river width before averaging.

PROVISIONAL DRAFT  
Subject to Revision  
DO NOT QUOTE OR RELEASE  
Pending Approval by Director  
U.S. Geological Survey

RM 140-225

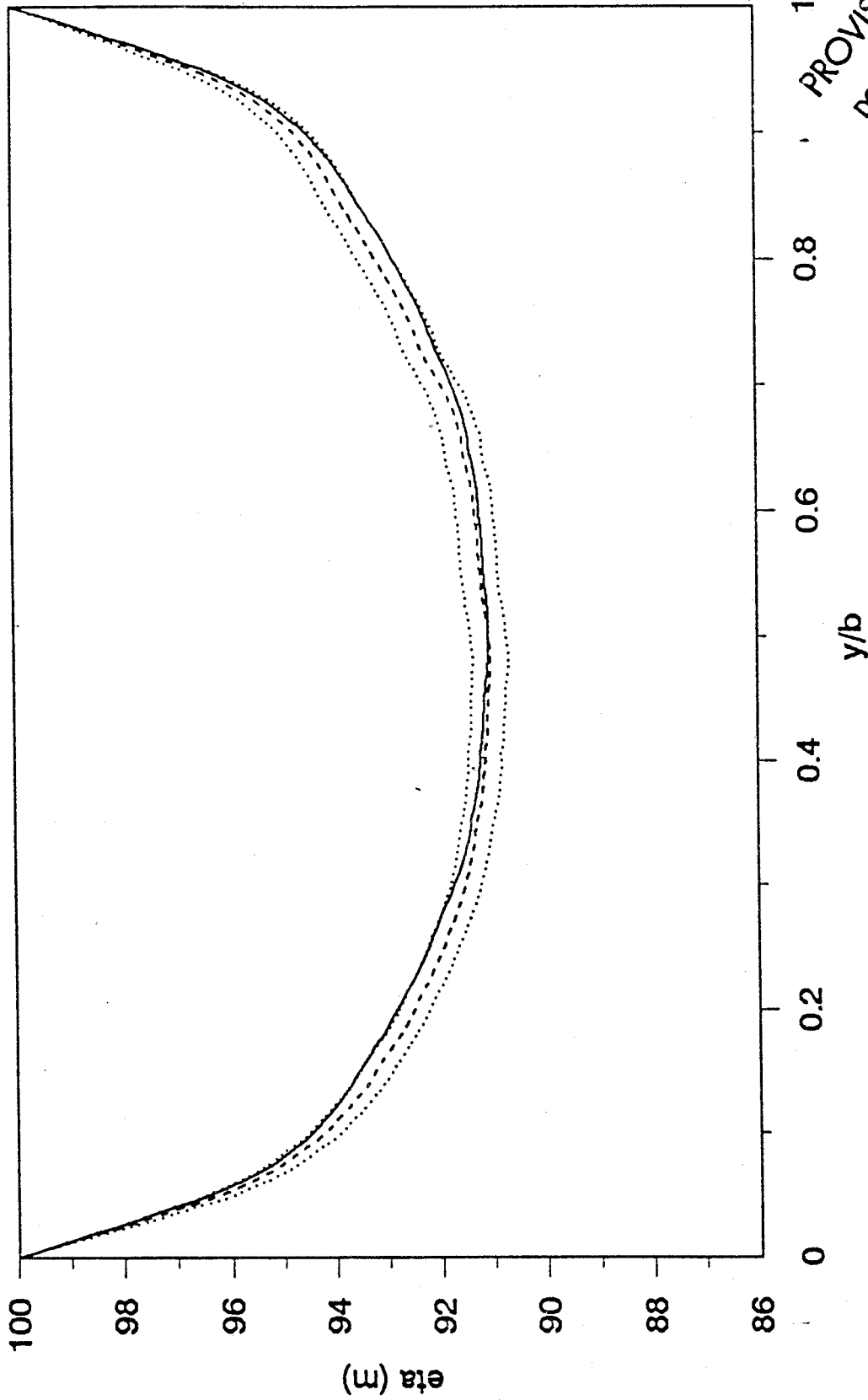


Figure 16: Block averaged cross-sectional shape for the set of channel profiles obtained by Wilson in the 140 to 225 reach. The solid line assumes the profiles must be symmetrical and the dashed line does not enforce this constraint. The dotted lines give the block averaged mean plus and minus one standard deviation. All profiles were scaled by river width before averaging.

PROVISIONAL DRAFT  
Subject to Revision  
DO NOT QUOTE OR RELEASE  
Pending Approval by Director  
U.S. Geological Survey

RM 0-225

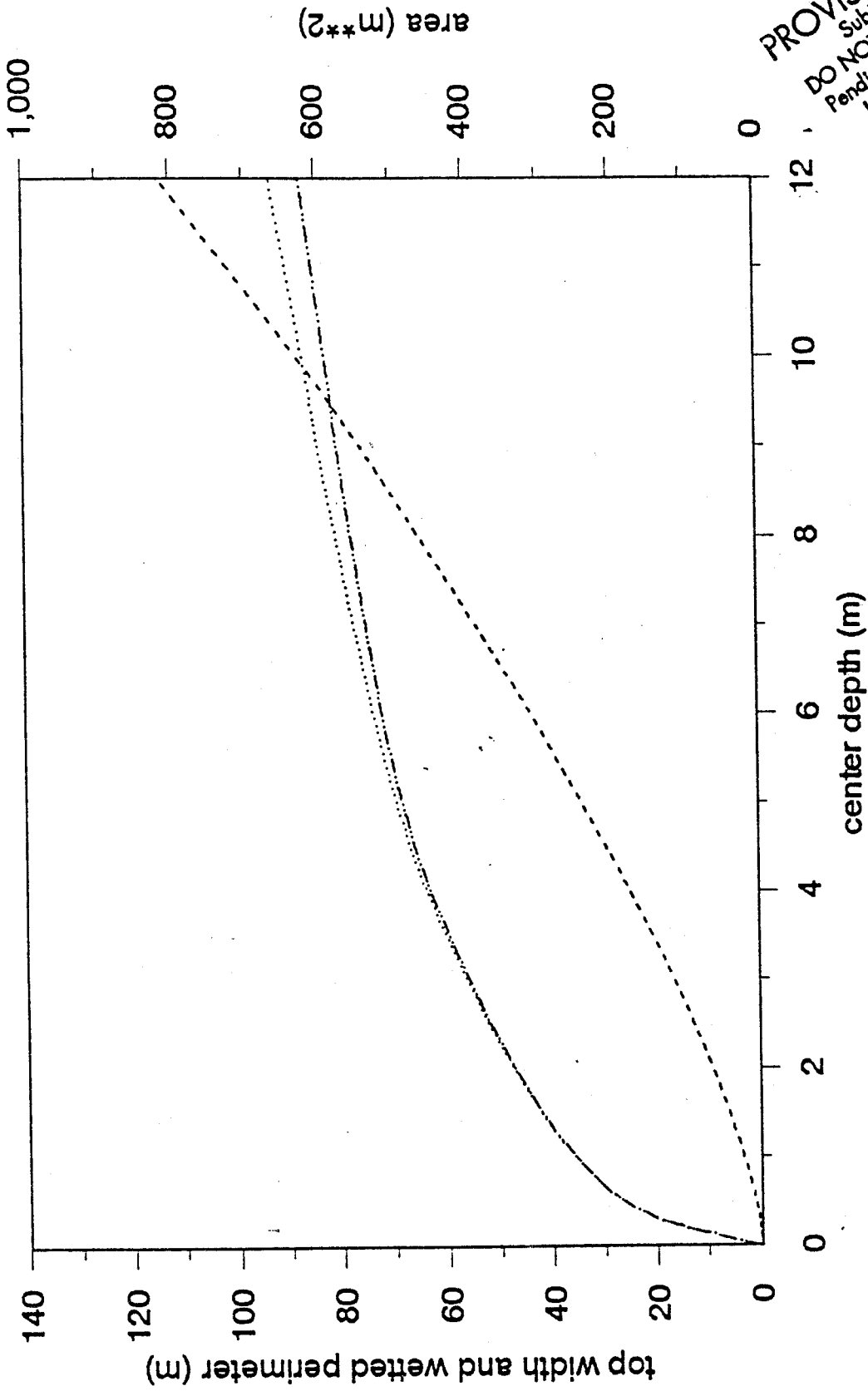


Figure 17: Morphologic properties of the reach averaged channel between River Miles 0 and 225 as functions of depth at the center of the channel. In this figure the dashed line represents cross-sectional area, the dashed line with double dots represents top width, and the dotted line represents wetted perimeter.

PROVISIONAL DRAFT  
Subject to Revision  
DO NOT QUOTE OR RELEASE  
Pending Approval by Director  
U.S. Geological Survey

RM 0-225

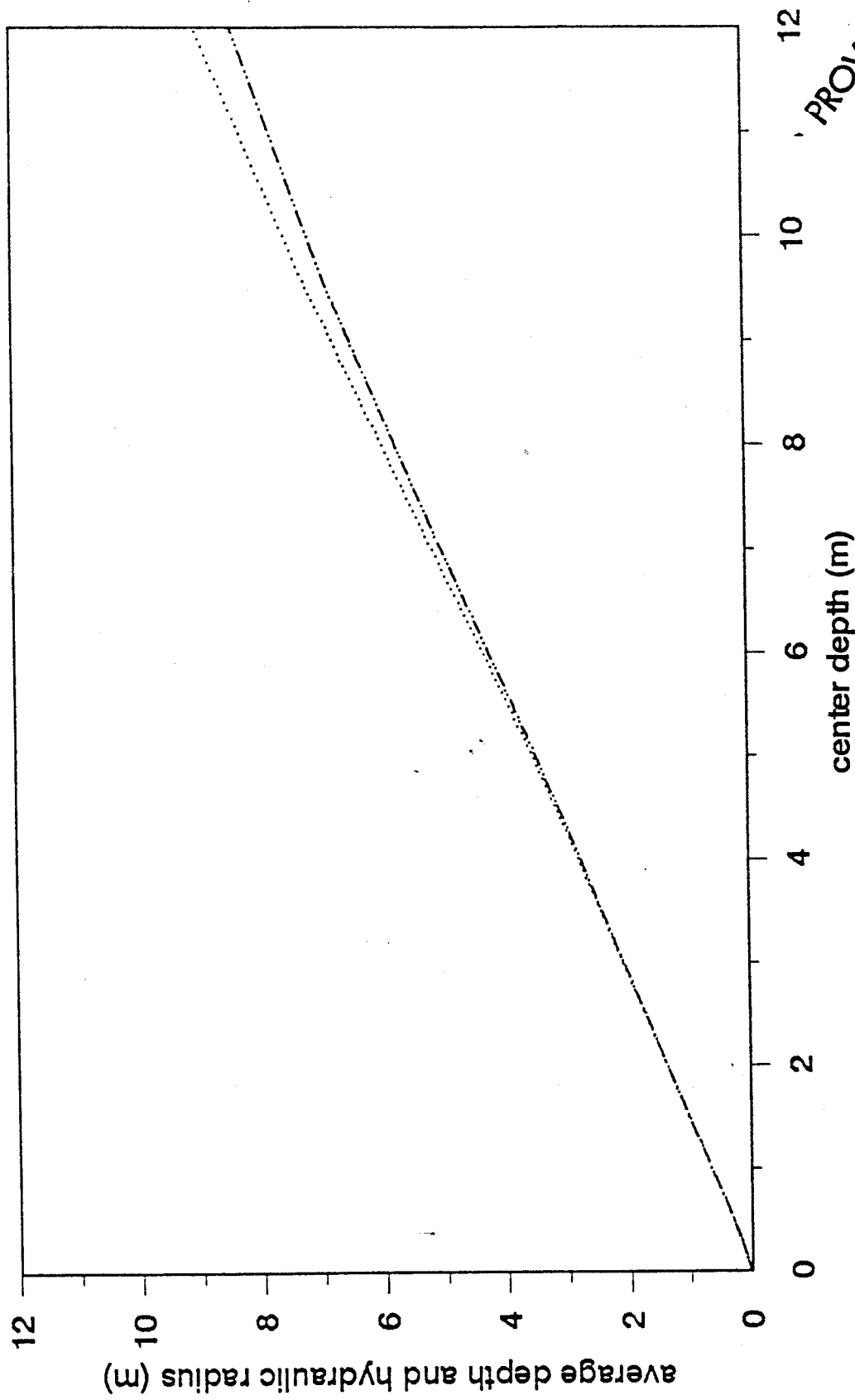
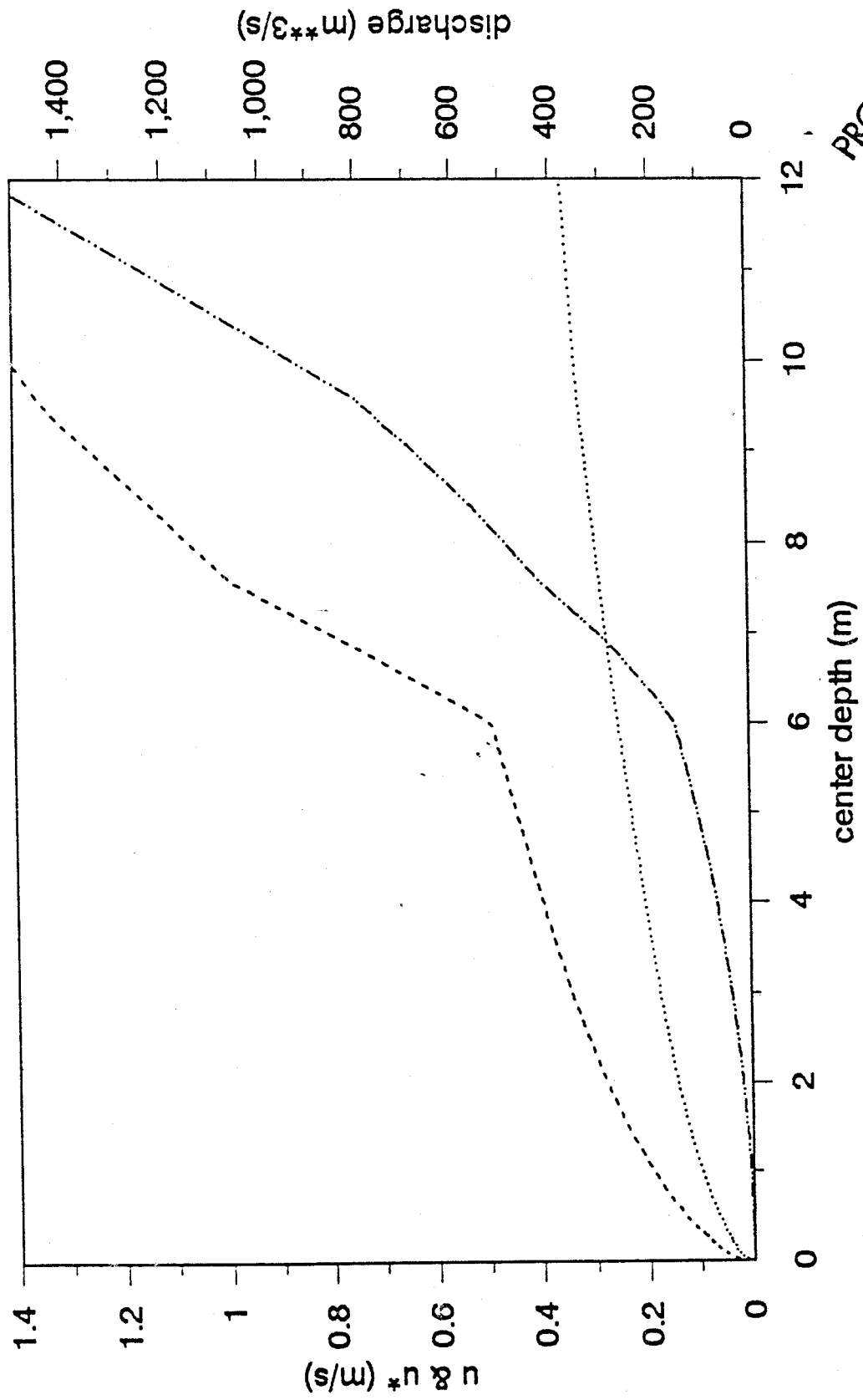


Figure 18: Morphological properties of the reach averaged channel between River Miles 0 and 225 as functions of depth at the center of the channel. In this figure average depth is indicated by the dotted line and hydraulic radius is indicated by the dashed line with double dots.

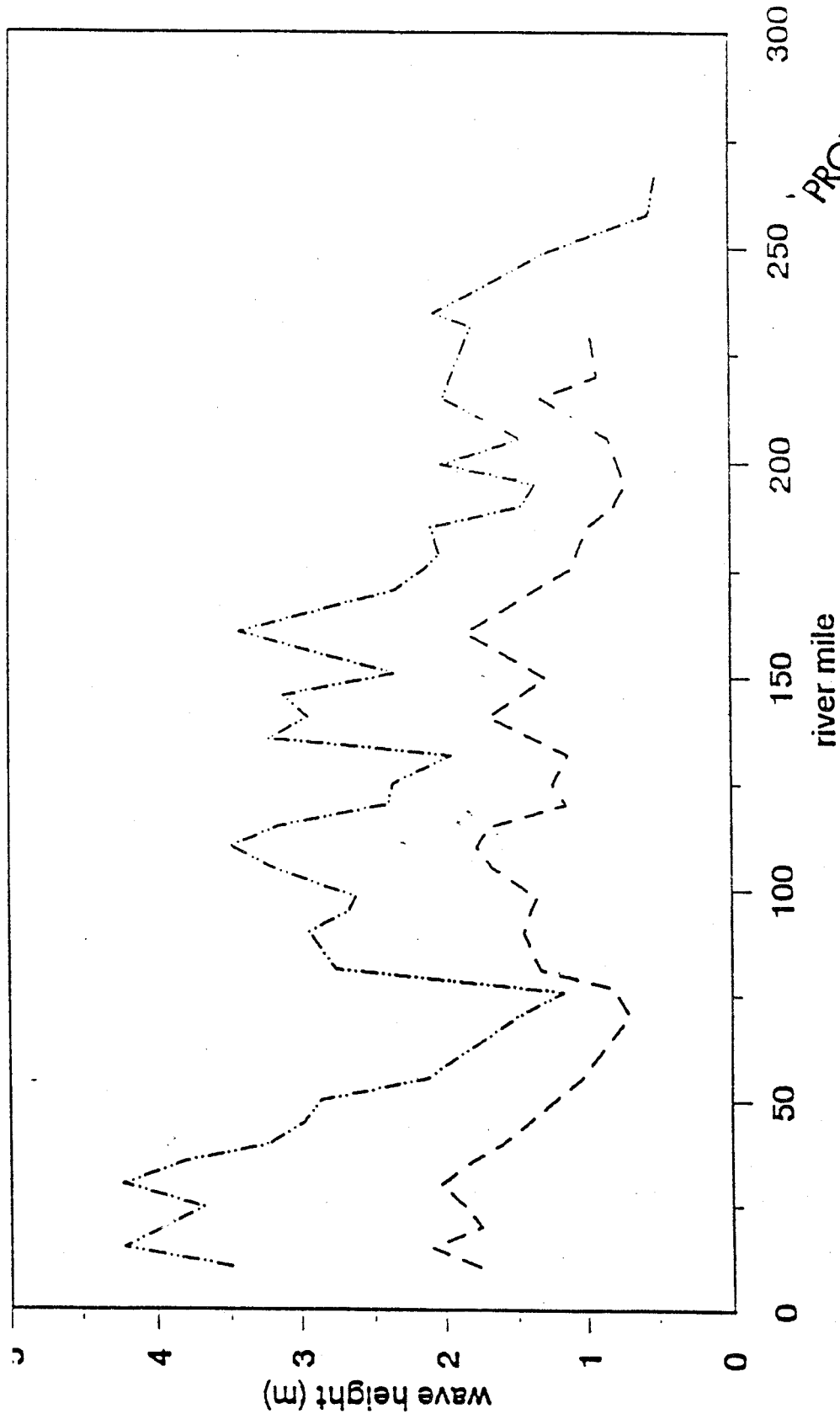
PROVISIONAL DRAFT  
Subject to Revision  
DO NOT QUOTE OR RELEASE  
Pending Approval by Director  
U.S. Geological Survey

RM 0-225



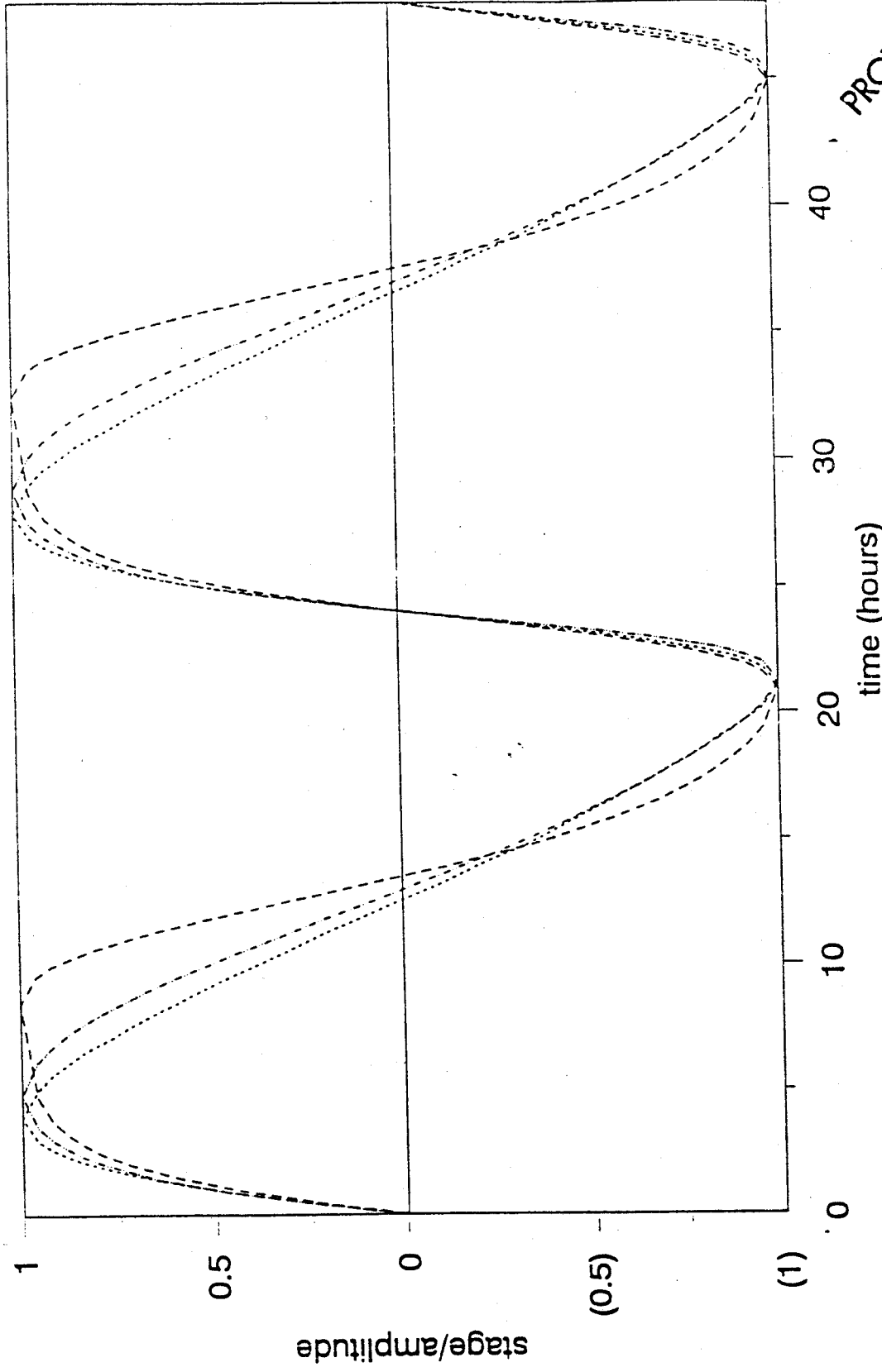
**PROVISIONAL DRAFT**  
 Subject to Revision  
 DO NOT QUOTE OR RELEASE  
 Pending Approval by Director  
 U.S. Geological Survey

Figure 19: Hydraulic properties of the reach averaged channel between River Miles 0 and 225 as functions of flow depth in the center of the channel. In this figure the dotted line represents shear velocity, the dashed line represents cross-sectionally averaged velocity, and the dashed line with double dots represents discharge.



**Figure 20:** Height of the discharge wave measured at temporary pressure gages along the Colorado River as a function of River Mile for Research Flow B (dashed line) and Research Flow D (dashed line with double dots). The discharge ranged from 5000cfs ( $142\text{m}^3/\text{s}$ ) to 15,000cfs ( $425\text{m}^3/\text{s}$ ) in the former case and from 3000cfs ( $85\text{m}^3/\text{s}$ ) to 26,000cfs ( $736\text{m}^3/\text{s}$ ) in the latter. The variations in stage at these localities correspond primarily to variations in river width.

**PROVISIONAL DRAFT**  
 Subject to Revision  
**DO NOT QUOTE OR RELEASE**  
 Pending Approval by Director  
 U.S. Geological Survey



**PROVISIONAL DRAFT**  
 Subject to Revision  
 DO NOT QUOTE OR RELEASE  
 Pending Approval by Director  
 U.S. Geological Survey

**Figure 21:** Shapes of the discharge wave in the *Morphologically Similar Reaches* just downstream of Lees Ferry (RM 0 to 11; dashed line), in the Inner Granite Gorge (RM 77 to 107; dashed line with double dots), and just upstream of Diamond Creek (RM 190 to 225; dotted line), for Research Flow B.

PROVISIONAL DRAI  
Subject to Revision  
DO NOT QUOTE OR RELEASE  
Pending Approval by Director  
U.S. Geological Survey

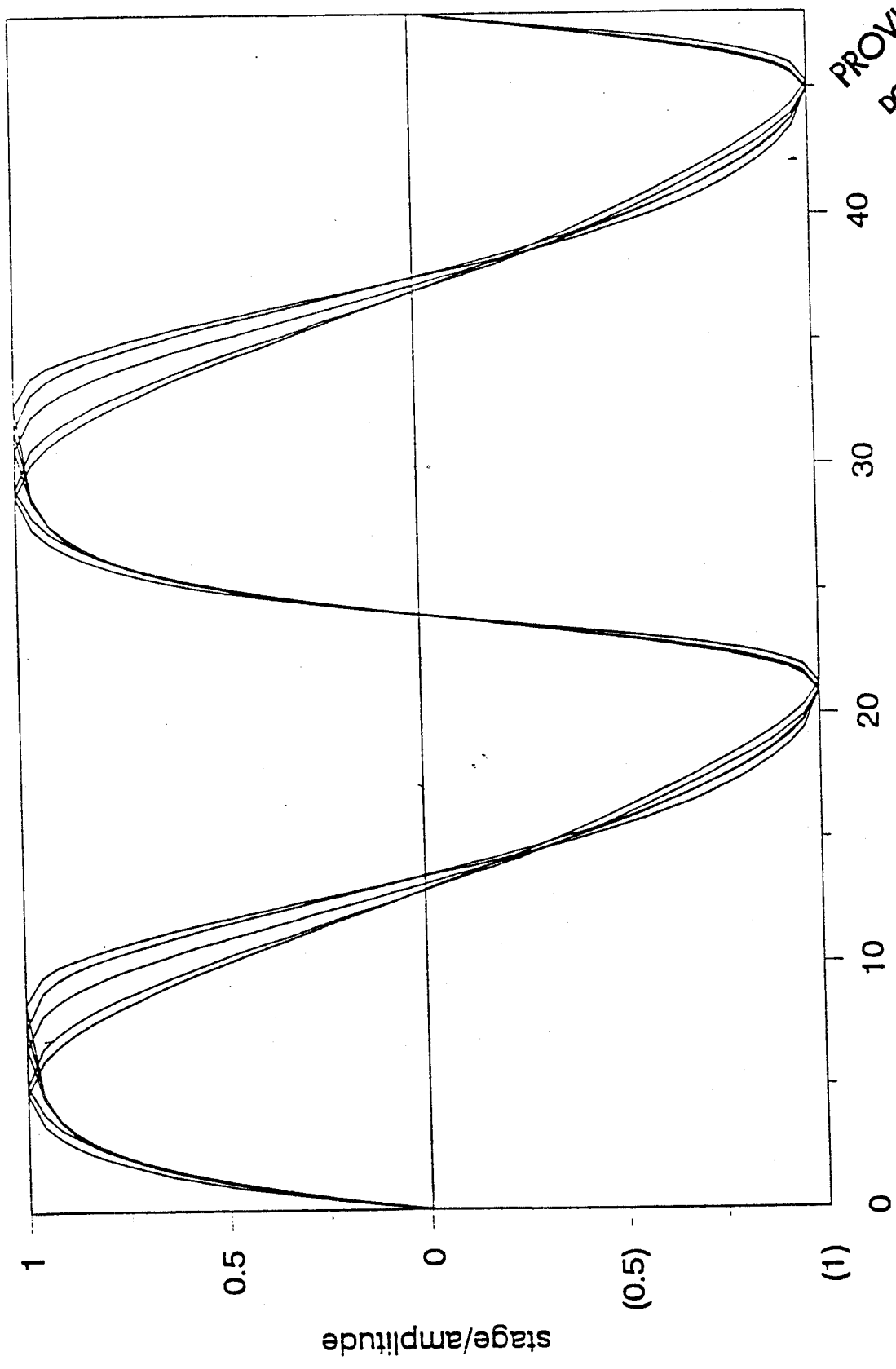
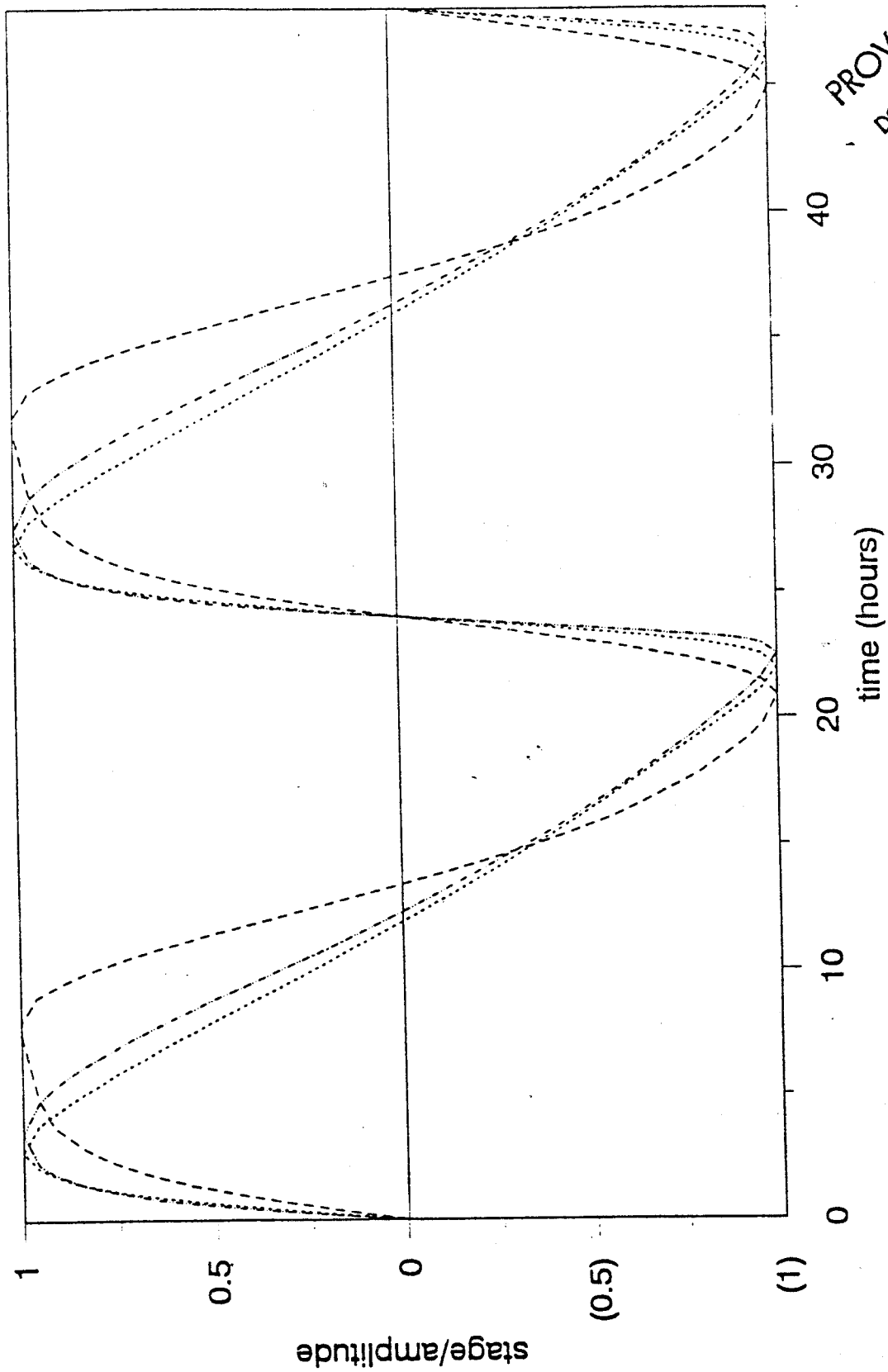
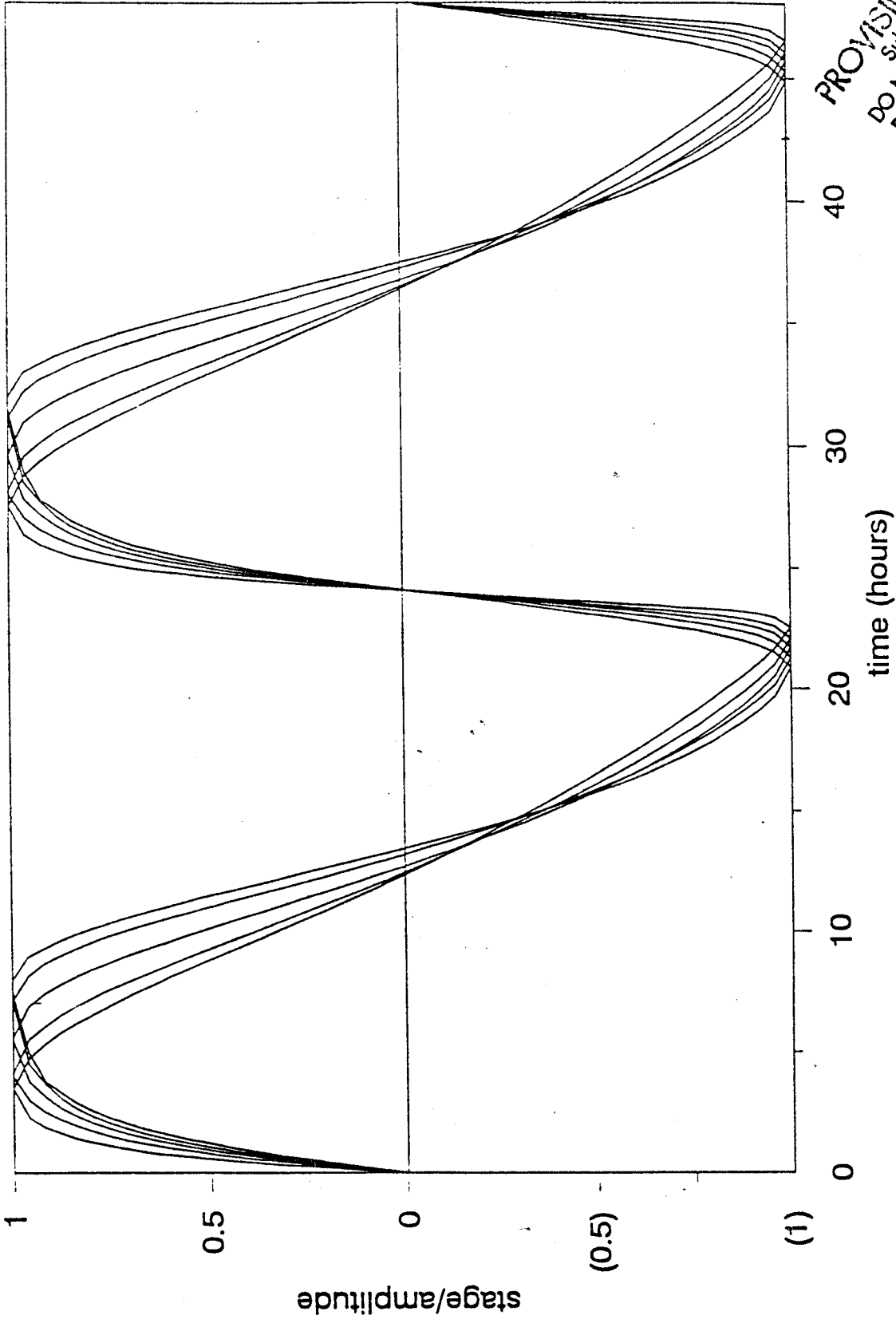


Figure 22: Shapes of the discharge wave in the Morphologically Similar Reaches between Lees Ferry and Phantom Ranch during Research Flow B. The waves transform systematically producing a steeper leading edge and a less steep trailing edge with distance downstream from the Dam.



**PROVISIONAL DRAFT**  
 Subject to Revision  
 DO NOT QUOTE OR RELEASE  
 Pending Approval by Director  
 U.S. Geological Survey

**Figure 23:** Shapes of the discharge wave in the *Morphologically Similar Reaches* just downstream of Lees Ferry (RM 0 to 11; dashed line), in the Inner Granite Gorge (RM 77 to 107; dashed line with double dots), and just upstream of Diamond Creek (RM 190 to 225; dotted line), for Research Flow D.



**PROVISIONAL DRAFT**  
 subject to Revision  
**DO NOT QUOTE OR RELEASE**  
 Pending Approval by Director  
 U.S. Geological Survey

**Figure 24:** Shapes of the discharge wave in the *Morphologically Similar Reaches* between Lees Ferry and Phantom Ranch during Research Flow D. The waves transform systematically producing a steeper leading edge and a less steep trailing edge with distance downstream from the Dam.

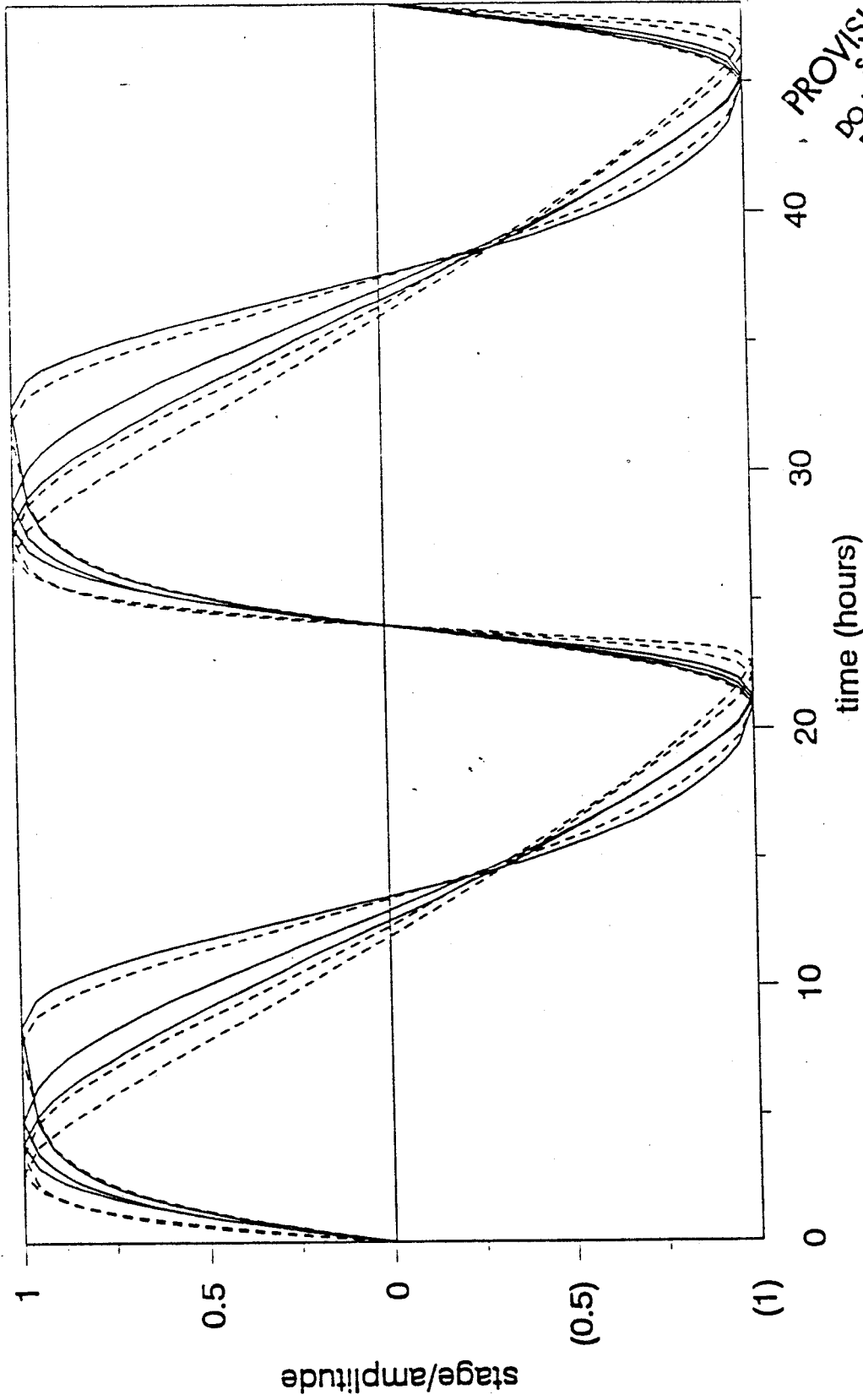


**Figure 25:** Comparison of the shapes of the discharge waves from Research Flows B (solid lines) and D (dashed lines) in the *Morphologically Similar Reaches 0 to 11, 77 to 107, and 190 to 225*.

**PROVISIONAL DRAFT**  
 Subject to Revision  
 DO NOT QUOTE OR RELEASE  
 Pending Approval by Director  
 U.S. Geological Survey

**PROVISIONAL DRAFT**  
Subject to Revision  
**DO NOT QUOTE OR RELEASE**  
Pending Approval by Director  
U.S. Geological Survey

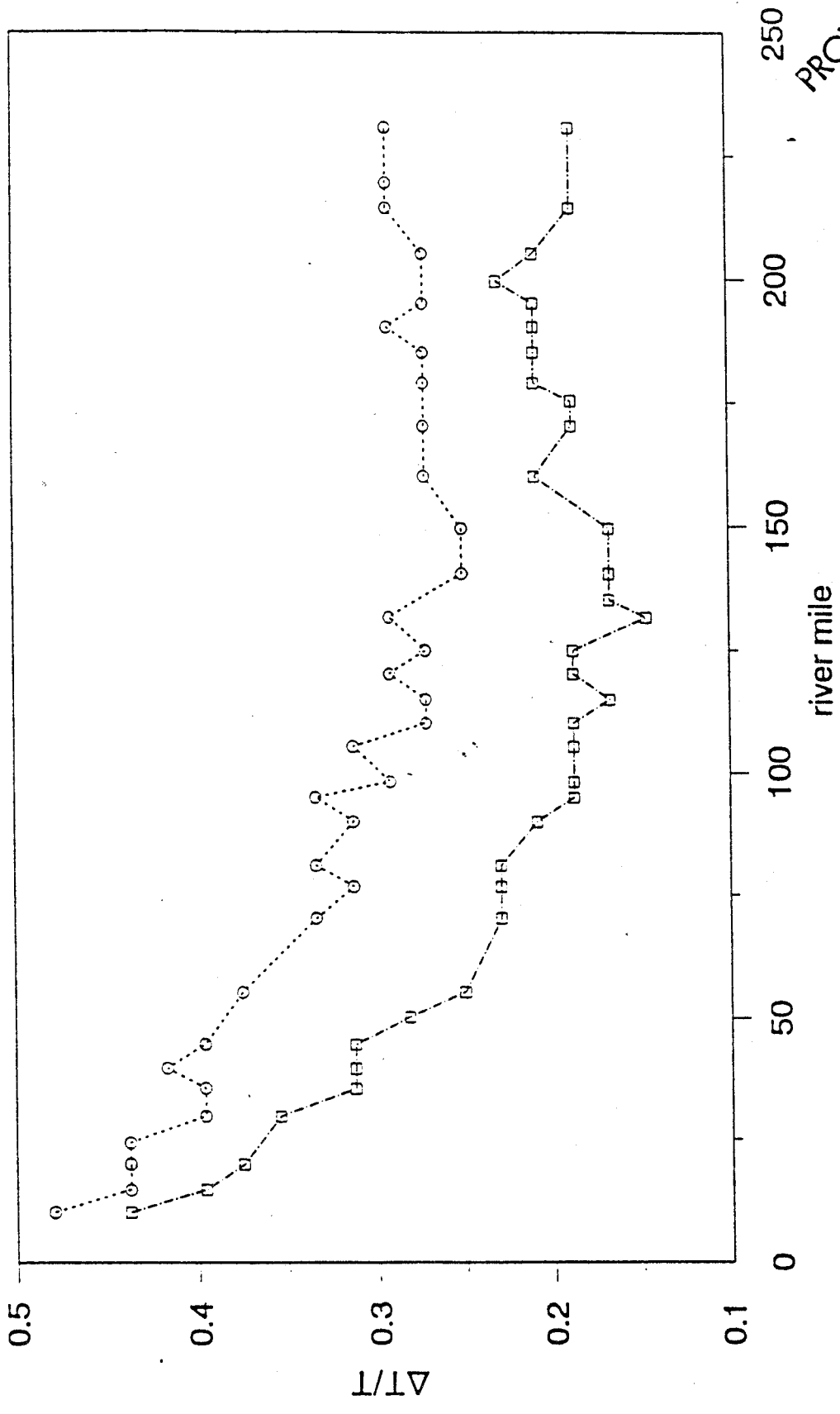


Figure 26: Time interval between leading trough and subsequent crest for Research Flows B (dashed line) and D (dashed line with double dots) as a function of River Mile.

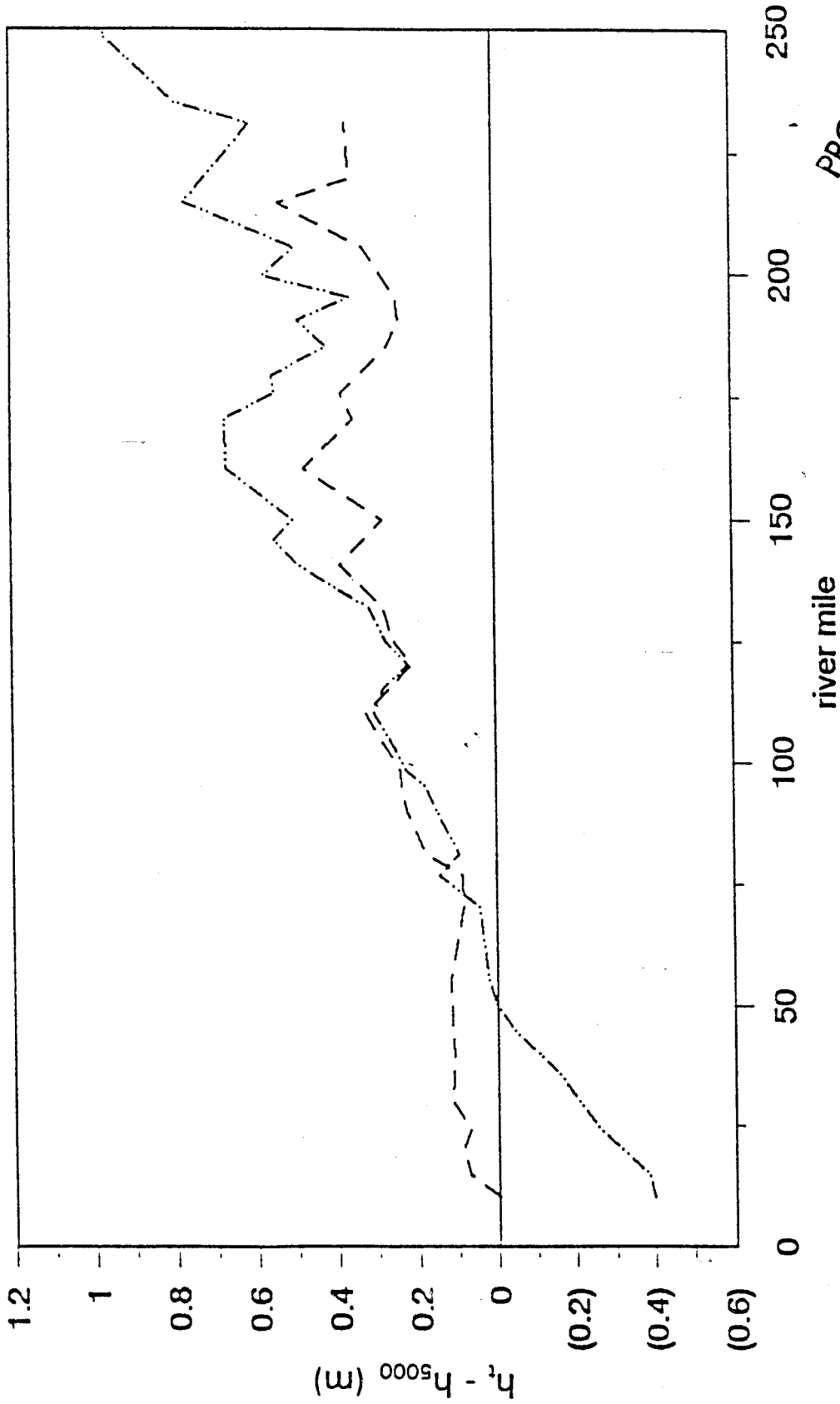


Figure 27: Differences in stage between the troughs of Research Flows B (dashed line) and (dashed line with double dots) and the preceding steady flow which had a discharge of 5,000cfs (142m<sup>3</sup>/s).

**PROVISIONAL DRAFT**  
 Do Not Subject to Revision  
 Pending Approval by Director  
 U.S. Geological Survey

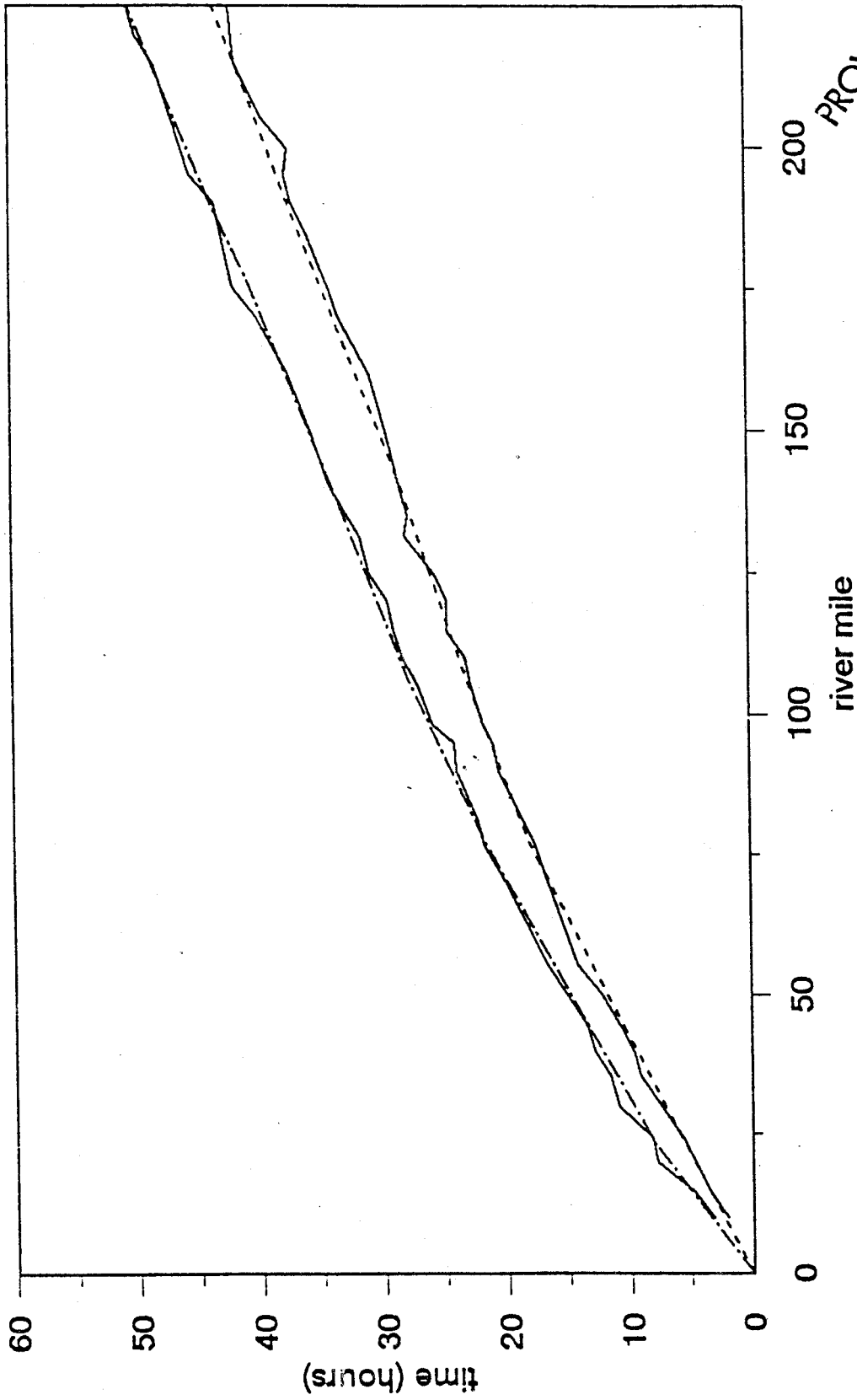


Figure 28: Travel time as a function of River Mile for the discharge waves during Research Flows B and D (solid line) compared to predicted travel times [dashed line with single dots (B) and dashed line (D)]. The smaller amplitude discharge wave of Research Flow B had a lower phase speed and, therefore, is the lower of the two solid lines.

**PROVISIONAL DRAFT**  
 Subject to Revision  
 DO NOT QUOTE OR RELEASE  
 Pending Approval by Director  
 U.S. Geological Survey

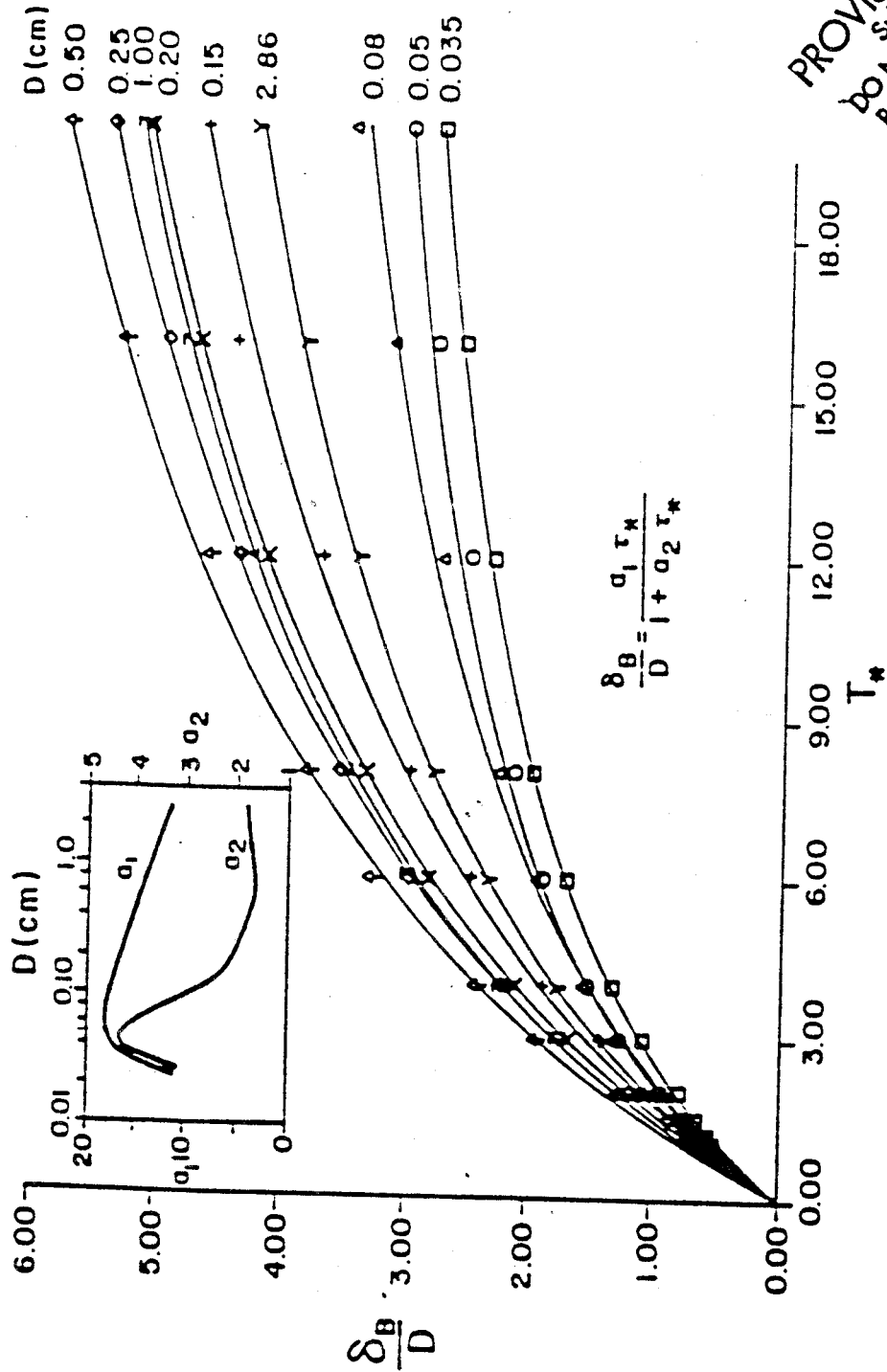


Figure 29: Height ( $\delta_B$ ) to which non-cohesive sediment grains with a density of  $\rho_s = 2.65 \times 10^{-3} \text{ kg/m}^3$  saltate as a function of transport stage ( $T^* = \tau_b / \tau_c$ ). The curves on the primary graph are for 9 sizes between  $D = 0.035 \text{ cm}$  and  $D = 2.86 \text{ cm}$ . They can be represented by the expression,  $\delta_B = \alpha_1 \tau_* (1 + \alpha_2 \tau_*)^{-1}$ , where  $\tau_*$  is the dimensionless boundary shear stress (Shields stress), and  $\alpha_1$  and  $\alpha_2$  are coefficients with values given in the inset as a function of grain size; the symbols on the primary graph denote values calculated using the saltation model of Wiberg and Smith (1985). The figure is from Wiberg (1987).

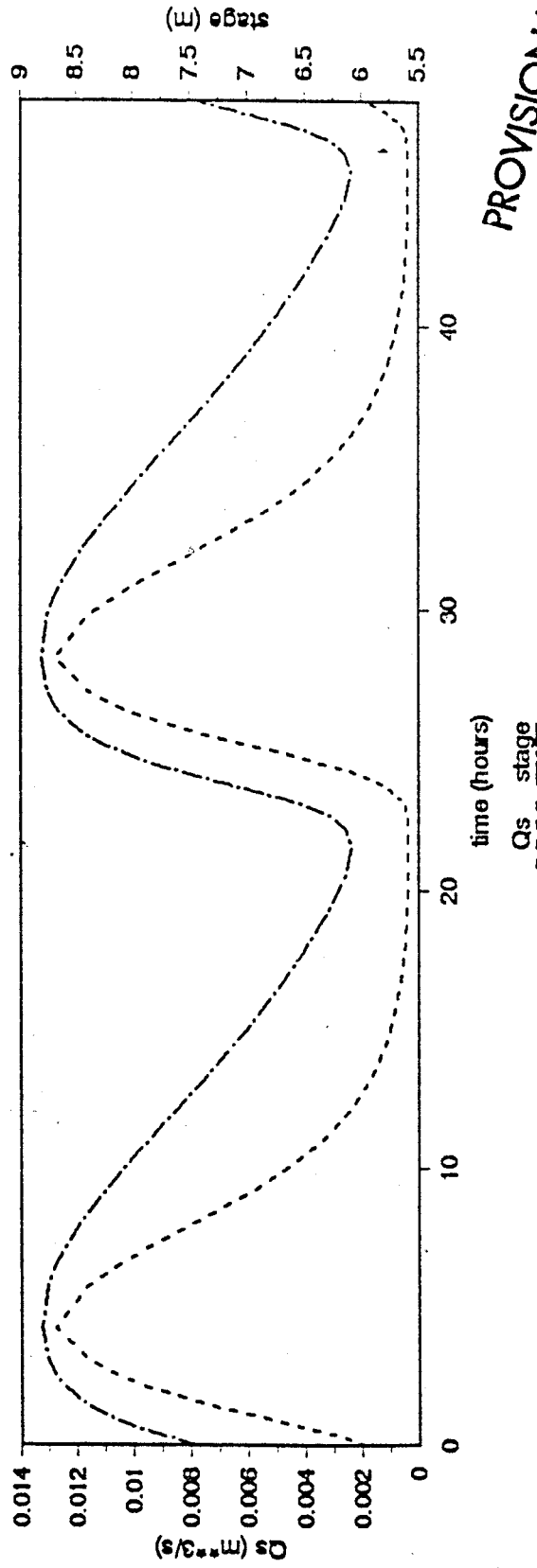
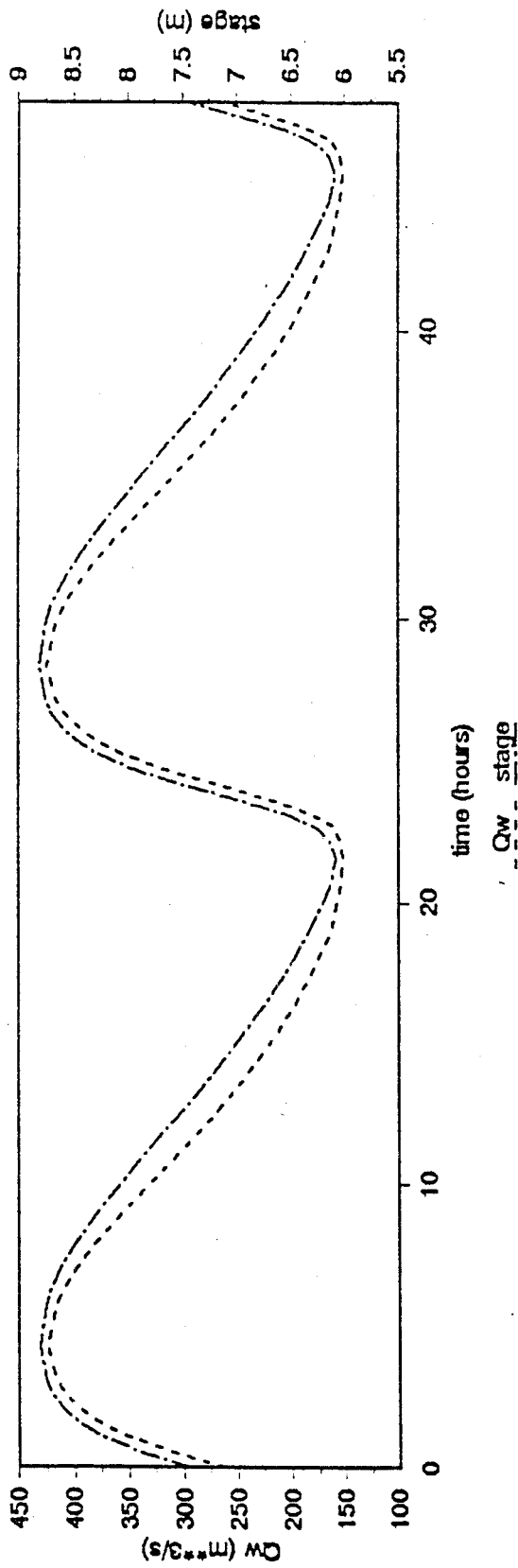


Figure 30: Comparison of the shapes of the measured stage, calculated water discharge and calculated suspended sand discharge waves over two cycles of Research Flow B. Note the nonlinear dependences of the suspended sand transport on stage and water discharge, producing a more peaked shape for that wave. These calculations are for the hydraulically characterized reach 140 to 169.

**PROVISIONAL DRAFT**  
 Subject to Revision  
 DO NOT QUOTE OR RELEASE  
 Pending Approval by Director  
 U.S. Geological Survey

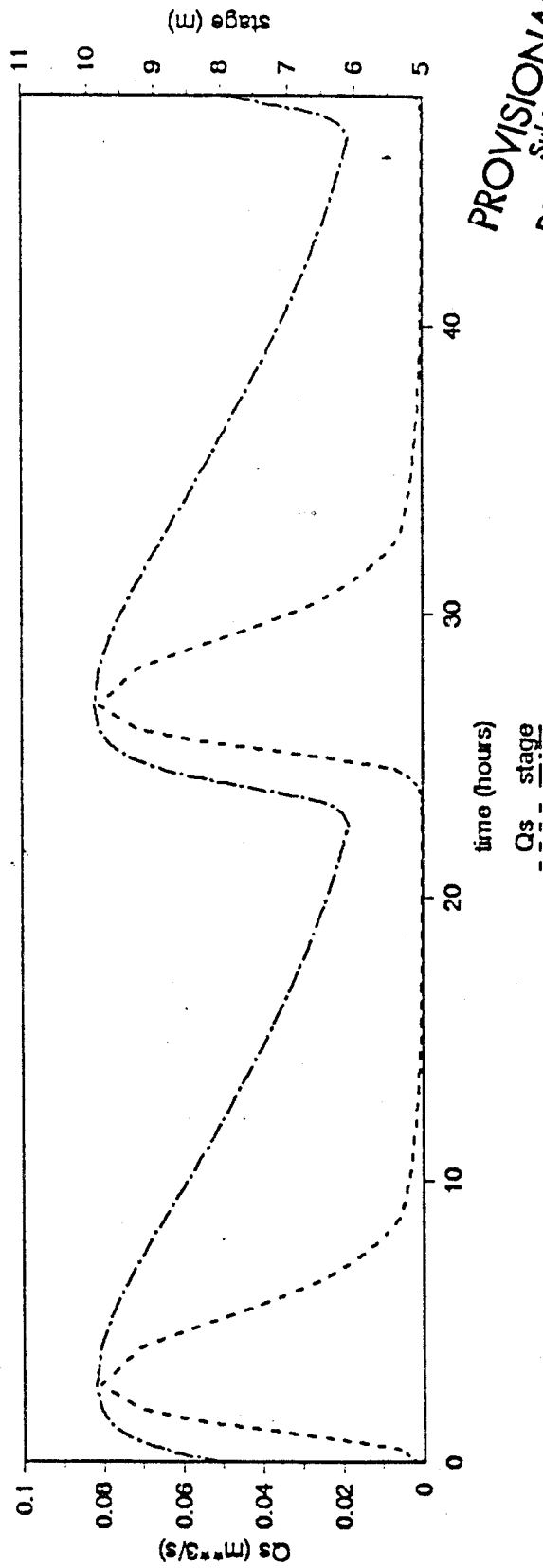
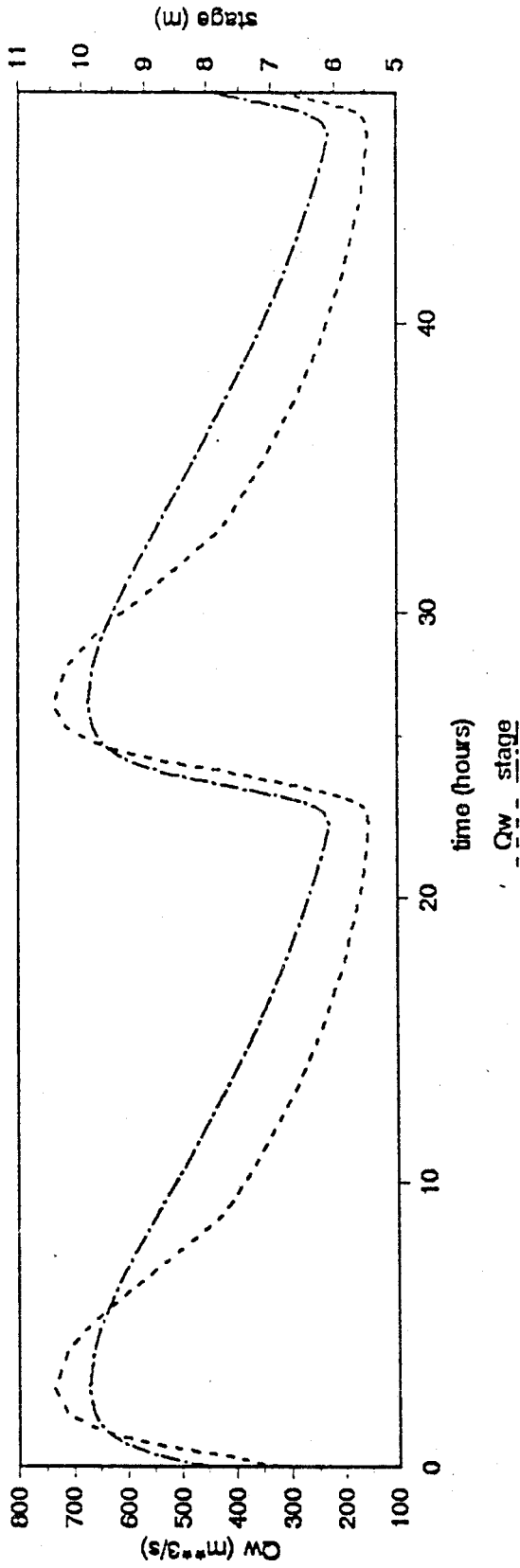


Figure 31: Comparison of the shapes of the measured stage, calculated water discharge and calculated suspended sand discharge waves over two cycles of Research Flow D. Note that most of the suspended sand transport occurs near the peak of the discharge wave during this research flow. These calculations are for the hydraulically characterized reach 140 to 169.

**PROVISIONAL DRAFT**  
 Subject to Revision  
 DO NOT QUOTE OR RELEASE  
 Pending Approval by Director  
 U.S. Geological Survey

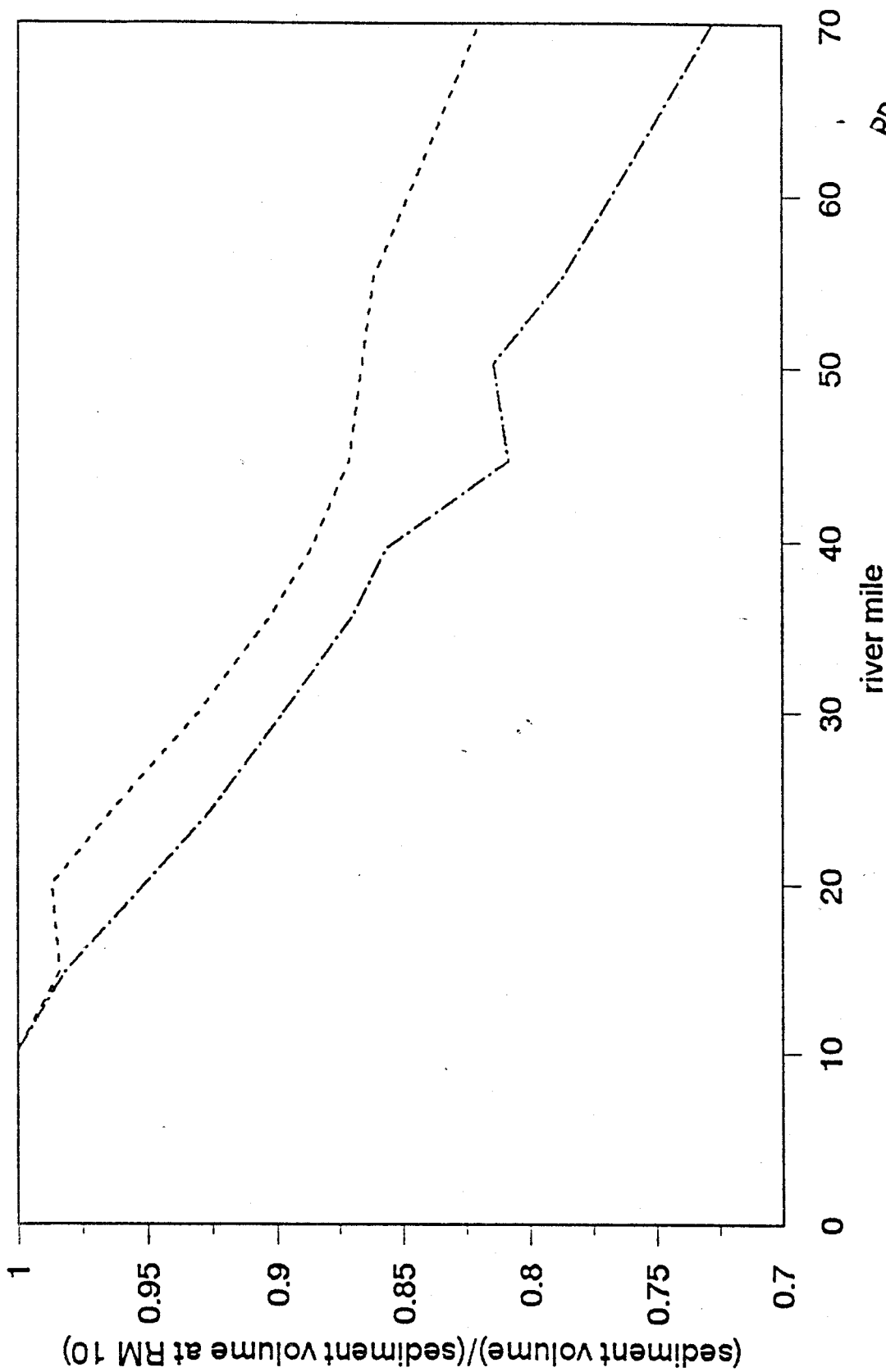


Figure 32: Decrease in sediment discharge in a channel of fixed average cross-section between Lees Ferry and River Mile 70 as a result only of the change in shapes of the discharge waves for Research Flows B (dashed line) and D (dashed line with single dots).

**PROVISIONAL DRAFT**  
 Subject to Revision  
 Do NOT QUOTE OR RELEASE  
 Pending Approval by Director  
 U.S. Geological Survey

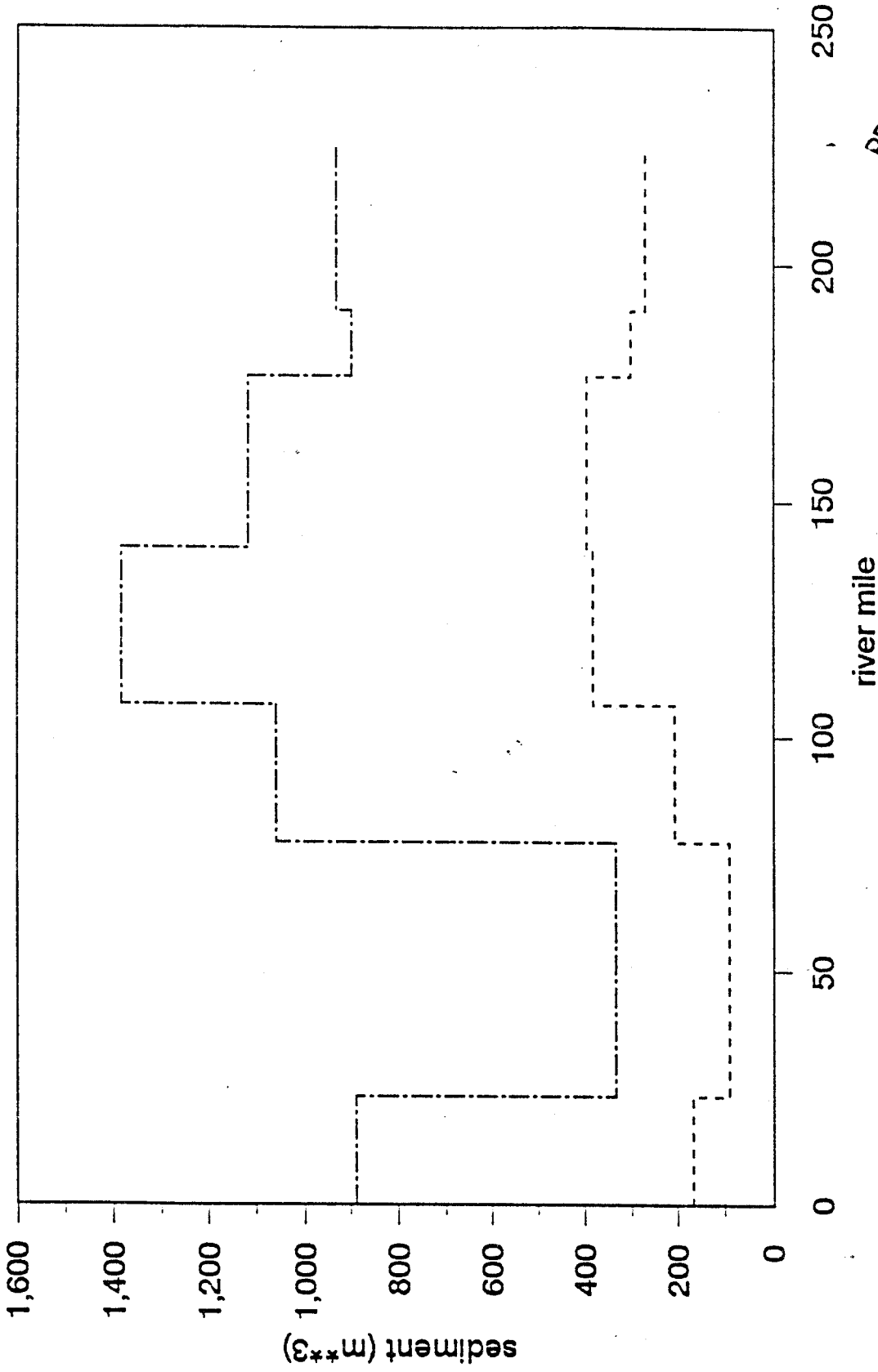


Figure 33: Suspended sand flux calculated for each hydraulically characterized reach during Research Flow B (dashed line) and Research Flow D (dashed line with single dots) assuming that 19% and 12% of the riverbed, respectively, in each of these reaches is covered by sand.

**PROVISIONAL DRAFT**  
 Do Not Subject to Revision  
 Do NOT QUOTE OR RELEASE  
 Pending Approval by Director  
 U.S. Geological Survey

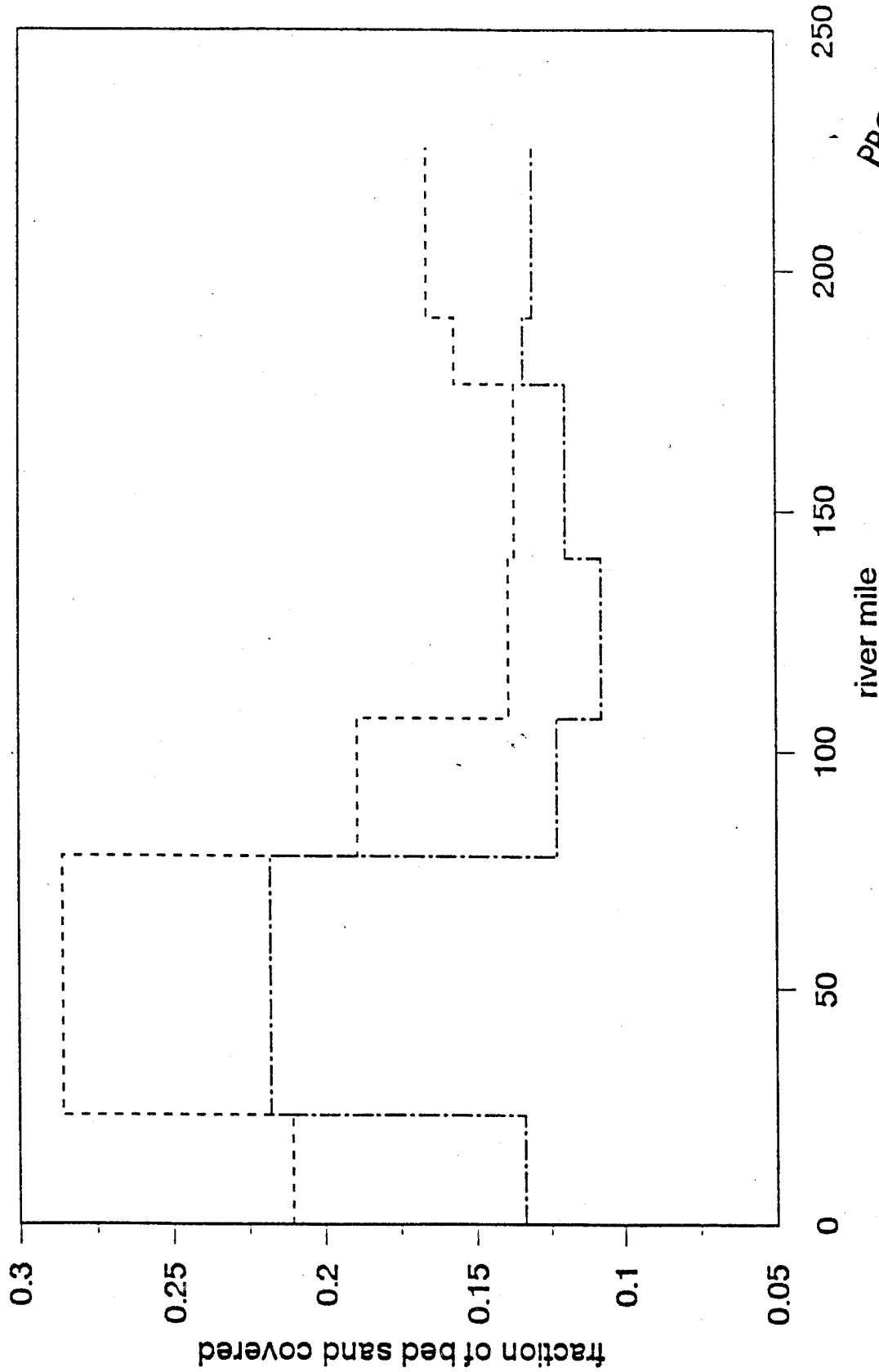


Figure 34: Percentage of the bed that would have to be covered by sand to produce a uniform downstream flux of this material during Research Flow B (dashed line) and Research Flow D (dashed line with single dots).

**PROVISIONAL DRAFT**  
 Subject to Revision  
 Do NOT QUOTE OR RELEASE  
 Pending Approval by Director  
 U.S. Geological Survey

Appendix I: Cross-sectional profiles for each of the morphologically similar reaches

Although mean cross-sectional profiles for several morphologically similar reaches are displayed in Figures 8 to 11, none of these provide comparisons of the symmetric to the asymmetric profiles or display the degree of variability of the profiles included in the block, as was done for the entire River in Figure 7. Therefore, Figures A1 through A10 are included in this report in order to display these properties for each of the morphologically similar reach. The format of each of these figures is the same as that used in Figure 7.

**PROVISIONAL DRAFT**  
Subject to Revision  
**DO NOT QUOTE OR RELEASE**  
Pending Approval by Director  
U.S. Geological Survey

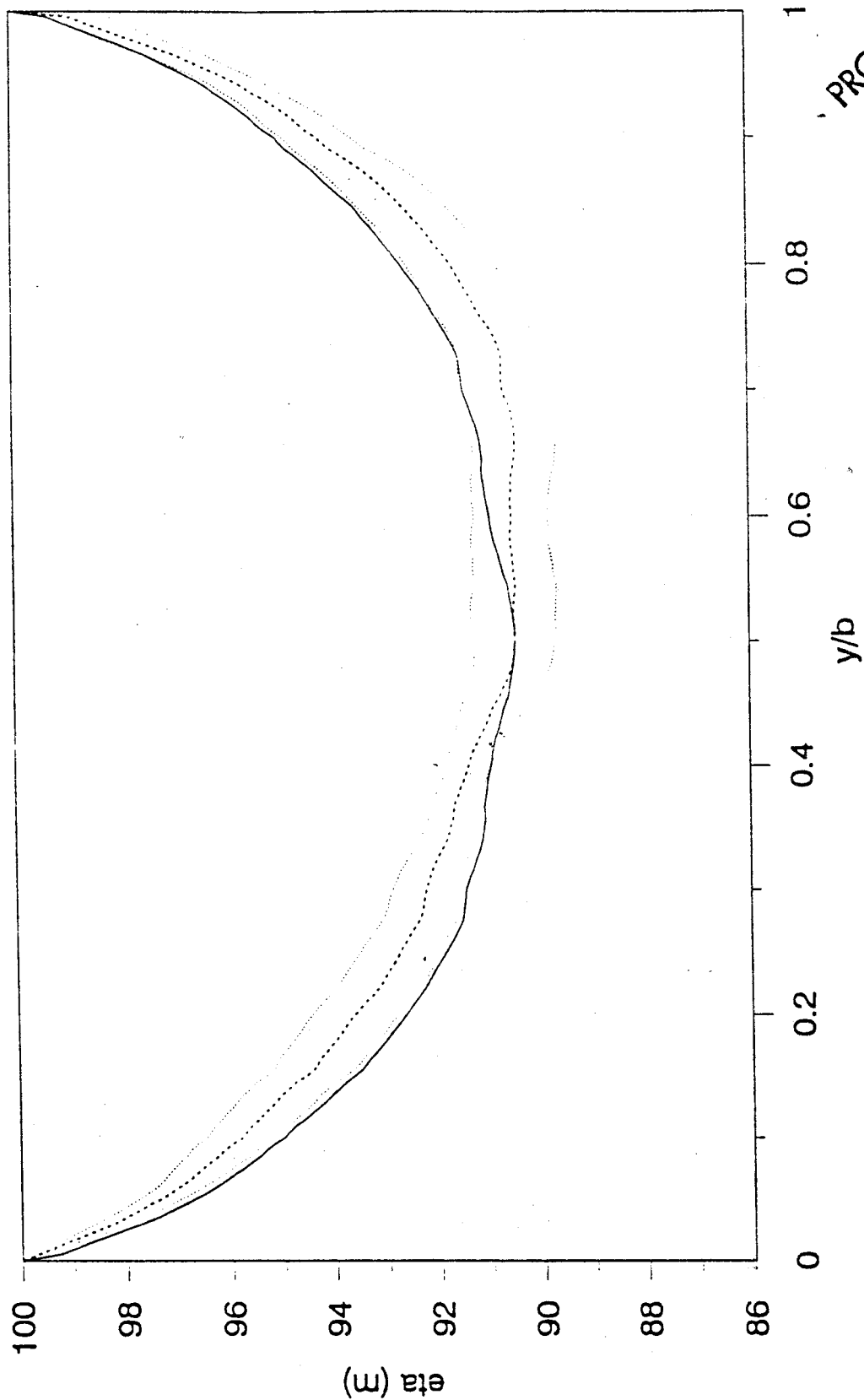


Figure A1: Block averaged cross-sectional shape for the set of channel profiles obtained by Wilson in the 0 to 11 reach. The solid line assumes the profiles must be symmetrical and the dashed line does not enforce this constraint. The dotted lines give the block averaged mean plus and minus one standard deviation. All profiles were scaled by river width before averaging.

PROVISIONAL DRAFT  
 Subject to Revision  
 DO NOT QUOTE OR RELEASE  
 Pending Approval by Director  
 U.S. Geological Survey

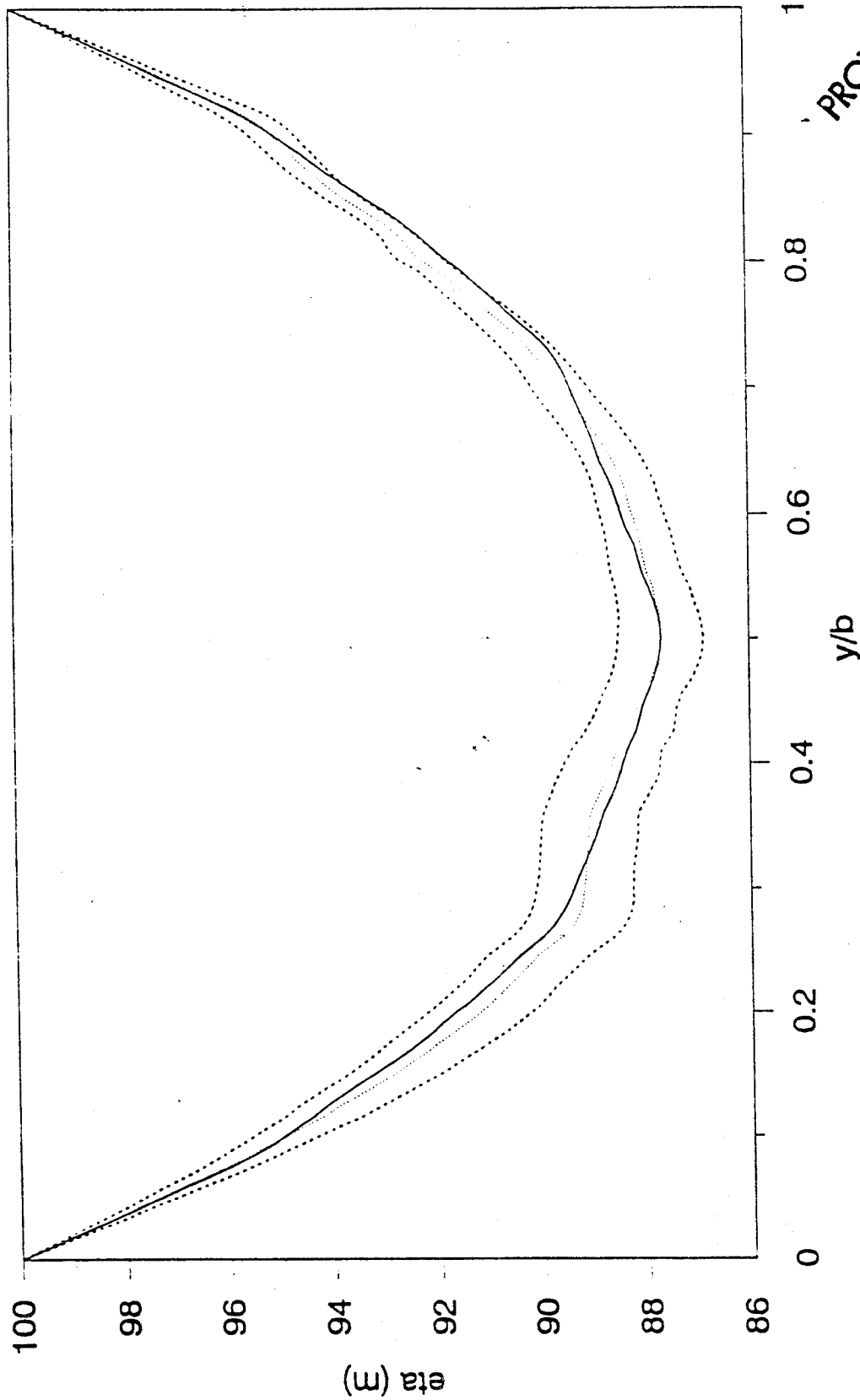
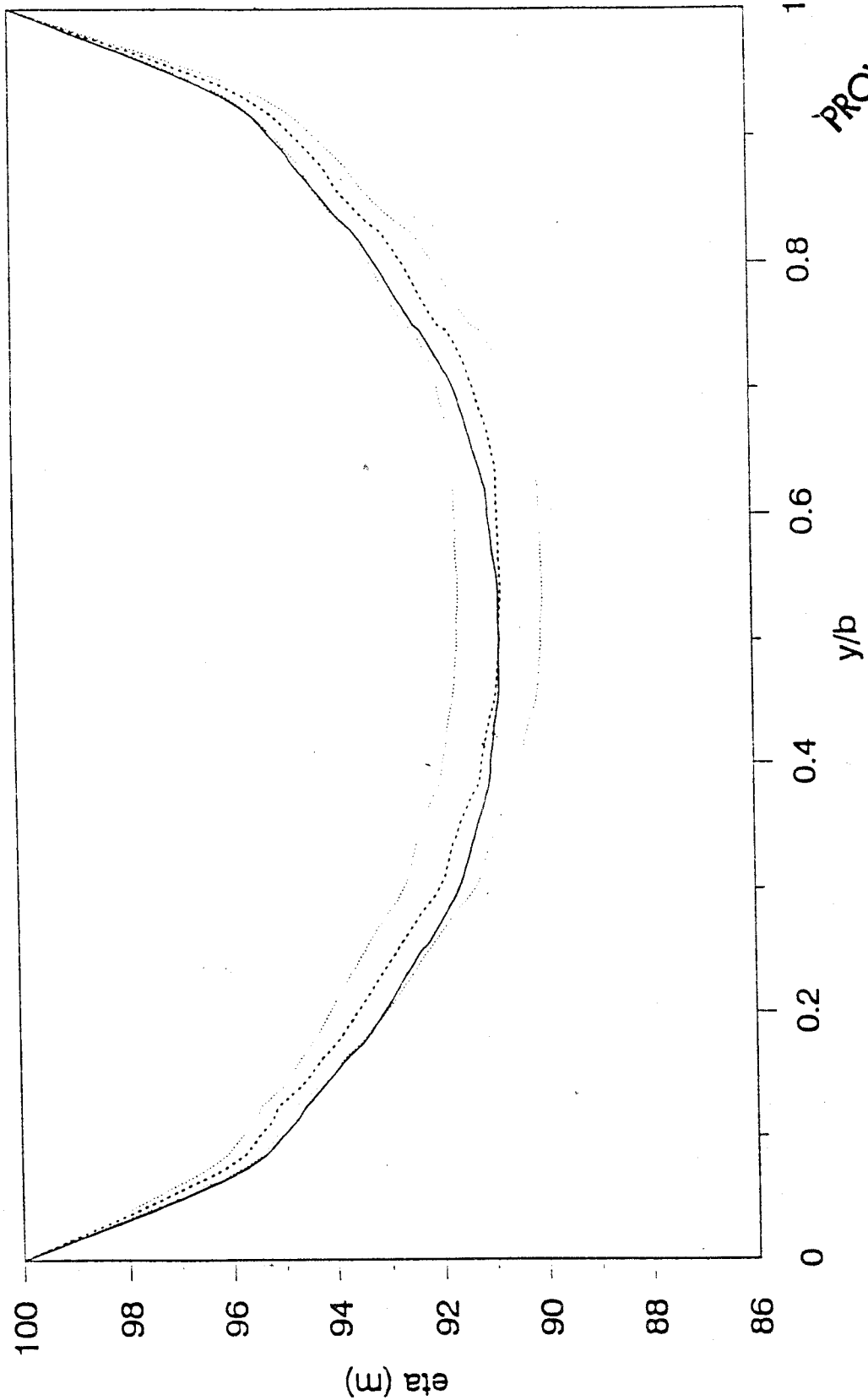


Figure A2: Block averaged cross-sectional shape for the set of channel profiles obtained by Wilson in the 11 to 23 reach. The solid line assumes the profiles must be symmetrical and the dashed line does not enforce this constraint. The dotted lines give the block averaged mean plus and minus one standard deviation. All profiles were scaled by river width before averaging.

**PROVISIONAL DRAFT**  
 Subject to Revision  
**DO NOT QUOTE OR RELEASE**  
 Pending Approval by Director  
 U.S. Geological Survey



**PROVISIONAL DRAFT**  
 Subject to Revision  
 DO NOT QUOTE OR RELEASE  
 Pending Approval by Director  
 U.S. Geological Survey

**Figure A3:** Block averaged cross-sectional shape for the set of channel profiles obtained by Wilson in the 23 to 50 reach. The solid line assumes the profiles must be symmetrical and the dashed line does not enforce this constraint. The dotted lines give the block averaged mean plus and minus one standard deviation. All profiles were scaled by river width before averaging.

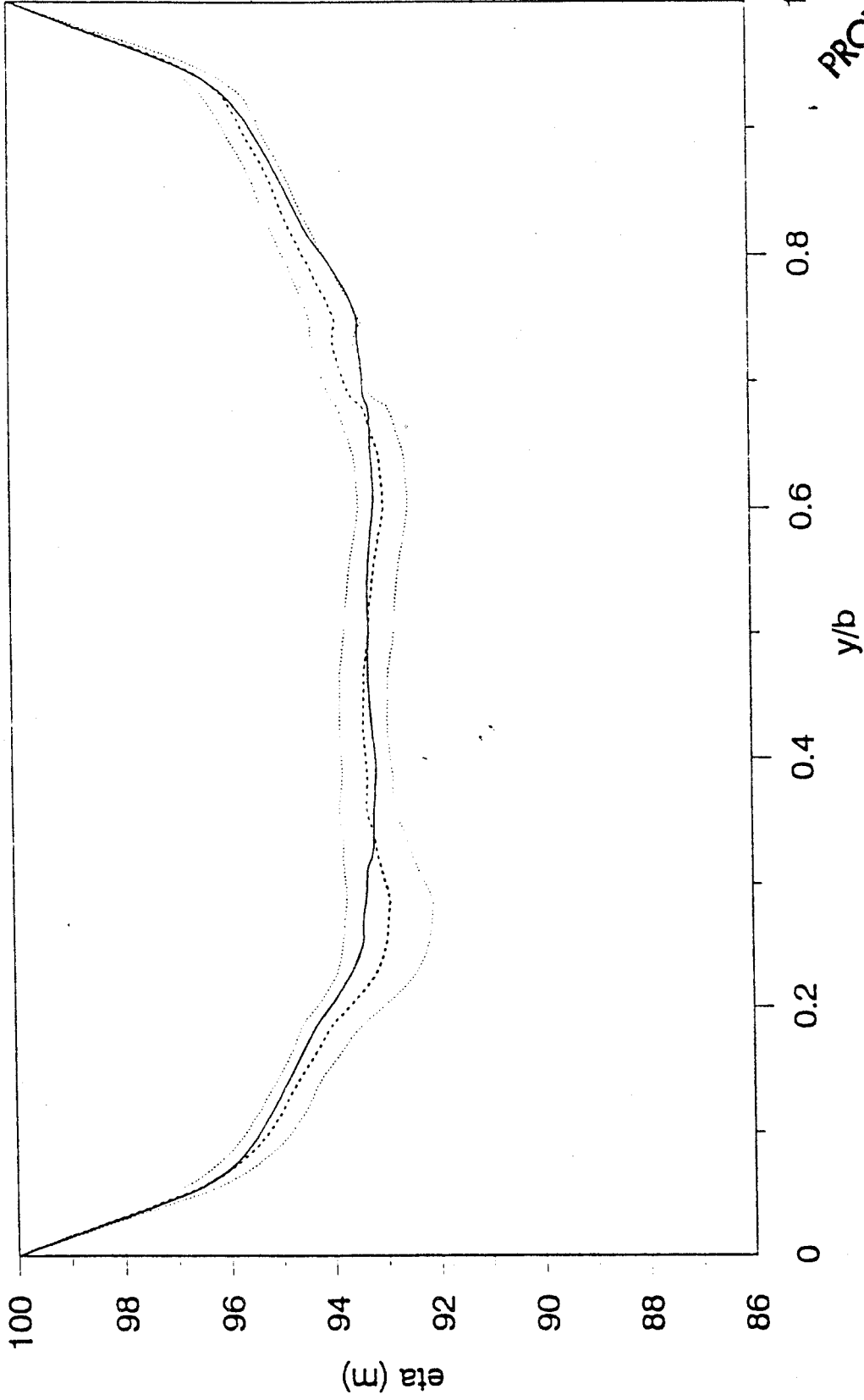


Figure A4: Block averaged cross-sectional shape for the set of channel profiles obtained by Wilson in the 50 to 77 reach. The solid line assumes the profiles must be symmetrical and the dashed line does not enforce this constraint. The dotted lines give the block averaged mean plus and minus one standard deviation. All profiles were scaled by river width before averaging.

**PROVISIONAL DRAFT**  
 Subject to Revision  
 DO NOT QUOTE OR RELEASE  
 Pending Approval by Director  
 U.S. Geological Survey

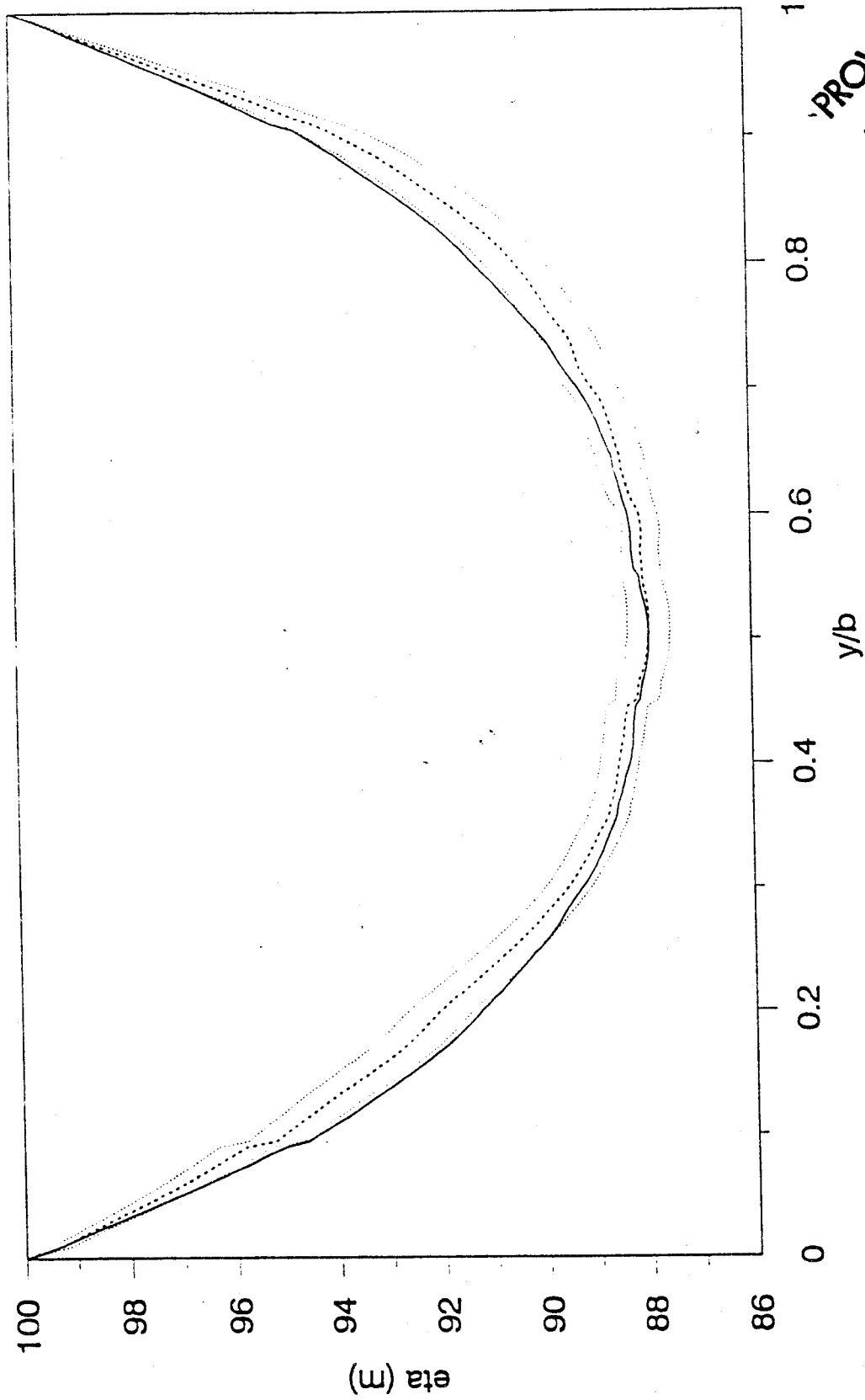
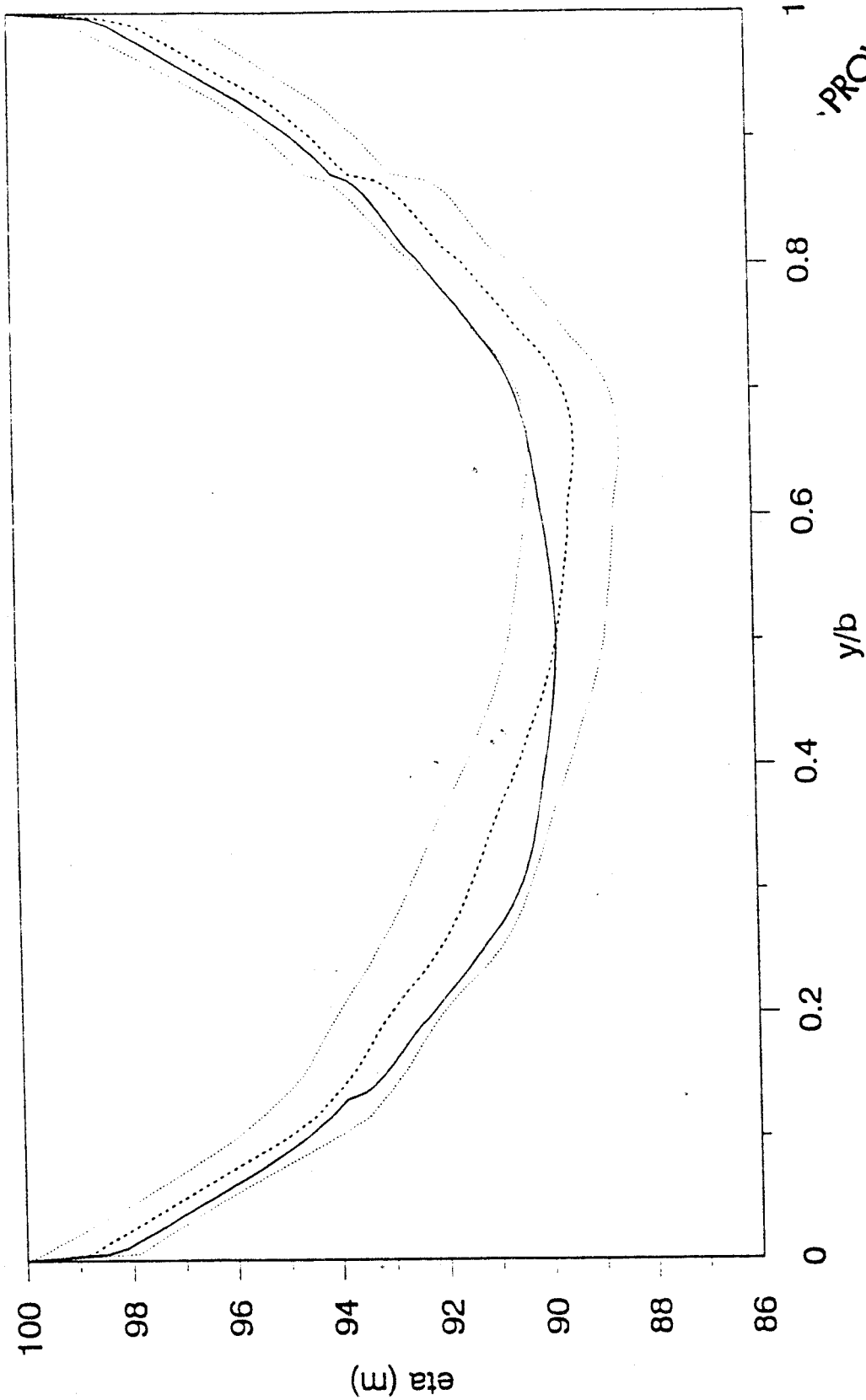


Figure A5: Block averaged cross-sectional shape for the set of channel profiles obtained by Wilson in the 77 to 107 reach. The solid line assumes the profiles must be symmetrical and the dashed line does not enforce this constraint. The dotted lines give the block averaged mean plus and minus one standard deviation. All profiles were scaled by river width before averaging.

**PROVISIONAL DRAFT**  
 Subject to Revision  
 DO NOT QUOTE OR RELEASE  
 Pending Approval by Director  
 U.S. Geological Survey



**PROVISIONAL DRAFT**  
 Subject to Revision  
**DO NOT QUOTE OR RELEASE**  
 Pending Approval by Director  
 U.S. Geological Survey

**Figure A6:** Block averaged cross-sectional shape for the set of channel profiles obtained by Wilson in the 107 to 117 reach. The solid line assumes the profiles must be symmetrical and the dashed line does not enforce this constraint. The dotted lines give the block averaged mean plus and minus one standard deviation. All profiles were scaled by river width before averaging.

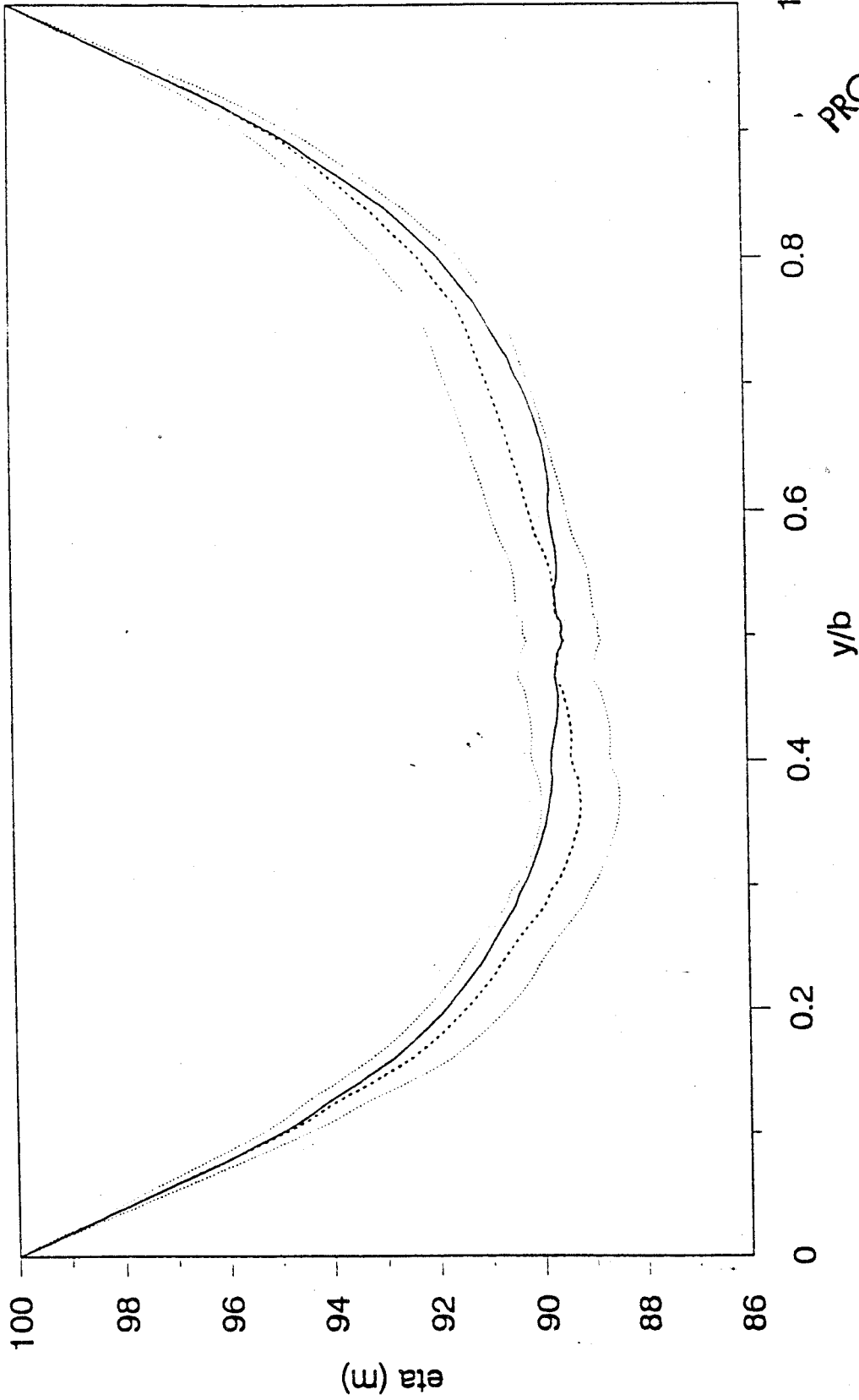


Figure A7: Block averaged cross-sectional shape for the set of channel profiles obtained by Wilson in the 117 to 140 reach. The solid line assumes the profiles must be symmetrical and the dashed line does not enforce this constraint. The dotted lines give the block averaged mean plus and minus one standard deviation. All profiles were scaled by river width before averaging.

**PROVISIONAL DRAFT**  
 Subject to Revision  
 DO NOT QUOTE OR RELEASE  
 Pending Approval by Director  
 U.S. Geological Survey

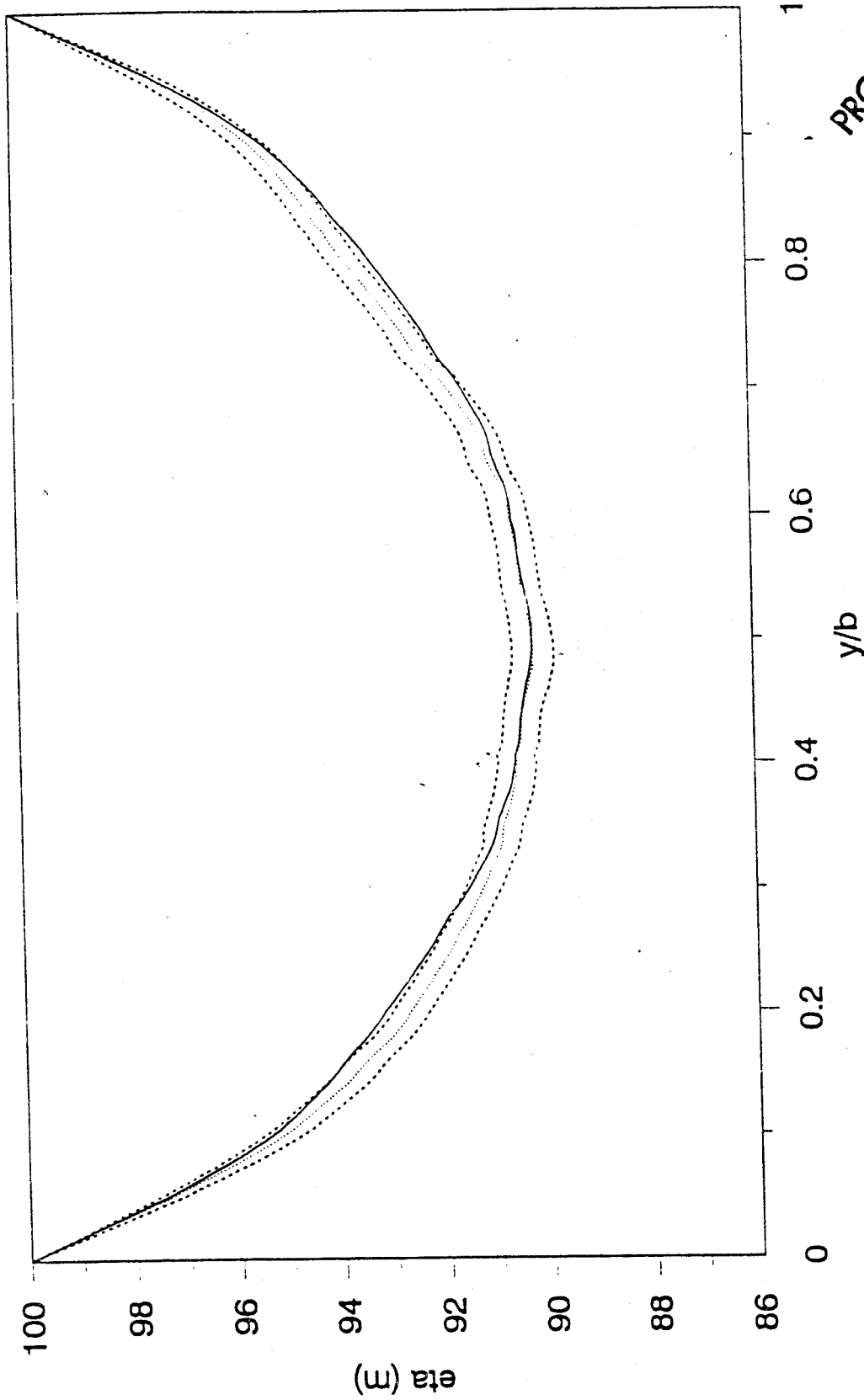
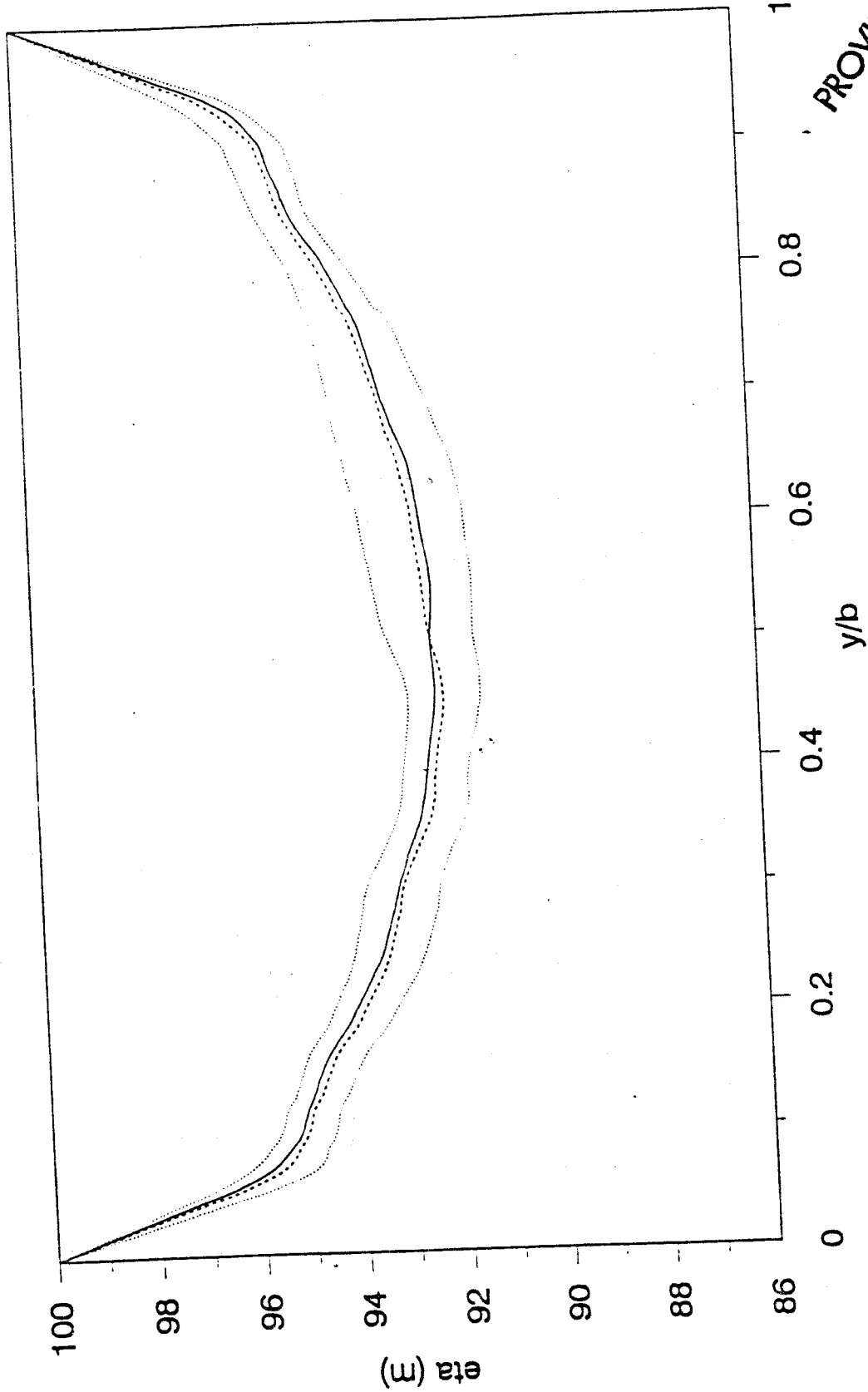


Figure A8: Block averaged cross-sectional shape for the set of channel profiles obtained by Wilson in the 140 to 169 reach. The solid line assumes the profiles must be symmetrical and the dashed line does not enforce this constraint. The dotted lines give the block averaged mean plus and minus one standard deviation. All profiles were scaled by river width before averaging.

**PROVISIONAL DRAFT**  
 Subject to Revision  
 DO NOT QUOTE OR RELEASE  
 Pending Approval by Director  
 U.S. Geological Survey



**PROVISIONAL DRAFT**  
 Subject to Revision  
 DO NOT QUOTE OR RELEASE  
 Pending Approval by Director  
 U.S. Geological Survey

**Figure A9:** Block averaged cross-sectional shape for the set of channel profiles obtained by Wilson in the 169 to 190 reach. The solid line assumes the profiles must be symmetrical and the dashed line does not enforce this constraint. The dotted lines give the block averaged mean plus and minus one standard deviation. All profiles were scaled by river width before averaging.

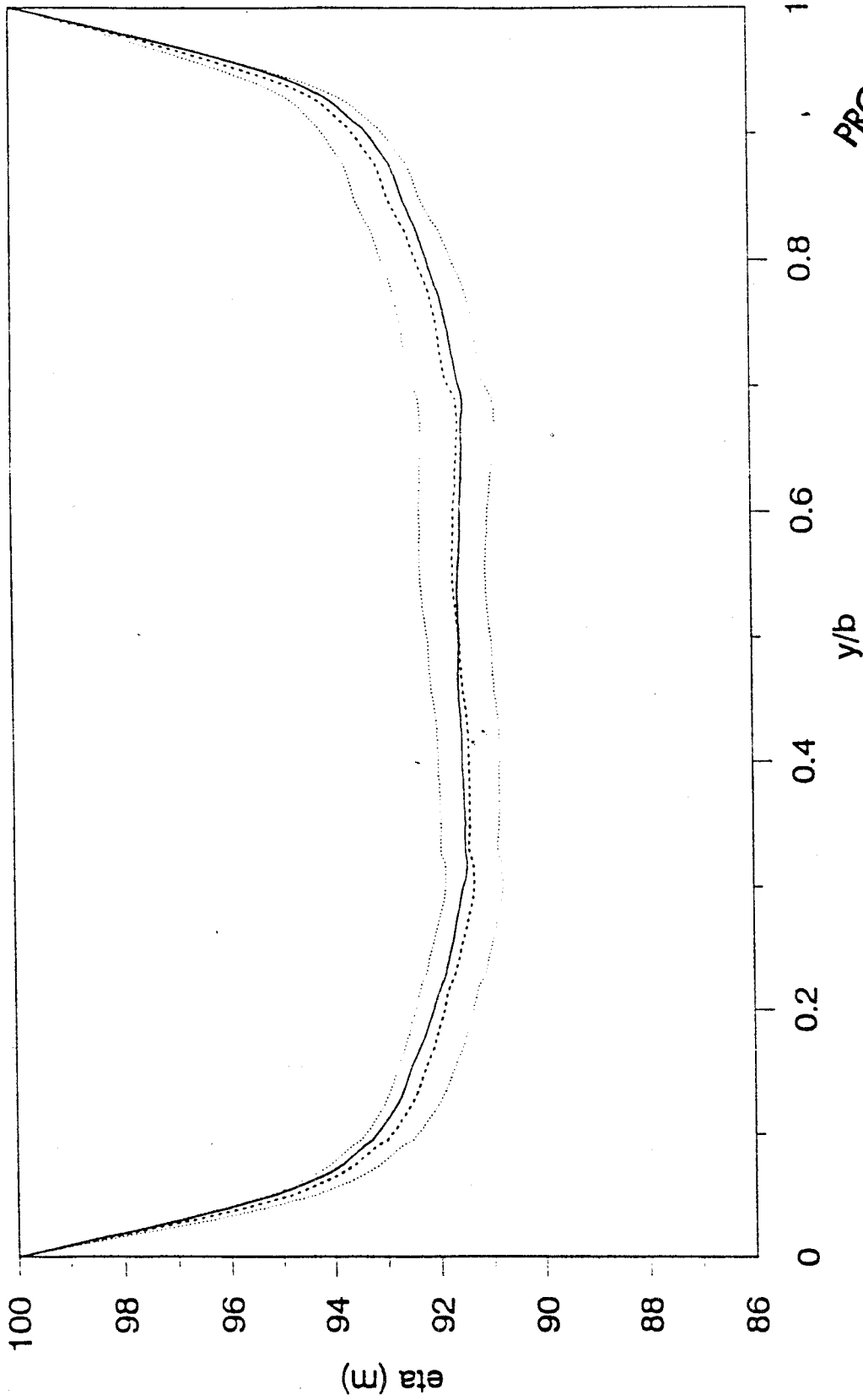


Figure A10: Block averaged cross-sectional shape for the set of channel profiles obtained by Wilson in the 190 to 225 reach. The solid line assumes the profiles must be symmetrical and the dashed line does not enforce this constraint. The dotted lines give the block averaged mean plus and minus one standard deviation. All profiles were scaled by river width before averaging.

**PROVISIONAL DRAFT**  
 Subject to Revision  
 DO NOT QUOTE OR RELEASE  
 Pending Approval by Director  
 U.S. Geological Survey



# United States Department of the Interior



GEOLOGICAL SURVEY

Water Resources Division  
2617 E. Lincolnway, Suite B  
Cheyenne, WY 82001

May 1, 1992

## Memorandum

To: Dave Wegner, GCES, USBR, Flagstaff, AZ

From: Jim Wilson, USGS, WRD, Cheyenne, WY

Subject: PUBLICATIONS--Transmittal of revised GCES report by USGS authors

ORIGINAL

A copy of the new report listed below is attached. I also am sending a copy to the Colorado River Studies office in Salt Lake City and the NEPA Manager in Denver.

*"Flow and sediment transport in the Colorado River between Lake Powell and Lake Mead,"* by  
J. Dungan Smith and Stephen Wiele

As with the other USGS reports, please treat this as an internal working document for use by Colorado River Studies personnel only. This report will be updated one or more times before it is published. USGS policy is that it not be made available to the public, nor should it be cited as a reference or listed in bibliographies, until it has been published.

James F. Wilson, Jr.

## Attachments

Copy to: R.D. Mac Nish, District Chief, WRD, USGS, Tucson, AZ  
G.R. Marzolf, WRD, USGS, Boulder, CO  
Tim Randle, USBR, Denver, CO

**GCES OFFICE COPY  
DO NOT REMOVE!**

440.00

RES-5.00

C 719

(18102)

#212

PH 4805-dr ft

E 7